Molecular Imprinting with Functional DNA and Nanozymes: Affinity Improvement and Selective Catalysis

by

Zijie Zhang

A thesis

presented to the University of Waterloo

in fulfilment of the

thesis requirement for the degree of

Doctor of Philosophy

in

Chemistry

Waterloo, Ontario, Canada, 2019

Examining Committee Membership

The following served on the Examining Committee for this thesis. The decision of the Examining Committee is by majority vote.

External Examiner	**Dr. Michael Serpe** Professor, Department of Chemistry, University of Alberta, Edmonton, Canada.
Supervisor	**Dr. Juewen Liu** Professor, Department of Chemistry, University of Waterloo, Waterloo, Canada.
Internal Member	**Dr. Xiaosong Wang** Professor, Department of Chemistry, University of Waterloo, Waterloo, Canada.
Internal Member	**Dr. Boxin Zhao** Associate Professor, Department of Chemical Engineering, University of Waterloo, Waterloo, Canada.
Internal Member	**Dr. Thorsten Dieckmann** Associate Professor, Department of Chemistry, University of Waterloo, Waterloo, Canada.
Internal-external Member	**Dr. Michael Pope** Assistant Professor, Department of Chemical Engineering, University of Waterloo, Waterloo, Canada.

Author's Declaration

This thesis consists of material all of which I authored or co-authored: see Statement of Contributions included in the thesis. This is a true copy of the thesis, including any required final revisions, as accepted by my examiners.

I understand that my thesis may be made electronically available to the public.

Statement of Contributions

The work presented in the thesis was performed by the author and several collaborators. The resulting publications and contributions of each collaborator are listed below in details.

The work in the Chapter 2 has been published as: Zijie Zhang and Juewen Liu. Molecularly Imprinted Polymers with DNA Aptamer Fragments as Macromonomers. ***ACS Applied Materials & Interfaces***, 2016, *8*, 6371-6378. All of experiments were performed by the first author. The manuscript was written by the two authors.

The work in the Chapter 3 has been published as: Zijie Zhang, Biwu Liu and Juewen Liu. Molecular Imprinting for Substrate Selectivity and Enhanced Activity of Enzyme Mimics. ***Small***, 2017, *13*, 1602730. All of experiments were performed by the first author. Biwu Liu helped for the experimental design. The manuscript was written by Zijie Zhang and Juewen Liu.

The work in the Chapter 4 has been published as: Zijie Zhang and Juewen Liu. Intracellular Delivery of a Molecularly Imprinted Peroxidase Mimicking DNAzyme for Selective Oxidation. ***Materials Horizons***, 2018, *5*, 738-744. All of experiments were performed by the first author. The manuscript was written by the two authors.

The work in the Chapter 5 has been published as: Zijie Zhang, Xiaohan Zhang, Biwu Liu and Juewen Liu. Molecular Imprinting on Inorganic Nanozymes for Hundred-fold Enzyme Specificity. ***Journal of the American Chemical Society***, 2017, *139*, 5412-5419. Xiaohan Zhang prepared the iron oxides nanoparticles. Biwu Liu helped for the experimental design. All of experiments were performed by the first author. The manuscript was written by Zijie Zhang and Juewen Liu.

The work in the Chapter 6 has been published as: Zijie Zhang, Yuqing Li, Xiaohan Zhang and Juewen Liu. Molecularly Imprinted Nanozymes with Faster Catalytic Activity and Better Specificity. ***Nanoscale***, 2019, *11*, 4854-4863. Xiaohan Zhang prepared the iron oxides nanoparticles. Yuqing Li helped for the experimental design. All of experiments were performed by the first author. The manuscript was written by Zijie Zhang and Juewen Liu.

Abstract

Molecular imprinting refers to polymerization of functional monomers in the presence of a template molecule. It is a general method to prepare stable and cost-effective artificial ligands as antibody mimics (also known as plastic antibodies), and the resulting materials are called molecularly imprinted polymers (MIP). Many molecules have been used as templates for imprinting ranging from metal ions, small molecules, peptides and proteins, nucleic acids, to whole cells with a wide range of applications including chromatography, solid-phase extraction, biosensors, therapeutics, organic synthesis and catalysis. MIP however suffer from low affinity and limited signaling mechanisms for binding. DNA oligonucleotides possess many functions such as specific molecular recognition (aptamers) and catalytic activities (DNAzymes). In addition, DNA is stable and easily modified. Combining MIP with DNA has several advantages. First, DNA aptamers can further improve the affinity of MIPs. At the same time, they may enable signaling of MIP binding. Second, some DNAzymes such as those with peroxidase-like activities (G-quadruplex DNAzymes), have low substrate selectivity, and MIP could solve this problem by introducing specific substrate binding sites on the DNAzymes. The approach can also extend to other type enzyme mimics such as nanozymes. Finally, the imprinted polymer shell can also protect enzymes from degradation and facilitate intracellular uptake. In this thesis, molecular imprinting with functional DNA and enzyme mimics were systematically studied. The main aims of the thesis include improving the binding affinity of MIPs and achieving selective catalysis of enzyme mimics. The mechanism of MIP for improved catalysis was also explored.

In Chapter 1, the introduction, relevant background knowledge about molecular imprinting, DNA and enzyme mimics was introduced. A state-of-the-art research progress of the fields was also reviewed. The research goals and outline of the thesis were described in the end of the chapter.

In Chapter 2, DNA aptamer fragments were used in the MIPs for affinity improvement and signalling. While previous research all used full-length aptamers, aptamer fragments with lower cost and higher stability have not been studied. In this work, DNA aptamer for adenosine was used as a model aptamer. It was first split into two halves, fluorescently labeled, and copolymerized into MIPs. With a fluorescence quenching assay, we found that the affinity of MIPs was improved with the aptamer fragments incorporated. Compared to the mixture of the free aptamer fragments, their MIPs doubled the binding affinity. Each free aptamer fragment alone cannot bind adenosine, whereas MIPs containing each fragment are effective binders. We further shortened the aptamer fragment, and the DNA length was pushed to as short as six nucleotides, yielding MIPs still having a high binding affinity (K_d ~27 μM). The study provides a new strategy for preparing functional MIP materials by combining high-affinity biopolymer fragments with low-cost synthetic monomers, allowing higher binding affinity and providing a method for signaling binding based on DNA chemistry.

In Chapter 3, molecularly imprinted nanogels were synthesized around a peroxidase-mimicking DNAzyme (G-quadruplex DNAzyme) to solve the problem of poor specificity of enzyme mimics. The polymer shell was demonstrated that improved the stability and activity of the DNAzymes by 2-fold. When the MIP was prepared with the DNAzyme and its substrate, the catalytic efficiency, k_{cat}/K_m, was enhanced by 6-fold for the imprinted substrate over the non-imprinted, true for both TMB and ABTS as substrates, indicating that selectivity can be achieved via imprinting. Within MIPs, the DNAzyme was also stable against high temperature and allowed

for repeated use. This study demonstrated that molecular imprinting provided a general and practical method to form hybrid materials and introduce substrate recognition to enzyme mimics.

In Chapter 4, following the work in the Chapter 3, a molecularly imprinted DNAzyme nanogel was prepared using Amplex red as the template. The MIP nanogels selectively oxidized Amplex red in the presence of H_2O_2 to form a fluorescent product resorufin, while the oxidations for other substrates (TMB, ABTS and dopamine) were inhibited. The MIP nanogel exhibited more than 1.6-fold higher activity than the free DNAzyme. At the same time, the gel matrix protected the DNAzyme from degradation by DNase I. The nanogel was then internalized by HeLa cells and an intracellular oxidation was achieved. This work provided an integrated solution for biocatalysis inside cells and it might be an interesting solution for intracellular therapeutic applications.

In Chapter 5, molecularly imprinted nanogels were grown on nanozymes to create substrate binding pockets. Fe_3O_4 NPs with peroxidase-mimicking activity were chosen as a model nanozyme. Electron microscopy confirmed a shell of nanogel encapsulating the nanozyme core. By imprinting with an adsorbed substrate, moderate specificity was achieved with neutral monomers (around 2.4-fold). Further introducing charged monomers led to nearly 100-fold specificity for the imprinted substrate over the non-imprinted compared to that of bare Fe_3O_4. Selective substrate binding was further confirmed by ITC tests. Besides Fe_3O_4, the same method was also successfully applied for imprinting on gold nanoparticles (a peroxidase mimic) and nanoceria (an oxidase mimic). In this work, molecular imprinting advanced the functional enzyme mimicking aspect of nanozymes, and such hybrid materials will find applications in biosensor development, separation, environmental remediation, and drug delivery.

In Chapter 6, following the work in Chapters 4 and 5, the catalytic mechanism of molecular imprinted enzyme mimics was systematically studied. A surface science approach was taken by dissecting the catalysis into three steps: adsorption of substrates, reaction, and product release. Each step was individually studied using reaction kinetics measurement, dynamic light scattering, UV-vis spectrometry. Through imprinting, the local substrate concentration around enzyme mimics was enriched by around 8-fold, which contributed to the increased activity. Diffusion of the substrate across the imprinted gel layer was studied by a pre-incubation experiment, demonstrating the improved molecular transportation in the imprinted gel layers. The activation energy (E_a) was measured and a substrate imprinted sample had the lowest activation energy of 13.8 kJ mol^{-1}. Product release was also improved after imprinting as indicated by ITC binding tests using samples respectively imprinted with the substrate and the product. This study has rationalized improved activity and specificity of molecularly imprinted enzyme mimics and guided further rational design of such functional materials.

Overall, molecular imprinting with DNA aptamer fragments improved the affinity and enabled binding signalling. Imprinting on the enzyme mimics including both DNAzyme and nanozymes effectively solved the problem of low substrate specificity. The catalytic activity was also improved due to the enriched local concentration of substrate and lowered activation energy. The thesis provides a new strategy for preparing functional materials by combining MIP with functional DNA and nanomaterials to advance the molecular recognition and selective catalysis field.

Acknowledgements

Firstly, I want to thank my supervisor Dr. Juewen Liu for being my advisor in the past four years. Thank him for giving me the opportunity to study in this great group. Four years of PhD study is short, but it is the most important period in my life. With his help, I have not only learned how to do works correctly and efficiently, but also learned how to be a positive thinker when encountering failures. I will always remember his advices, especially the "*Keep doing things that you're not good at over and over again until you are the expert*".

I would like to thank my committee members Dr. Boxin Zhao, Dr. Thorsten Dieckmann, and Dr. Xiaosong Wang. Thanks for their professional guidance and suggestions for my research projects. I also want to thank my external examiner Dr. Michael Serpe, and my internal-external examiner Dr. Michael Pope for attending my examination. Thanks for their precious time. I also want to say many thanks to Cathy and Kim. They are always kind and patient to help me during my PhD study.

I also want to thank all our lab members with whom I spent unforgettable moment, Dr. Po-Jung Jimmy Huang, Dr. Feng Wang, Dr. Biwu Liu, Dr. Wang Li, Dr. Li Xu, Dr. Liu Wang, Dr. Jinyi Zhang, Dr. Runjhun Saran, Dr. Dai Li, Dr. Wenhu Zhou, Yibo Liu, Yuqing Li, Zhicheng Huang, Lingzi Ma, Xiaohan Zhang, Woohyun J. Moon, Mohamad Zandieh, Tianmeng Yu, Anand Lopez, Ziyi Sun, Olatunji Oni, Michael Hoang, Mahsa Vazin, Lei Chen, Howard Tsai, Qingyun Chen, Yichen Zhao and other members and visiting scholars. I would like to thank Prof. Hao Liang for encouraging me studying abroad. Finally, I would like to thank my parents. They are always being with me and encouraging me no matter where I am and how hard it gets.

Dedication

I would like to dedicate this thesis to my family,

thanks for their love and support!

Table of Contents

List of Figures

List of Tables

List of Abbreviations

AA	Acrylic acid
AAm	Acrylamide
AMP	Adenosine monophosphate
AMPS	2-acrylamido-2-methyl-1-propanesulfonic acid
APS	Ammonium persulfate
AR	Amplex red (10-acetyl-3,7- dihydroxyphenoxazine)
ATP	Adenosine triphosphate
AuNPs	Gold nanoparticles
cDNA	Complementary DNA
DLS	Dynamic Light Scattering
DMPA	*N*-[3-(dimethylamino)propyl]methacrylamide
DMSO	Dimethyl sulfoxide
DNA	Deoxyribonucleic acid
DOPA	Dopamine
DVB	Divinylbenzene
EDMA	Ethylene glycol dimethacrylate
EDX	Energy-dispersive X-ray spectroscopy
ELISA	Enzyme-linked immunosorbent assays
FAM	6-carboxyfluorescein
FRP	Free radical polymerization
GMP	Guanosine monophosphate

GOx	Glucose oxidase
GTP	Guanosine triphosphate
HEPES	4-(2-hydroxyethyl) piperazine-1-ethanesulfonic acid
HRP	Horseradish peroxidase
ICP-MS	Inductively coupled plasma mass spectrometry
ITC	Isothermal titration calorimetry
$\boldsymbol{K}_{\mathbf{cat}}$	Rate constant
$\boldsymbol{K}_{\mathbf{m}}$	Michealis-Menten constant
LOD	Limit of detection
MAA	Methacrylic acid
MBAA	*N*, *N'*-methylenebisacrylamide
MIP	Molecularly imprinted polymers
NIP	Non-imprinted polymers
NIPAAm	*N*-isopropylacrylamide
NMR	Nuclear magnetic resonance
OPD	o-phenylenediamine dihydrochloride
PBS	Phosphate-buffered saline
QCM	Quartz crystal microbalance
QDs	Quantum dots
SDS	Sodium dodecyl sulfate
SEM	Scanning electron microscopy
TEMED	*N,N,N',N'*-tetramethylethylenediamine
ThT	Thioflavin T

TMB	3,3',5,5'-tetramethylbenzidine
UCNPs	Upconverting nanoparticles

Chapter 1 Introduction

1.1 Molecular imprinting

1.1.1 Definition of molecular imprinting

Molecular imprinting is known as a technique to prepare synthetic materials that are capable of selective binding the target molecules. The concept was inspired by the 'lock-and-key' model of enzymes and antibodies.[1] Conceptually, the target molecules were used as the 'key' templates. Various functional monomers that could form reversible specific interactions with the templates were used as the pieces of the 'lock'. With the interactions, the 'key' template would drive the arrangement of the monomer pieces in favored positions and form a pre-polymerization complex. By introducing crosslinking agents and performing polymerizations, the complex was fixed into polymer matrix. The templates were then removed by disrupting the pre-formed interactions and the resulting cavities could specifically rebind the templates due to the complementary binding sites with memory of the shape, size and functional groups of the templates. The prepared materials are called molecularly imprinted polymers (MIPs).[2-3] An integrated definition of molecular imprinting was elected by Alexander *et al.*, as followed,[4] and the Figure 1.1 shows a schematic presentation for the molecular imprinting process.

> "The construction of ligand selective recognition sites in synthetic polymers where a template (atom, ion, molecule, complex or a molecular, ionic or macromolecular assembly, including micro-organisms) is employed in order to facilitate recognition site formation during the covalent assembly of the bulk phase by a polymerization or polycondensation process, with subsequent removal of some or all of the template being necessary for recognition to occur in the spaces vacated by the templating species".[4]

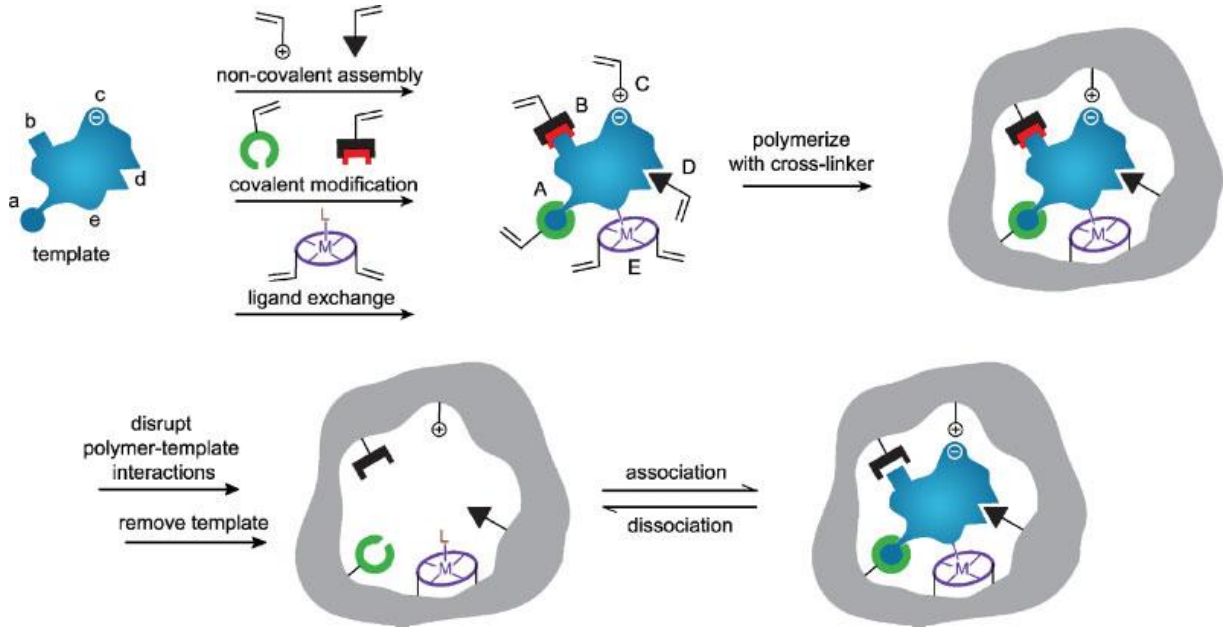

Figure 1.1 Schematic representation of the molecular imprinting process: The formation of reversible interactions between the template and functional monomers may involve one or more of the following interactions: (A) reversible covalent bond(s); (B) covalent bonds combined with non-covalent interactions; only non-covalent interactions of (C) electrostatic, (D) hydrophobic or van der Waals forces, and (E) co-ordination with a metal center. Each formed with complementary functional groups or structural elements of the template, (a-e) respectively]. Figure adapted with permission from ref ([4]). Copyright © 2006 John Wiley & Sons, Ltd.

1.1.2 Imprinting approaches

1.1.2.1 Covalent imprinting

The choice of functional monomers is highly important for MIPs. To achieve specific binding, MIPs are prepared using covalent and non-covalent interactions for imprinting. Covalent imprinting, pioneered by Wulff and co-workers,[5] uses functional monomers that could form reversible covalent bonds with template molecules (Figure 1.1A). For example, carboxylic ester

bonds for carboxylic acids,[6-7] boronate ester bonds for diols,[8] and Schiff's bases for amine or aldehyde.[9-10] After polymerization, the covalent bonds are cleaved with the templates removal and re-formed upon rebinding the templates. Due to the specificity of covalent bonds, covalent imprinting usually generates homogenous binding sites in MIPs.[11] Therefore, the covalent approach has the advantages of high affinity and stability. However, covalent imprinting suffers from difficulties in template removal and slow binding kinetics. Furthermore, the available templates for covalent imprinting are limited and usually needs prior modifications[11-12]

1.1.2.2 Non-covalent imprinting

In contrast, the non-covalent approach, first proposed by Mosbach group,[13-14] relies on weaker intermolecular interactions, such as hydrogen bonding, electrostatics, van der Waals forces, ion–pairing, π-π stacking and hydrophobic forces (Figure 1.1C and D).[11, 15] Many functional monomers are available to be used individually or combined for non-covalent imprinting (Figure 1.2). For example, methacrylic acid (MAA) is commonly used to form hydrogen bonds with template molecules. Acrylic acid (AA) and allylamine are usually used to form electrostatic interactions.[4] Furthermore, the functional monomers are mostly commercially available, and many others are being developed.[16] Therefore, with non-covalent imprinting, the available template molecules are vastly expanded, ranging from small molecules,[17] metal ions,[18] peptides, [19] proteins,[20] nucleic acids,[21] and even whole cells.[22-23] Due to the simplicity in operation, non-covalent imprinting has become the most widely used method for MIP preparation.[4, 24] In this thesis, MIPs were prepared based on non-covalent approach.

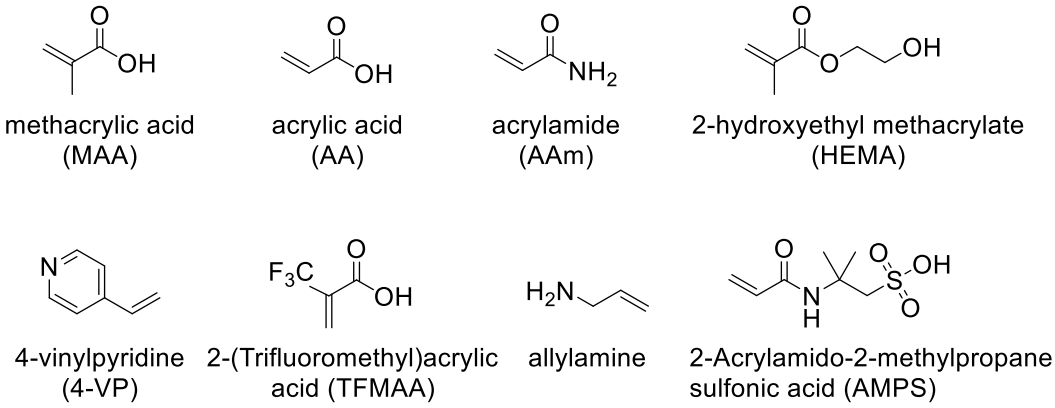

Figure 1.2 Chemical structures of some commonly used functional monomers for non-covalent imprinting.

1.1.2.3 Other approaches

Besides the two main methods, MIPs are also prepared by combining both covalent and non-covalent imprinting, called semi-covalent imprinting (Figure 1.1B). This approach was first proposed by Whitcombe and co-workers.[25-26] In their process, templates were coupled with a covalent bond for polymerization and the specific rebinding still relied on non-covalent interactions. The method attempts to combine the advantages of both the approaches and offers an intermediate alternative. Metal coordination is another imprinting approach by copolymerizing metal ions as functional monomers in MIPs for specific ligand recognition or exchanges.[9] This approach is widely used for ion sensors development and preconcentration studies.[27] Though effective, these approaches are either difficult in operation or can be only used for specific templates.

1.1.3 Preparation of MIPs

1.1.3.1 Free radical polymerization

MIPs can be prepared using various polymerization methods, including free radical polymerization, sol-gel polymerization [28] and controlled radical polymerization.[29] Among them, free radical polymerization (FRP) is the most commonly used method due to its simplicity, effectivity and compatibility with large numbers of monomers and various solvent systems.[30] In addition, FRP can be performed in mild reaction conditions, e.g., low temperature and atmospheric pressures, which are critical for the formation of interactions between functional monomers and templates during imprinting. A typical FRP follows three elementary steps: initiation, propagation and termination (Figure 1.3A).[31-32] In (1) initiation, the initiators, such as 2,2'-azobisisobutyronitrile (AIBN) or ammonium persulfate, generate free radicals (R*) that attack the double bonds of monomers and produce intermediate radicals. In (2) propagation, the main step of FRP, the produced radicals successively react with other monomers and grow to macromolecular polymer chains with high molecular weight. In (3) termination, the chain growth is terminated by either (a) disproportionation or (b) combination of two radical chain ends.

FRP usually generates linear polymer chains. To prepare MIPs, crosslinkers that have two or multiple polymerizable vinyl groups need to be introduced so that cross-linked polymers, such as bulk network gels, micro or nanogel particles, are produced. Crosslinkers play important roles in stabilizing the imprinted cavities and fixing the functional groups for templates rebinding. The type and amount of used crosslinkers could affect imprinting efficiency. The crosslinker ratio, i.e., the molar percentage of crosslinkers to total monomers, is also important. High crosslinker ratio results in more rigid polymer matrix but with lower swelling property and smaller pore size, which may prevent templates transportation.[33-34] Low crosslinker ratio (e.g., < 5%) leads to invalid imprinting due to less stabilized binding sites and cavities. In addition, the reactivity of crosslinkers needs to be similar as the functional monomers for an equivalent copolymerization.[30] Figure 1.3B

shows some commonly used crosslinkers for imprinting. Ethylene glycol dimethacrylate (EGDMA) and divinylbenzene (DVB) are widely used for imprinting in organic solvents and *N,N'*-methylenebisacrylamide (MBAA) is a common crosslinker for aqueous imprinting.

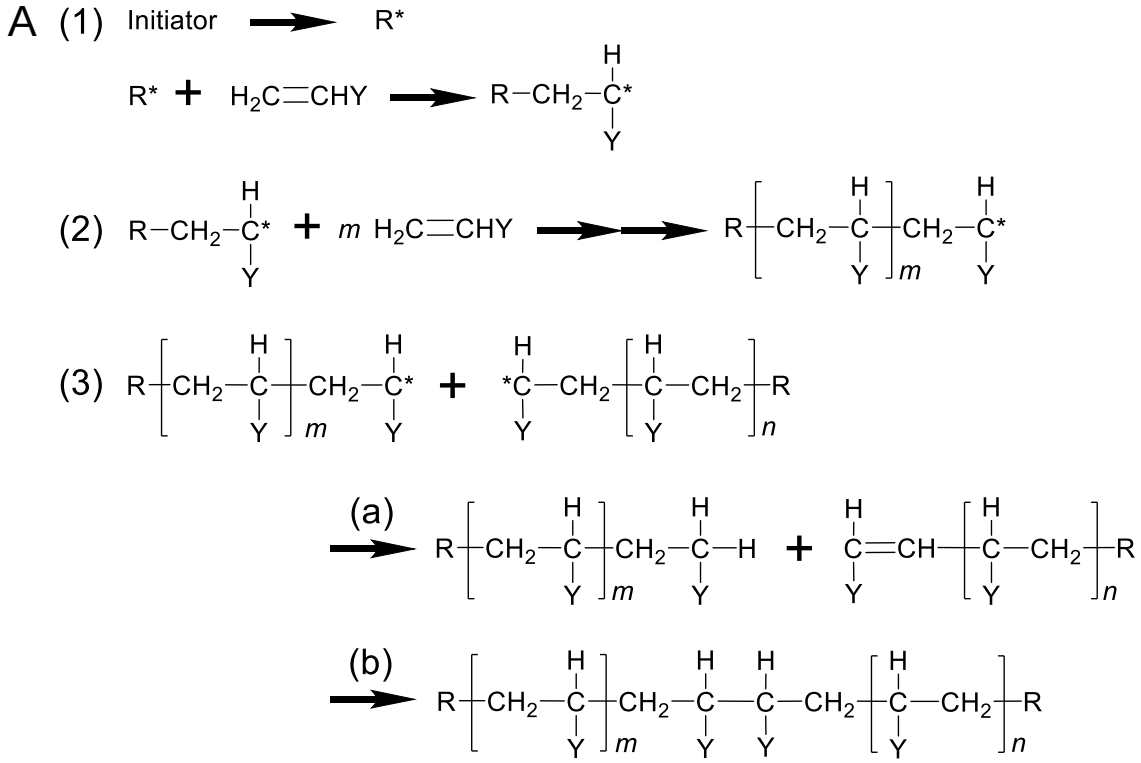

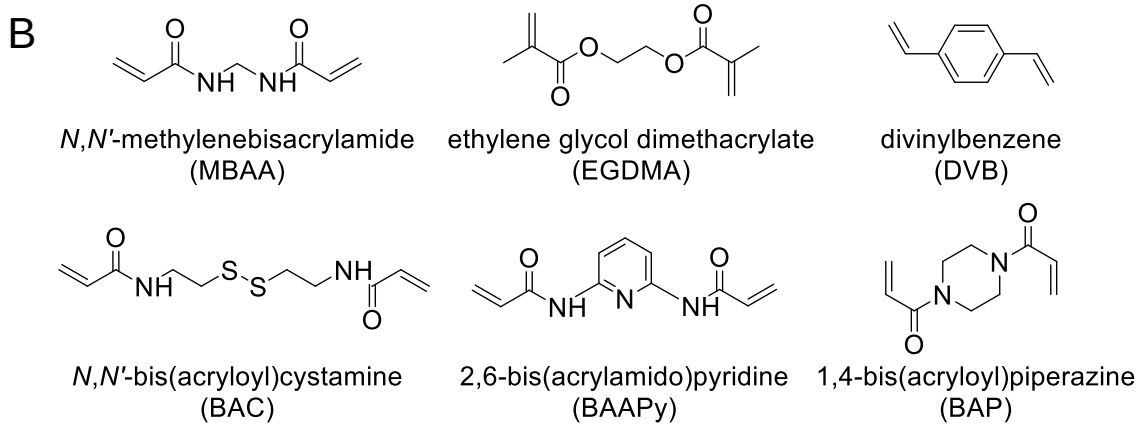

Figure 1.3 (A) Mechanism of free radical polymerization: (1) initiation, (2) propagation, (3) termination by either (a) disproportion or (b) combination. (B) Chemical structures of some commonly used crosslinkers for preparing MIPs.

1.1.3.2 Synthetic methods of MIPs

MIPs can be prepared using various synthetic methods. The most general and simplest method is bulk polymerization, where bulk MIP gels are polymerized in solutions followed by cutting or grinding the bulk gels into small particles with diameters usually more than hundreds of micrometers.[35-36] Although rapid and simple, the prepared MIPs are irregular and have low surface areas for target rebinding. Grinding or cutting also lead to the damage of the imprinted cavities. To overcome the limits, many methods that aim to prepare spherical MIPs with micro or nanometer sizes are developed, such as suspension polymerization,[37] emulsion polymerization,[38-39] solid-phase polymerization[37, 40] and precipitation polymerization. Among them, precipitation polymerization has been recognized as the most effective and simplest method for preparing MIP nanoparticles.

Precipitation polymerization is a type of heterogeneous polymerizations.[31] It begins from a homogeneous solution, in which the monomers, crosslinkers, templates and initiators were evenly mixed. The solution is highly diluted with an excess of solvent used (usually more than 95%, wt).[41] As polymerization proceeds, polymer particles grow individually and without overlapped by capturing free monomers or oligomers to react with the vinyl groups on their surface. As size becoming bigger and the crosslinking process preventing the polymer from freely mixing in the solvent, the polymer particles become insoluble and precipitate out of the system. The particle obtained by the method usually has a diameter ranges of 0.1 μm to 10 μm and with a

narrow distribution.[42] The first example of MIPs prepared using precipitation polymerization was reported by Ye and co-workers.[43] Estradiol and theophylline were imprinted as the templates and methacrylic acid was used as the functional monomer. The polymerization was performed in acetonitrile solution. The obtained MIP particles have a uniform size around 300 nm and showed a higher binding specificity than those prepared by the conventional bulk polymerization.

Since this seminal work, precipitation polymerization has been widely used to prepare a variety of targets imprinted MIP nanoparticles.[44] In addition, the method has also been developed as a facile synthetic approach for preparing functional MIPs, such as fluorescent,[45] thermo- or pH-responsible,[46-47] degradable and core shell MIPs by simply incorporating relevant monomers or crosslinkers or nanomaterials.[48] In 2008, an aqueous precipitation polymerization method was reported by the Shea group.[19, 49] A type of peptide imprinted MIP nanoparticles was prepared in diluted aqueous solutions by using acrylamide-based monomers in the presence of an ionic surfactant sodium dodecyl sulfate (SDS) at room temperature (Figure 1.4). The size of the prepared MIPs was measured close to proteins (diameter ≈40 nm), and the binding affinity was optimized by adjusting the monomer composition. In 2009, Haupt and co-workers developed this method and prepared a series of proteins or other small molecules imprinted MIP nanoparticles with no surfactant added through either photo- or enzyme-initialized polymerizations.[50-51] The MIP nanoparticles had a size range of 50-300 nm and were used as specific enzyme inhibitors. The aqueous precipitation polymerization has extended the range of available monomers and templates for imprinting that are only compatible in aqueous solutions. Many biopolymer-based functional monomers, such as antibodies and DNA, have been successfully used to prepare MIPs.

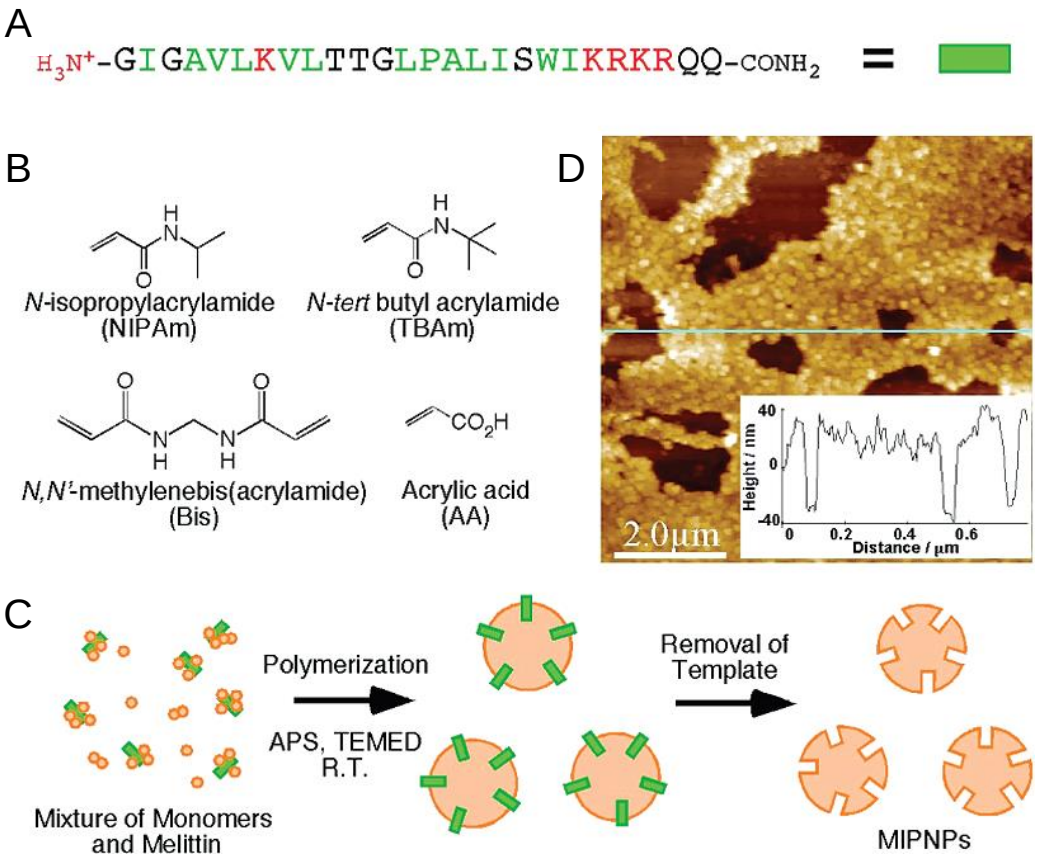

Figure 1.4 Preparation and characterization of the peptide imprinted MIP nanoparticles through aqueous precipitation polymerization. (A) Amino acid sequence of the target peptide, melittin. (B) Monomers and crosslinker used for MIP synthesis. (C) Schematic of the preparation of MIP nanoparticles. (D) Solution-phase AFM images of the prepared MIP nanoparticles. A height profile of the cross section (sky-blueline) is shown in the inset. Figures adapted with permission from ref ([19]). Copyright © 2010 American Chemical Society.

1.1.4 Biopolymers as monomers used in MIPs

Despite these achievements, MIPs still suffer from low affinity and specificity. The choice of functional monomers is often a trial-and-error process and ineffective. During the past decade, attempts have been made on using biomolecules such as antibody, peptides and aptamers as

monomers to solve the problem. In 2006, Miyata and co-workers used a vinyl conjugated antibody and lectin to imprint glycoproteins in bulk hydrogels.[52] Upon rebinding the target, the gels responded with a volume shrinkage, providing an interesting way to detect tumors. In 2011, Bowen *et al.*, introduced a short peptide (polymyxin) as a monomer for MIP,[53] although further optimization is likely needed to show its effect. The Scheller group incorporated a modified sugar ligand (mannose) and the imprint factor increased by 8-fold.[54] Antibodies and peptides still suffer from high cost and low stability, while mannose works only for limited targets. In this thesis, I used functional DNA to solve the problem.

1.2 Deoxyribonucleic acid (DNA)

1.2.1 The Structure of DNA

DNA is a linear biopolymer composed of two complementary strands forming a double helical structure. Besides being genetic carriers, DNA also has functional properties such as molecular recognition and catalysis due to its unique structure. The two DNA strands are antiparallel and coil each other around a common axis forming a right-hand twisted duplex (~ 20 Å in diameter, B-DNA) (Figure 1.5A). Each DNA strand is composed of nucleotides as monomeric units that are covalently linked by phosphodiester bonds resulting in an alternative sugar-phosphate backbone (Figure 1.5B). Each nucleotide contains a sugar (deoxyribose), a phosphate group and a nucleobase that has four different types named as adenine (A), guanine (G), cytosine (C) and thymine (T). The nucleobases can form hydrogen bonds according to the Watson–Crick base pairing rules (i.e., adenine with thymine and guanine with cytosine) contributing the formation of double-stranded DNA (Figure 1.5C).

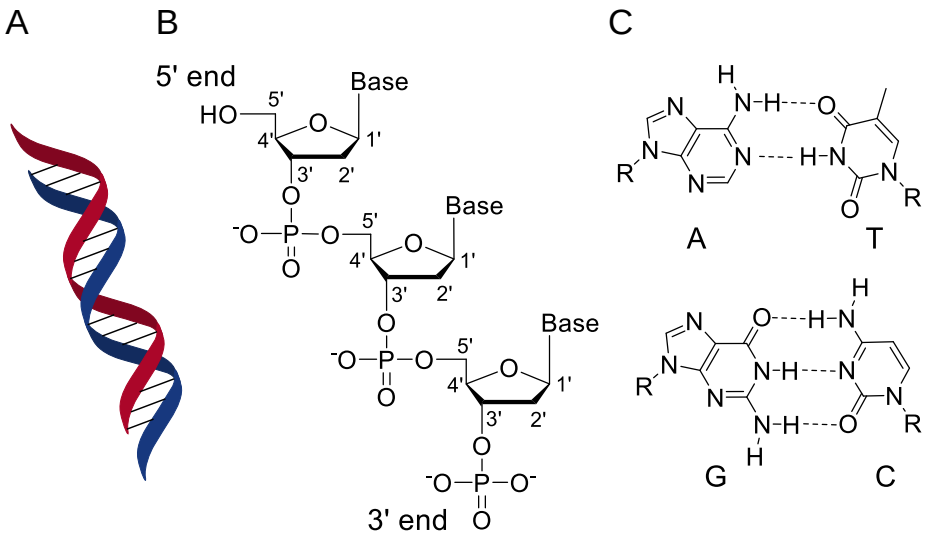

Figure 1.5 Chemical structures of DNA. (A) The double helix structure of double-stranded DNA. (B) A single-stranded DNA. (C) Four types of nucleobases forming Watson–Crick base pairs.

1.2.2 DNA aptamers

DNA aptamers are single-stranded DNAs that can specifically bind to target molecules.[55] They are usually isolated by in vitro selection called systematic evolution of ligands by exponential enrichment (SELEX) technique.[56] Through selections, DNA aptamers can bind to essentially any type of chemicals including ions, small molecules, proteins and surfaces.[57] Figure 1.6 shows examples of three DNA aptamers and their binding targets. In 1995, the Szostak group isolated the adenosine DNA aptamer that has a similar affinity to a few adenosine derivatives including AMP, cAMP and ATP, but it cannot bind other nucleosides such as guanosine (Figure 1.6A).[58] This aptamer has been extensively used as a model for biosensor development.[59] Another example is cocaine aptamers that are widely used for detecting cocaine with an affinity (K_d) around 0.4-10 μM.[60] Hg^{2+} aptamer is a thymine rich DNA sequence than can bind Hg^{2+} to form the T- Hg^{2+}-T base pairs, which has been widely used for developing Hg^{2+} biosensors.[61] The binding affinities of

aptamers to small molecules are often in the low micromolar range. Compared to antibodies, aptamers for small molecules have its advantages in terms of excellent binding affinity and specificity.

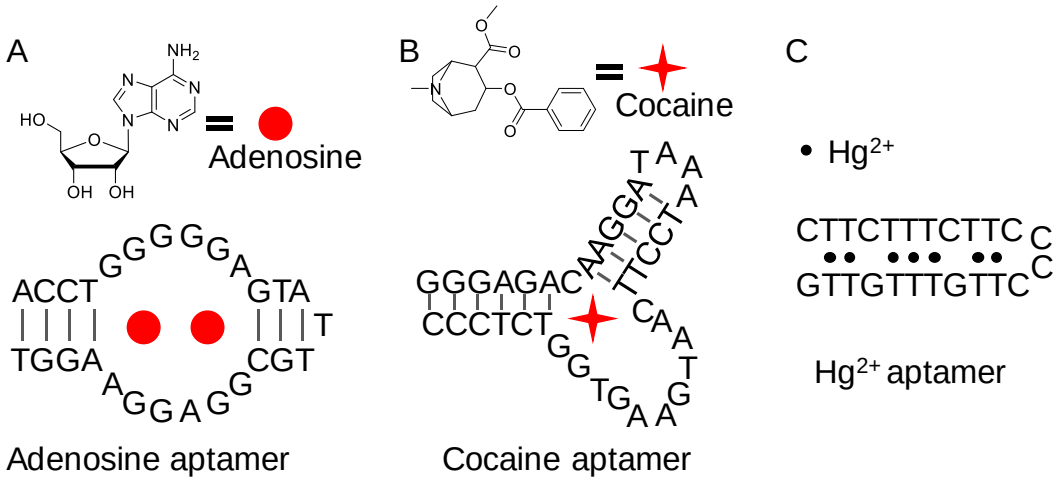

Figure 1.6 Examples of DNA aptamers for binding (A) adenosine or ATP, (B) cocaine and (C) Hg^{2+} ions.

1.2.3 DNAzymes

DNA with catalytic activities are known as DNAzymes.[62-63] Since 1994, many types of DNAzymes have been produced via in vitro selection. DNAzymes can catalyze many types of reactions such as RNA/DNA cleavage, ligation, phosphorylation.[64] One particularly interesting DNAzyme is G-quadruplex that has peroxidase-mimicking activity (Figure 1.7A).[65] It forms a G-quadruplex structure and requires a hemin as a cofactor (Figure 1.7B).[65-66] In the presence of H_2O_2, this DNAzyme can oxidize many substrates such as TMB, ABTS and Amplex Red.[67-68] These substrates are commonly used since they can produce a color change or fluorescent signal upon oxidation and thus are analytically useful. DNAzyme serves as an enzyme mimic that can catalyze enzyme-like reactions under near physiological conditions. Unlike proteins, DNAzyme is highly

stable, cost-effective and easy to modify. They have been widely tested for biosensor development, environmental remediation, and medicine.[69-70]

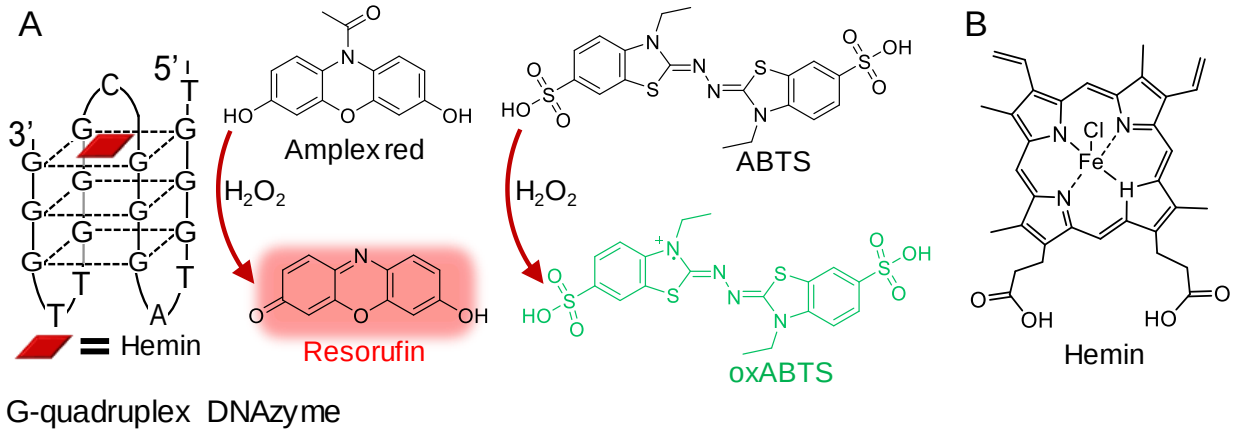

Figure 1.7 (A) The G-Quadruplex DNAzyme with peroxidase activity oxidizing Amplex red (AR) and ABTS in the presence of H_2O_2. The products of oxABTS has a green color (λ_{max} = 420 nm) and resorufin has fluorescence (Ex/Em: ~571/585 nm). (B) The structure of hemin.

1.2.4 DNA modification

The relative ease of synthesis allows for DNA to be modified with a variety of functional groups. One of the most performed modification is labelling fluorescent groups on DNA (e.g., FAM) for biosensor development.[71] To incorporate into polymer matrix, DNAs are commonly modified with arydite on the 5'-end. By adding an acrydite group, DNA can be easily incorporated into acrylic polymers (Figure 1.8A). This property allows DNA to be used as a macromonomer for MIP.

Besides acrydite modification, a nucleotide-modification approach was also reported by Poma and co-workers[72] They modified deoxyuridine with an alkene group on the C5 position to generate a polymerizable nucleotide (T*) (Figure 1.8B). The modified nucleotide was used to

substitute thymidines in the cocaine aptamer, and the aptamer hence contained multiple potential points to be polymerized in the polymer matrix (e.g., T*6 cocaine aptamer with six polymerizable points, Figure 1.8B). Although effective, this approach positioned polymerizable sites very close to the binding core of aptamers and may directly influence aptamer binding. In contrast, the acrydite approach allows a flexible conjugation of aptamers in gel matrix that does not have the concern, making it the most popular method of DNA conjugation.

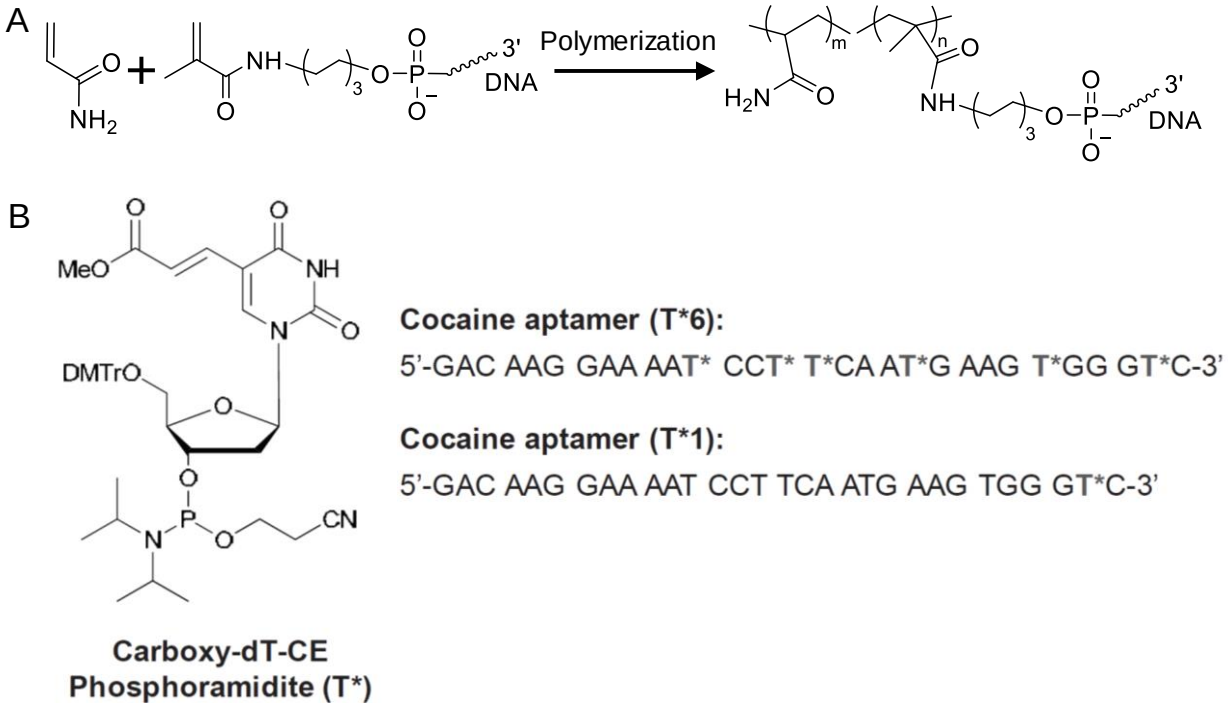

Figure 1.8 (A) Copolymerization of an acrydite-modified DNA into polyacrylamide. (B) The modified deoxyuridine (Carboxy-dT-CE Phosphoramidite, T*) and the cocaine aptamers with one (T*1) or six (T*6) thymidines substituted. Figure B adapted with permission from ref ([72]). Copyright © 2015, Wiley-VCH.

1.2.5 DNA used in molecular imprinting

Combining DNA with molecular imprinting has several advantages. First, DNA has specific molecular recognition functions, such as DNA aptamers, that may improve binding affinity of MIPs. Second, the polymer matrix of MIPs can in turn be part of a DNA sequence or structure. DNA sequences with low or no binding affinity might be rescued through imprinting. Third, DNA can be modified in many ways, such as with fluorophores, thiolate, biotin and acrydite, facilitating bioconjugation and signal transduction.[73-74]

The first example of using DNA in molecular imprinting was reported by the Spivak and co-workers who used two acrydite-modified aptamers that can bind to different positions on thrombin (Figure 1.9).[75] After removing the targets, the aptamer-MIPs worked as volume-responsive hydrogels for detecting thrombin and the detection limit was down to femtomolar. In addition to thrombin, the authors also tested another glycoprotein demonstrating the generality of this method. Besides, DNA aptamers functionalized MIPs were also used to detect virus,[76] antibiotics,[77] and gene sequences,[78] mainly based on electrochemical sensors with high sensitivities (detection limits down to femtomolar) and fast responses (10-60 min). However, the above studies all used full-length DNA aptamers for imprinting. Efforts need to be made to test aptamer fragments. Comparing to full-length aptamers, short fragments are more stable and have a lower cost. Moreover, MIPs might be able to rescue the binding affinity of aptamer fragments.

A limitation of MIPs for biosensor applications is the lack of optical signals. Molecular binding to MIPs is usually monitored using microgravimetric analysis, electrochemical, chromatography or isothermal titration calorimetry (ITC). Optical approaches such as convenient fluorescence or color based signaling methods are rarely reported. DNA may provide a solution to

this problem since DNA is programmable and easy to be modified. For example, DNA can be modified with fluorophore and quencher to generate fluorescent signals.[71] Many dyes can stain DNA and generate fluorescence, and they may also be used for signaling binding by MIPs. Li and coworkers removed a guanosine from a G-quadruplex sequence.[79] By using a specific dye thioflavin T (ThT), the structure served as a MIP sensor that specifically bound guanosine but not its nucleotides (e.g., GMP, GDP, GTP). In addition, DNA was also combined with luminescence/fluorescence nanoparticles and quantum dots signaling of MIP binding.[80 81]

In addition to DNA aptamers, imprinting using double-strand DNA was also reported.[82] By anchoring one of the strands as a monomer and removing the other strand as the target, the generated DNA-MIPs specifically recognized the target DNA strand through complementary binding. Furthermore, a single nucleotide (e.g., polymerizable 2'-deoxyuridine, dU) was also used as a monomer to imprint deoxyadenosine (dA).[83-84] The "tailored" MIP had specificity for the Watson-Crick paired dA, but not other nucleotides (e.g., dG or dC). So far, molecular imprinting with DNAzymes have not been studied yet. With the ability of engineering specific binding sites, imprinting could be applied to solve the problem of poor substrate selectivity of DNAzymes.

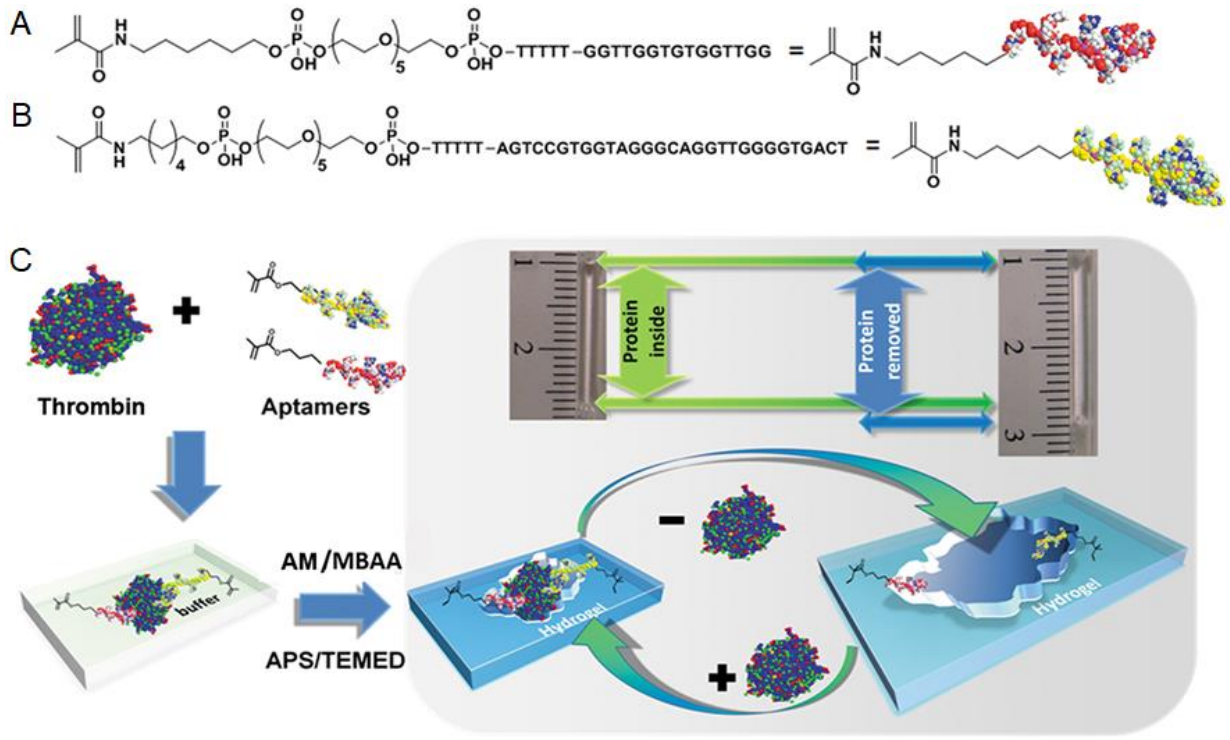

Figure 1.9. MIPs with two aptamers to create thrombin-responsive hydrogels. The sequence and modification of (A) aptamer 1, and (B) aptamer 2 modified with a polymerizable methacrylamide terminus. (C) Scheme of the imprinting process and visualization of the volume change of the imprinted hydrogel shown on the upper right corner. Figures adapted with permission from ref ([75]). Copyright © 2013 American Chemical Society.

1.3 Nanomaterials as enzyme mimics (nanozymes)

Nanozymes refer to inorganic nanomaterials that catalyze enzyme-like reactions under near physiological conditions.[85] Since the first nanomaterial (fullerene derivatives) was reported with activity of DNA cleavage in 1993,[86] remarkable progress has been made in nanozymes developments. In the past few decades, a diverse range of nanomaterials including metal oxides, gold nanoparticles and carbon-based nanomaterials were discovered with oxidase,[87-89] peroxidase,[90-92] catalase,[93] superoxide dismutase,[94] and laccase mimicking activities.[95] The term

"nanozymes" was firstly coined by Scrimin and co-workers to report the ribonuclease-like activity of thiol layer coated gold clusters.[96] In 2004, a surface "naked" gold nanoparticles were reported having glucose oxidase-mimicking activity by Rossi group.[88] Since then, the term was extended to nanomaterials with intrinsic enzyme-like activities.[85] Comparing to protein enzymes, nanozymes have advantages of much higher stability and lower cost, so that are very attractive for various applications ranging from biosensor development,[97-99] environmental remediation,[70, 100] to nanomedicine.[101] Among them, iron oxide nanoparticles, nanoceria and gold nanoparticles are the most widely used materials as enzyme mimics in a diverse range of applications.

1.3.1 Iron oxide as peroxidase mimics

The magnetite iron oxide nanoparticle (Fe_3O_4 NP) is well known of its magnetic property with a broad applications in separation, tumor targeting, and resonance imaging.[102-103] In 2007, Yan and co-workers unexpectedly discovered that the Fe_3O_4 NPs exhibited an intrinsic peroxidase-mimicking activity.[90] Peroxidases, such as the horseradish peroxidase (HRP), catalyze its substrate oxidation in the presence of hydrogen peroxide (H_2O_2). Yan and co-workers used three Fe_3O_4 NPs with different sizes (Figure 1.10A) to catalyze the substrate TMB oxidation to blue colored products (oxTMB) in the presence of H_2O_2 (Figure 1.10B). With only H_2O_2 or only Fe_3O_4 NPs, there were no reactions found demonstrating the peroxidase-like activity of the Fe_3O_4 NPs. The activity was then tested with other two substrates, DAB and OPD, which were also respectively oxidized to their colored products (Figure 1.10B, brown and red colored tubes). In addition, the activity of the Fe_3O_4 NPs was size-dependent where smaller size NPs had higher activities likely due to the larger surface area. The activity was also affected by pH and temperatures but were much more robust than the mimicked HRP when tested at a range of temperatures (4–90 °C) and pH (0–12). The Michaelis constants (K_m, represents the substrate binding affinity) suggested that

Fe_3O_4 NPs had a higher affinity than HRP for binding the substrate TMB, while lower affinity for binding H_2O_2. However, the catalytic rates (k_{cat}, represents the catalytic speed) by Fe_3O_4 NPs were demonstrated around 40 times higher than that by the HRP indicating the efficiency of the Fe_3O_4 NPs as catalyst.

Since this seminal work, Fe_3O_4 nanozymes have been widely used to detect H_2O_2 by using the chromogenic substrates (e.g., TMB and ABTS).[104-105] Because glucose oxidase (GOx) catalyzes the oxidation of glucose producing H_2O_2, Fe_3O_4 nanozymes were also commonly combined with GOx used for glucose detection. For example, Wei and Wang developed novel sensing platforms with Fe_3O_4 and GOx to detect glucose with a detection limit down to 30 μM.[105] Besides that, Fe_3O_4 nanozymes were also widely used for virus detection,[106] tumor treatment[107] and immunoassays.[108]

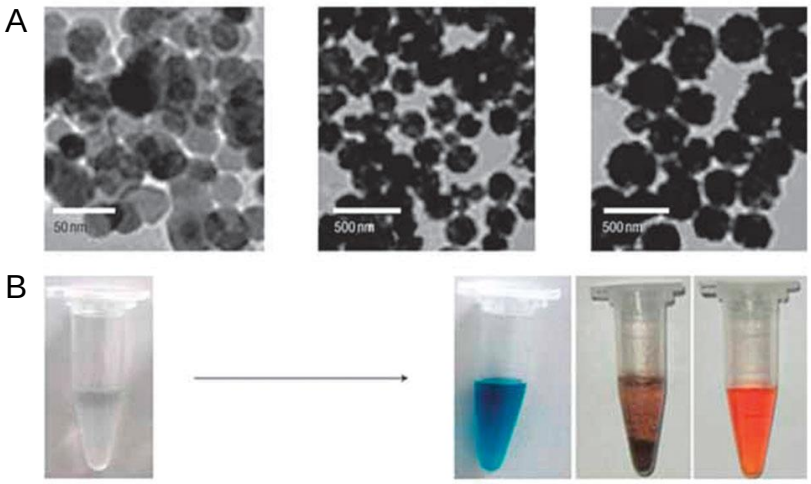

Figure 1.10. Fe_3O_4 NPs with peroxidase-mimicking activity. (A) TEM image of Fe_3O_4 NPs with different sizes. (B) Fe_3O_4 NPs catalyse the oxidations of various substrates (TMB, DAB and OPD) in the presence of H_2O_2 producing colored products. Figures reprinted with permission from ref ([90]). Copyright © 2007 Nature Publishing Group.

1.3.2 Nanoceria as oxidase mimics

Unlike peroxidase, oxidase catalyzes its substrate using oxygen as oxidant. Nanoceria is cerium oxide nanoparticles (CeO_2 NPs) usually with diameter ranges of 5-20 nm[109] Due to the presence of mixed valence of Ce^{3+}, Ce^{4+} and oxygen vacancies, CeO_2 has been widely used as catalysts in many applications.[110] In 2009, Asati and co-workers reported nanoceria having oxidase-like activity by using several colorimetric substrates, e.g., TMB, ABTS and DOPA (levodopa), tested in pH 4 without H_2O_2 added (Figure 1.11A).[87, 111] The activity of CeO_2 was highly dependent on the particle size, surface coating and pH conditions. In the best optimization, the catalytic rate (k_{cat}) of the CeO_2 NPs was 10 times faster than that of the HRP with H_2O_2 indicating its efficiency used as catalyst.

Nanoceria has been widely used in enzyme-linked immunosorbent assays (ELISA). Comparing with traditional ELISA using protein enzymes (e.g., HRP), CeO_2-based immunoassays have several advantages. First, CeO_2 is more stable and costs lower than protein enzymes. Second, CeO_2 catalyzes oxidation without H_2O_2 eliminating the toxic effect. Third, CeO_2 is capable of surface modification allowing targeting design. For example, Asati and co-workers conjugated folic acids on CeO_2 surface to specifically recognize tumor cells.[87] By using the colorimetric substrates (e.g., TMB), targeted cancer cells were detected with generating blue-colored products of TMB under the catalysis of CeO_2 (Figure 1.11B). However, CeO_2 cannot catalyze the oxidations of these substrates (TMB, ABTS and DOPA) at neutral pH (e.g.,pH at 6-7). In 2011, the author developed the method by using a fluorogenic substrate Ampliflu (also called Amplex red) that can be catalyzed in neutral pH to generate a fluorescent product resorufin (Figure 1.11C),[111] extending the CeO_2-based immunoassays performing in near physiological conditions.

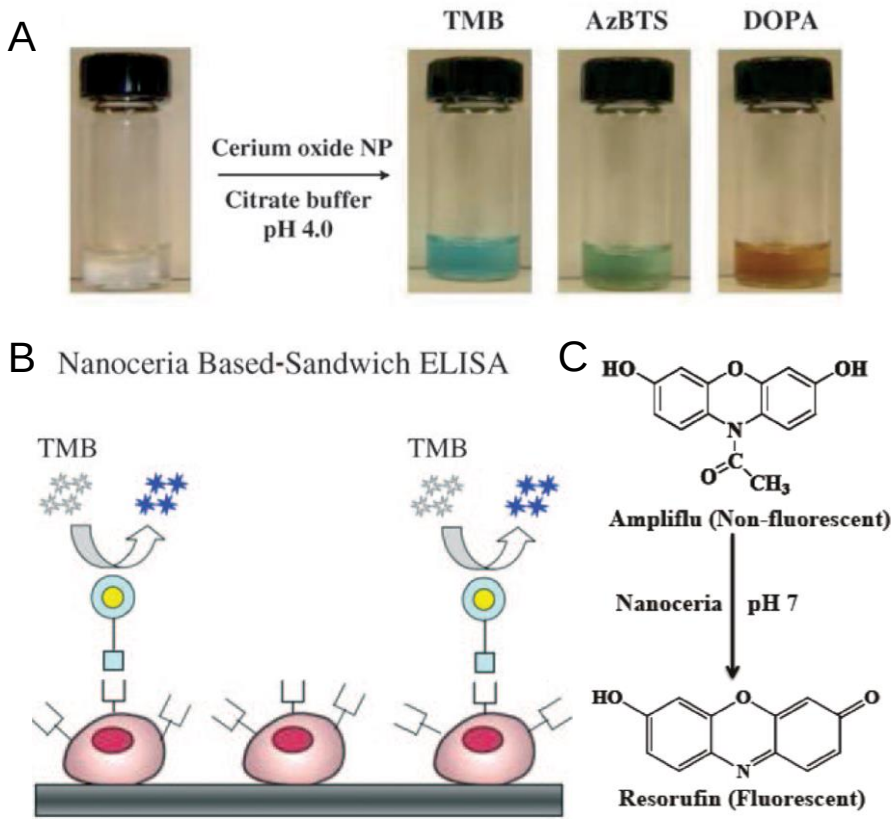

Figure 1.11. Nanoceria with oxidase-mimicking activity. (A) CeO_2 catalyzes oxidation of various substrates in pH 4. (B) A schematic of using nanoceria in immunoassays. (C) Nanoceria catalyzed the oxidation of Ampliflu (also called Amplex red) to fluorescent product resorufin in pH 7. Figures A and B adapted with permission from ref ([87]). Copyright © 2009 Wiley-VCH Verlag GmbH & Co. KGaA, Weinheim. Figure C reprinted with permission from ref ([111]). Copyright © 2011 American Chemical Society.

1.3.3 Gold nanoparticles as oxidase mimics

Unlike Fe_3O_4 and CeO_2 are metal oxides based nanozymes, gold nanoparticles (AuNPs) are metal nanomaterials with enzyme-mimicking activity. In 2004, Rossi and co-workers reported the AuNPs catalyzed the oxidation of glucose in aerobic condition (Figure 1.12A).[88] The reaction was similar to the glucose oxidations catalyzed by GOx indicating the oxidase-like activity. While

gold processing mimetic activity, other metal nanoparticles such as Ag, Pd and Pt were not found active (Figure 1.12B). The following mechanism studies suggested that AuNPs catalysis follows the Eley-Rideal model that glucose first adsorbed on the surface of AuNPs and then reacted with oxygen in the solution producing gluconic acids and H_2O_2.[88, 112]

Although possess activities, these nanozymes suffer from the problem of no substrate selectivity for reactions. Any type of substrates could be catalyzed upon diffusing on their surface. Previous studies mainly focused on the activity improvement of theses nanozyme, the substrate specificity, a feature of most natural enzymes, had rarely been addressed. Molecular imprinting might be an ideal method to solve the problem (studied in the Chapter 5).

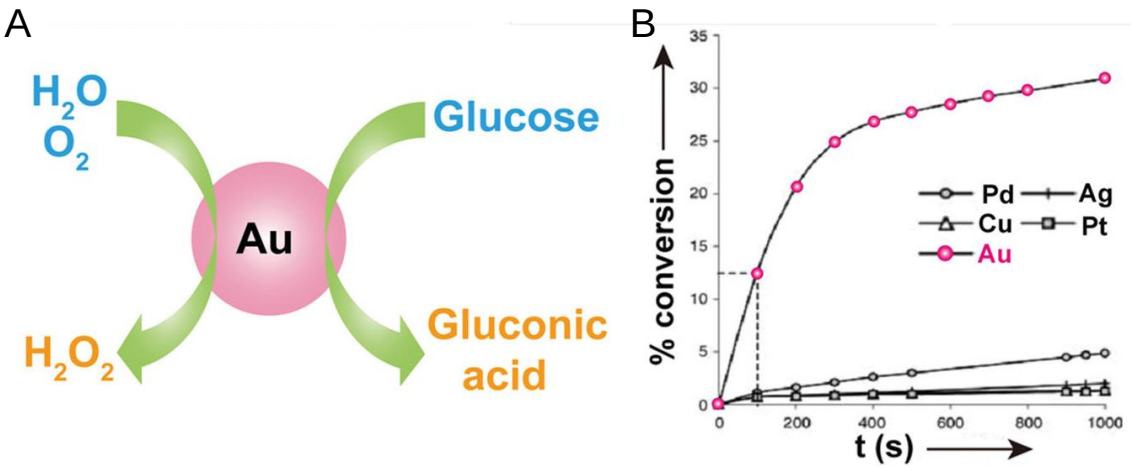

Figure 1.12 AuNPs with oxidase-like activity. (A) AuNPs catalyze glucose oxidation. (B) The GOx-like catalytic activity of different metal particles. Figures adapted with permission from ref ([112]). Copyright © 2014 WILEY-VCH Verlag GmbH & Co. KGaA, Weinheim.

1.4 Research goals and thesis outline

The main goals of this thesis include improving the binding affinity, enabling binding signaling of MIP by using DNA aptamer fragments with modifications. By preparing molecular imprinted nanogels on enzyme mimics, including both DNAzymes and nanozymes, to solve the problem of low substrate selectivity. The effect of imprinting on the activity and stability of the enzyme mimics and the catalytic mechanism were also the research goals of the thesis. To achieve these goals, the thesis was outlined as the following sections.

The Chapter 2 describes the study of using DNA aptamer fragments in MIPs. The adenosine aptamer were split to two fragments and copolymerized into MIPs with acrydite modification. The two fragments were labeled with fluorophore and quencher for fluorescent assays to determine the binding affinity. Next, single aptamer fragments were used in the MIP and the binding affinity were tested using ITC. To challenge the sequence limits, the single aptamer fragment was further shorten to only 6 base pairs, and its affinity was compared with free aptamer fragments, MIP nanogels and NIP nanogels to determine the affinity improvement.

The Chapter 3 describes the work of molecular imprinting on DNAzymes. G-quadruplex DNAzymes was co-imprinted with the substrate TMB or ABTS into nanogels. The gels were characterized by DLS and TME. The catalytic activity and substrate specificity of the MIP gels were determined by oxidizing the two different substrates and analyzed by Michaelis–Menten model (k_{cat} and K_m). In addition, the stability of the DNAzyme incorporated nanogels and recycle tests were also measured.

The Chapter 4 followed the work in the Chapter 3 aimed at intracellular catalysis. The imprinted DNAzyme nanogels were prepared using Amplex red (AR) as a template. The substrate

selectivity of the MIP nanogels was measured by using four different substrates (TMB, ABTS, dopamine and AR). The imprinted nanogels were internalized by HeLa cells and the intracellular catalysis were measured by using confocal microscopy.

The Chapter 5 describes the study of molecular imprinting on nanozymes. Three commonly used nanozymes, Fe_3O_4 NPs, CeO_2 and gold nanoparticles, were polymerized into nanogels with imprinted certain substrates as templates, e.g., TMB, ABTS and dopamine. The nanogels were characterized by SEM, EDX ICP-MS to determine the incorporation of the nanozymes. The catalytic activity and specificity of the MIP nanogels were determined based on the Michaelis–Menten kinetics using different substrates for oxidation. The specificity improvement was determined using Michaelis constant k_{cat}/K_m in comparison with the free nanozmes and non-imprinted nanogels. ITC binding tests were also performed to confirm the specificity improvements.

The Chapter 6 followed the work of the Chapter 4 and 5 aimed at understanding the catalytic mechanism of imprinted enzyme mimics. The study was divided into three steps: substrate adsorption, reaction and product release. Each step was studied individually. The adsorption capability of MIP, NIP nanogels and free Fe_3O_4 NPs were determined by UV-vis spectrometry. The local substrate concentration was calculated based on the gel volume and substrate content. The activation energy (E_a) was measured to probe reaction step. The catalytic kinetics of nanogels imprinted with the product resorufin and substrate AR were compared based on oxidation kinetics and ITC binding tests to probe the transportation efficiency in the gel matrix.

The Chapter 7 concludes the results in the Chapter 2-6 and provides the future plan and original contributions of the thesis.

Chapter 2 Molecularly Imprinted Polymers with DNA Aptamer Fragments as Macromonomers

2.1 Introduction

Molecular recognition is critically important in biology, biomaterials science, analytical chemistry, and medicine. Biologically derived molecules, for example antibodies and aptamers, are general platforms for molecular recognition.[113] Though possessing high binding affinity and specificity, they are expensive, unstable and prone to denaturation. MIPs are attractive alternatives. Compared to antibodies and aptamers, MIPs can be prepared in much larger quantities at a lower cost with higher stability.[114] As a result, MIPs have been widely applied in analytical chemistry, separation, and environmental remediation.[48] MIPs are usually prepared with various types of monomers, mostly of which are acrylic and silane based. However, the binding affinity of most MIPs needs to further improve. In addition, it is difficult to produce a detectable signal for MIP binding.[115]

We are interested in exploring the feasibility of combining biopolymers and MIPs by introducing a fragment of biological ligands as macromonomers in MIPs. DNA aptamers are oligonucleotides that selectively bind to target molecules. Incorporation of aptamers in MIPs have been reported for thrombin,[75] antigen[116] and cocaine bindings[72] via either terminal acrydite modification or nucleotides modification approaches.

In all the previous cases, however, full-length aptamers were used. Our idea is to use aptamer fragments as macromonomers to improve MIPs, and then gradually shorten the aptamer fragment length. Shorter fragments allow a lower cost and better stability. We hypothesize that

good binding might still be achieved with the help of the MIP matrix. For easy handling and good template accessibility, MIP hydrogel nanoparticles (or nanogels) were prepared in this study.

2.2 Materials and methods

2.2.1 Chemicals

All the DNA samples were purchased from Eurofins (Huntsville, AL). For the DNA used for polymerizations, acrydite groups were modified on the 5' end. For fluorescence signaling, DNA were modified with carboxyfluorescein (FAM) and black hole quencher 1 groups. Acrylamide (AAm), *N*-isopropylacrylamide (NIPAAm), methylene bis(acrylamide) (MBAAm), *N*-[3-(dimethylamino)propyl]methacrylamide (DMPA) and sodium dodecyl sulfate (SDS) were from Sigma-Aldrich. Ammonium persulfate (APS) and *N*,*N*,*N*',*N*'-tetramethylethylenediamine (TEMED) were from VWR. Sodium chloride, magnesium chloride, 4-(2-hydroxyethyl)-1-piperazineethanesulfonic acid (HEPES), adenosine, cytidine and other nucleosides were from Mandel Scientific (Guelph, Ontario, Canada). Mill-Q water was used to prepare all the buffers and solutions. All other reagents and solvents were of analytical grade and were used as received.

2.2.2 Preparation of nanogels

All the nanogels were prepared using aqueous precipitation polymerization method.[47, 49] Same concentrations of monomers, cross-linker, and initiator were used to achieve maximal consistency. For the nanogels containing FAM (or quencher)-labeled DNA aptamers, AAm (2.9 mg, 42 μmol), NIPAAm (4.6 mg, 42 μmol), aptamer fragments (20 μM each), and the template molecule adenosine or cytidine (1 mM) were dissolved in buffer A (50 mM HEPES, pH 7.6, 100 mM NaCl, 5 mM $MgCl_2$). The mixture was incubated for 30 min with slow stirring at 25 °C to form binding complexes. Then, the crosslinker MBAAm (2.4 mg, 16 μmol), DMPA (0.5 μL) and

surfactant SDS (0.8 mg) were added. After purging the mixture with N_2 for 1 h, polymerization was initiated by adding APS (0.6 mg) and TEMED (0.3 μL). The final reaction volume was standardized to 1 mL in a 1.7 mL plastic microtube. The reaction was continued for 4 h at 25 °C under a N_2 atmosphere and the solution was gently shaken several times after initiation. The resultant imprinted nanogels were collected by centrifugation at 15 000 rpm for 10 min and then washed extensively using Milli-Q water until completely removed the unreacted monomers and templates (confirmed by UV−vis spectrometry).

The collected nanogels were freeze-dried for 24 h and weighed to measure the reaction yield. The nanogels prepared for the ITC tests were prepared using the same method except that 70 μM of aptamer fragments were used. A higher DNA concentration was used for ITC because this technique is less-sensitive compared to fluorescence. Nonimprinted nanogels (NIPs) were also prepared and washed in the same way except that no template was added during polymerization. The concentration of the template adenosine was chosen to be 1 mM to avoid stacking of adenosine forming multimers at high concentrations (Adenosine has relatively low solubility).

2.2.3 Dynamic light scattering (DLS)

The hydrodynamic size and distribution of the nanogels were measured by DLS (Zetasizer Nano ZS90, Malvern). Each nanogel sample (50 μg/mL) was dispersed in the buffer A, and the temperature was maintained at 25 °C during measurements.

2.2.4 Coupling efficiency

The coupling efficiencies of the FAM-labeled aptamer incorporated in nanogels were determined by using fluorescence spectroscopy (excitation at 485 nm, emission at 525 nm). For other nanogels, the coupling efficiencies were determined by UV−vis absorbance at 260 nm. After

preparation, the nanogel samples were purified by centrifugation (15000 rpm, 10 min). The supernatant and a standard solution (containing the same initial aptamer concentration during preparation) were diluted to the same volume in buffer A. Their fluorescence emission or absorbance was measured to calculate coupling efficiency.

2.2.5 Fluorescence assays

The fluorescence intensity of FAM-labelled free aptamers and aptamer-incorporated nanogels were measured using a Varian Eclipse fluorescence spectrometer (Agilent Technologies, Santa Clara, CA) with excitation at 485 nm and emission at 525 nm at 25 °C. The fluorescence kinetics were measured by using a microplate reader (Infinite F200Pro, Tecan).

2.2.6 Isothermal titration calorimetry (ITC)

ITC was performed using a VP-ITC Microcalorimeter instrument (MicroCal). Prior to each measurement, each solution and suspension were degassed to avoid air bubbles. The sample of aptamer fragments (20 μM) or nanogel sample in buffer A was loaded in a 1.45 mL ITC cell at 25 °C. Adenosine (281 μL, 3 mM) in the same buffer was titrated into the cell through a syringe (10 μL each time, except for the first injection of 2 μL). The enthalpy (ΔH) and binding constant (K_a) were obtained through fitting the titration curves to a one-site binding model using the Origin software. The K_d values were calculated from $1/K_a$ and $\Delta G = -RT \ln (K_a)$, where R is the gas constant. ΔS was calculated from $\Delta G = \Delta H - T\Delta S$.

2.3 Results and discussion

2.3.1 Aptamer split and modification

The adenosine DNA aptamer has been extensively studied as a model for biosensor development.[58] The full-length aptamer contains only 27 nucleotides (Figure 2.1A). It can be split into two halves (Figure 2.1B, F1 and F2), and binding still occurs when both fragments are present.[117] To be co-polymerized into MIPs, each aptamer fragment was labeled on the 5′ end with an acrydite group. To measure binding, one fragment was labeled with a dark quencher on its 3′ end (Q-F1), and the other with an internal FAM (F-F2, Figure 2.1B). Upon forming the aptamer complex, the fluorescence is expected to quench (Figure 2.1C). Two small molecule monomers, AAm and NIPAAm, were included to form the gel matrix, and MBAAm was used as a crosslinker.

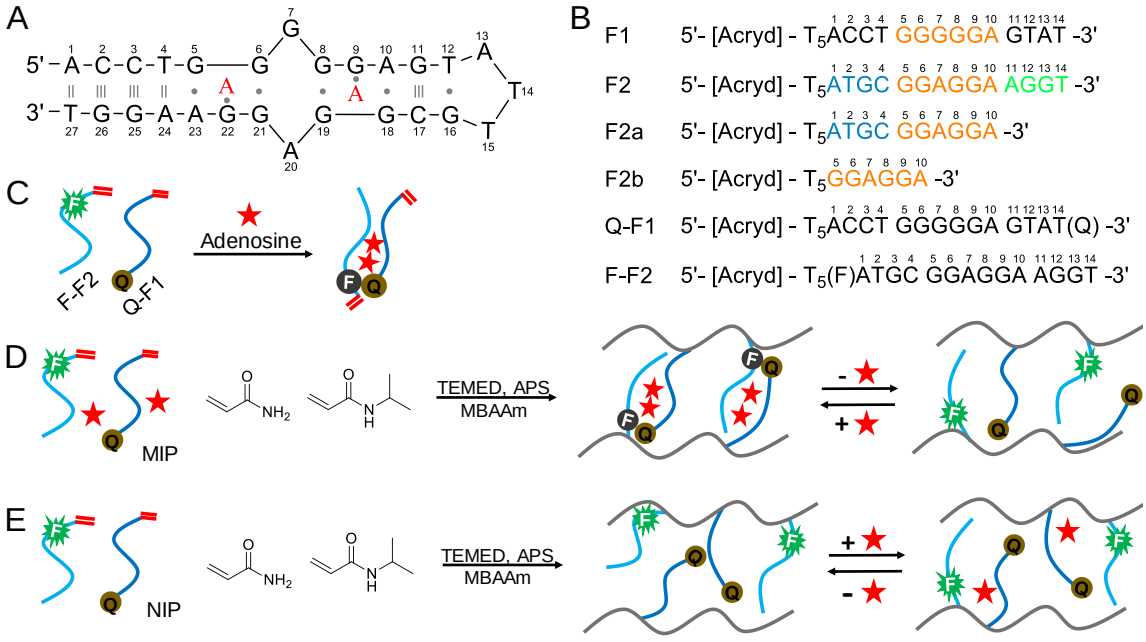

Figure 2.1 (A) The secondary structure of the full-length adenosine aptamer binding two adenosine molecules (the 'A' in red). (B) The sequences of the adenosine aptamer fragments used

in this work named F1, F2, F2a, F2b, Q-F1 (Black Hole Quencher 1 (Q) labeled) and F-F2 (carboxyfluorescein, FAM (F) labeled), respectively, all modified with a 5'-acrydite. (C) Schematic presentation of the two adenosine aptamer fragments (F-F2 and Q-F1) binding adenosine and fluorescence quenching. Schematic presentation of (D) adenosine imprinted (MIP) and (E) non-imprinted (NIP) MIPs with the aptamer fragments. TEMED and APS are used to initiate the polymerization reaction. MBAAm is the crosslinker.

2.3.2 Molecular imprinting with both aptamer fragments

We first tested the effect of molecular imprinting with the both half aptamer fragments were copolymerized. To compare the imprinting effect, three types of nanogels were prepared by precipitation polymerization: one in the absence of any target (named NIP), one with 1 mM cytidine (C-MIP), and the last one with 1 mM adenosine (A-MIP). We reason that the aptamer binding complex might form in the presence of adenosine, positioning the two aptamer halves forming a high affinity cavity (Figure 2.1D). Without adenosine, polymerization is random and the resulting gel particles may not bind adenosine (Figure 2.1E). A similar outcome is expected when cytidine is added into the pre-polymerization mixture as it does not form complex with the aptamer monomers. Among the various nucleotides, we only chose cytidine here as a negative control since this adenosine aptamer is a well-studied model system. It has a similarly high affinity for adenosine, AMP, and ATP, but has no binding when the base part is changed to C, T, or G.[58]

All the nanogels used for the tests have a similar size of 200 ±36 nm as determined by DLS and can be easily dispersed in water (Figure 2.2E). The DNA coupling efficiency was determined to be 30.2 ± 2.6 % by UV-vis spectroscopy and fluorescence. The low coupling efficiency maybe attributed to DNA damage by radicals.[118-119] After washing away the template

molecules and free monomers, the three nanogels were re-dispersed in the buffer A with the same final aptamer concentration (128 nM, each fragment, confirmed from UV-vis spectroscopy and fluorescence).

We next measured the fluorescence quenching. Upon adding 1 mM adenosine, the fluorescence intensity at 520 nm of the A-MIP gel decreased significantly (Figure 2.2C), suggesting the two aptamer halves reassembled. In comparison, the signal from the NIP (Figure 2.2A) and C-MIP (Figure 2.2B) only dropped slightly indicating the lack of aptamer binding. As a control, none of these samples were quenched by 1 mM cytidine. This study indicates that imprinting during gel formation is critical for re-binding.

To quantitatively understand binding, relative fluorescence quenching (F/F_0) of these gels were measured as a function of adenosine concentration (Figure 2.2D). With increasing adenosine concentration, the signal from the NIP and C-MIP samples decreased slightly reaching a final ratio around 0.80, while a final ratio of 0.46 was achieved for the A-MIP. We also compared the same concentration of the free split aptamers without any gel (Figure 2.2D, blue trace). Interestingly, it only decayed to a final ratio of 0.66. The dissociation constant (K_d) of the free aptamer fragments (1.6 mM) is four times higher than that for the A-MIP gels (0.4 mM). Therefore, with imprinting, the split aptamer fragments are positioned at a more favorable binding configuration than the free aptamers in solution.[120] This improved binding is also related to an increased effective concentration of the aptamers by linking them to the gel matrix. In this regard, the gel matrix helped aptamer binding.

From this initial test, we confirmed that imprinting indeed took place during preparation of these gels. Without adenosine, the two aptamer fragments were randomly distributed during

polymerization. Confined by the crosslinked gel network, they may not reach each other in the presence of adenosine (Figure 2.1E). The presence of fluorescence signal in this method allows for convenient detection of adenosine, which is a significant advantage brought by DNA. Many fluorescent sensors were reported using this aptamer for adenosine detection and the limit of detection was usually down to micromolar concentrations.[121-124] The aptamer-MIPs may serve as a better type of sensors to this aim because of the improved binding affinity by imprinting and reusability of the nanogels.

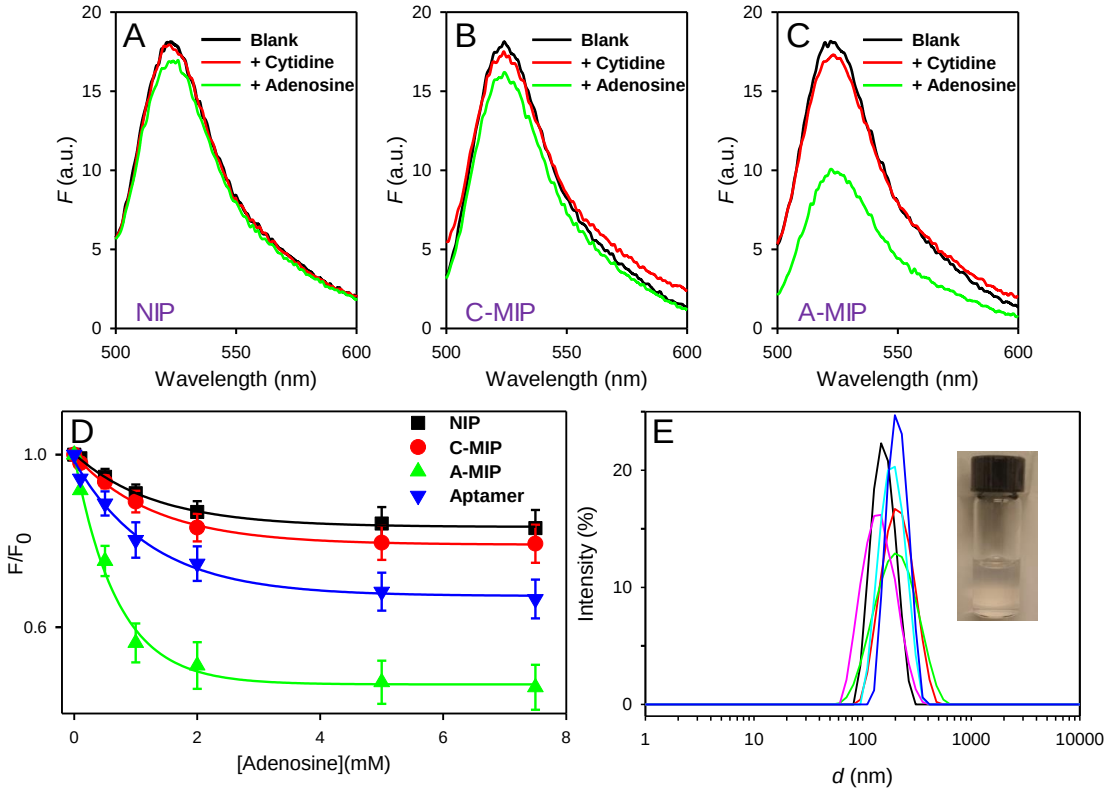

Figure 2.2 Fluorescence spectra for the (A) NIP, (B) C-MIP and (C) A-MIP nanogels before and after adding 1 mM cytidine or adenosine. (D) Fluorescence quenching of the three nanogels and the free split aptamer (128 nM, each fragment) at 520 nm as a function of adenosine concentration. For all the experiments, the nanogels (~0.13 mg/mL) all contained a final of 128 nM aptamers in buffer A. (E) The particle size distributions of used nanogels by DLS: MIP (Black), A-MIP (Red),

F2-MIP (Green), F1F2-MIP (Blue), F2a-MIP (Pink) and F2b-MIP (Cyan) (50 μg/mL nanogels in the buffer A for the measurements). Other used nanogels have average hydrodynamic size between 170 and 210 nm. Inset: A photograph of the F1F2-MIP nanogel dispersed in the buffer A.

2.3.3 Probing the initial aptamer binding complex

Because the two aptamer halves can partially base-pair with each other (Figure 2.1A and B), it is possible that a fraction of the aptamers is already hybridized in the nanogels in the absence of adenosine. For this population, further addition of adenosine may not induce further fluorescence quenching. Therefore, it is important to measure the fraction of the initial binding complex in the gels. For this purpose, we designed an experiment as shown in Figure 2.3E. The complementary DNAs (cDNAs) of the two aptamer fragments were added to the gels to disrupt the aptamer binding structures and to increase fluorescence. For the A-MIP sample without adenosine, the cDNAs led to a slight fluorescence increase of ~10% (Figure 2.3A); for the NIP gel, the increase was only ~5% (Figure 2.3B). The free DNA aptamer fragments (no gel) after binding with its cDNA also has a slight fluorescence of 3.3% (Figure 2.3C). Based on this, we conclude that ~2% initial binding complexes formed for the NIP, while ~7% of the aptamers were in the complex form for the A-MIP in the absence of adenosine. This is reasonable since the aptamer fragments in the A-MIP were closer to each other due to imprinting. As a positive control, we add adenosine to the A-MIP gel first. We then observed a large fluorescence increase of ~80% after adding the cDNAs (Figure 2.3D). Therefore, most of aptamer fragments did not form the binding complex in the absence of adenosine. This is important for the analytical applications to achieve a large signal change.

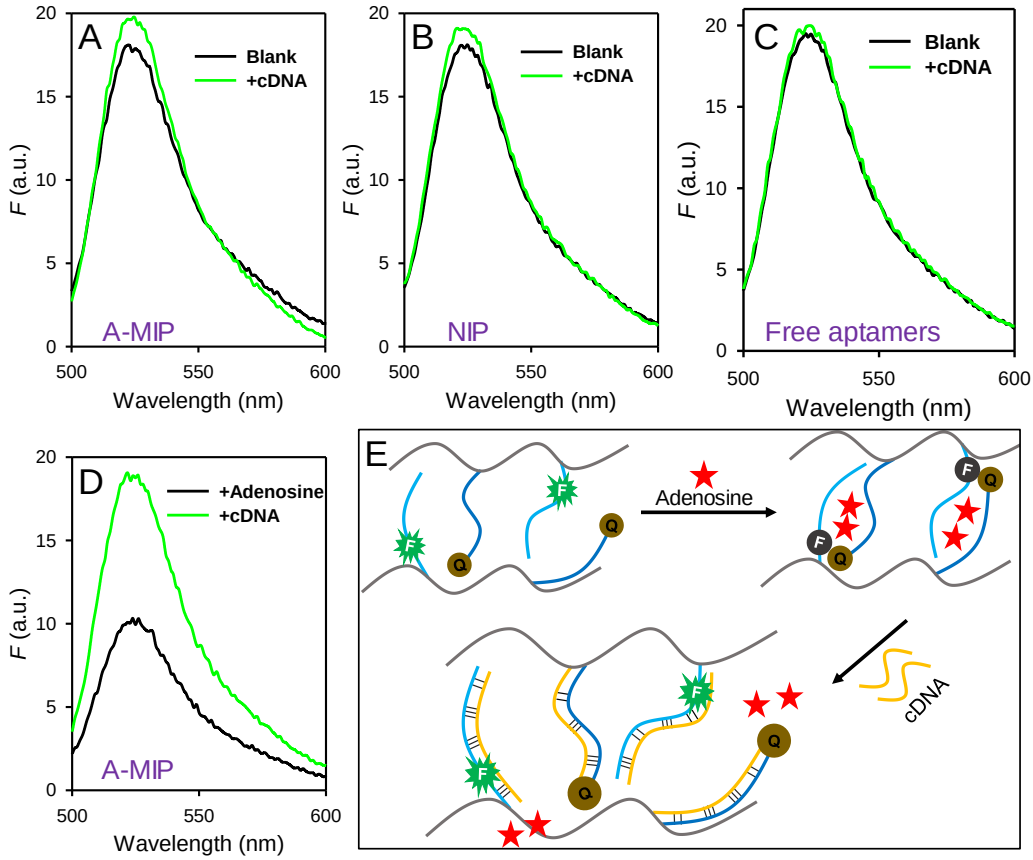

Figure 2.3 Fluorescence spectra for (A) the A-MIP, (B) the NIP nanogels and (C) the free aptamer fragments after adding the two cDNAs (128 nM each) of the two aptamer fragments. (D) Fluorescence spectra of the A-MIP gels with 1 mM adenosine and then adding the cDNAs. (E) Schematic presentation of using the cDNAs to open the aptamer binding complex.

2.3.4 The binding tests of free individual aptamer fragments

With both aptamer halves, it is not surprising that the A-MIP gel binds adenosine. A more challenging question is to take a single fragment that cannot bind adenosine for imprinting. Before imprinting into gels, we first tested the binding abilities of the free aptamer fragments. Because this design makes fluorescence-based assay difficult, we employed non-labeled DNA and

characterized binding using ITC. The two fragments are named F1 and F2, respectively (See the sequences in the Figure 2.1B).

When adenosine was titrated into either aptamer fragment (F1 or F2, no gels), barely any heat was detected (Figure 2.4A and B), suggesting no binding by the individual fragments. On the other hand, a strong binding was detected for the sample containing both fragments (F1 + F2, no gels, Figure 2.4C). The thermodynamic values of the above experiments were calculated (Table 2.1). The enthalpy change (ΔH) for each aptamer fragment binding adenosine was at least 18-fold lower than that when both fragments were used. Since the heat was very small, we cannot obtain an accurate fitting for other thermodynamic values. Based on the NMR structure of the aptamer,[125] both halves contribute indispensable purine bases (G9 and G22) and base stacking to stabilize the G·A pair for binding the target adenosine (see the aptamer structure in the Figure 2.1A). It is not surprising that each fragment alone failed to bind. The both fragments (F1+F2) had a lower binding affinity than that of the original aptamer (full length adenosine aptamer without split, Figure 2.4D and Table 2.1). The both fragments (F1+F2) also bond more targets than by the original aptamer likely due to the split conformation (the binding site *N*, Table 2.1).

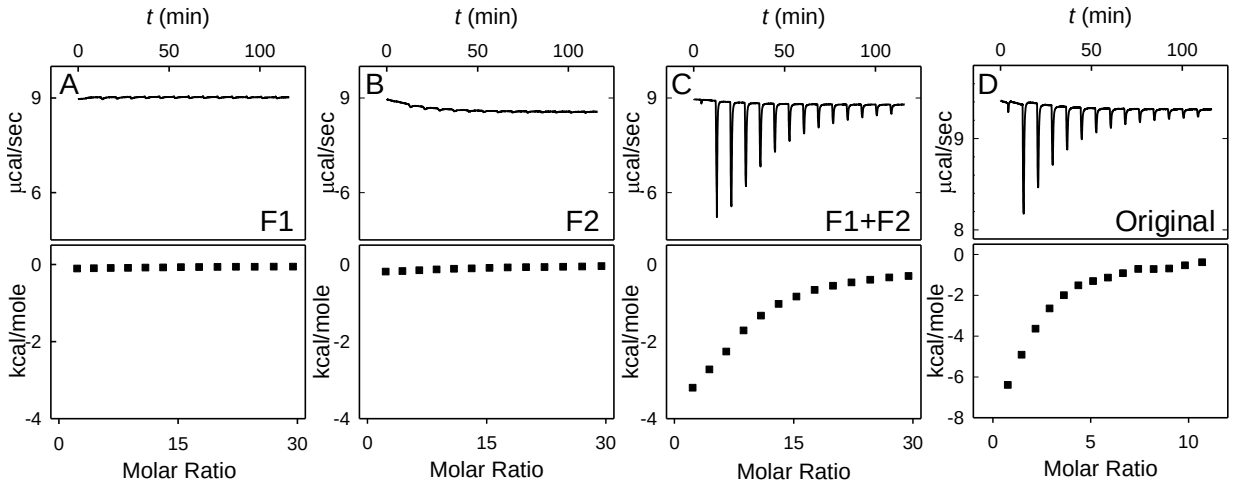

Figure 2.4 ITC titration curves obtained at 298 K (25°C) for binding between 20 µM of (A) F1, (B) F2 and (C) F1+F2 aptamer fragments with 3 mM adenosine in the buffer A. (D) The titration curve between 10 µM of the original aptamer (full length adenosine aptamer without split) binding with 0.5 mM adenosine in the buffer A. The original titration traces (top) and the integrated heat (bottom) of each reaction are shown.

Table 2.1. Thermodynamic data for adenosine titrating to the aptamers by ITC.[a]

Aptamers	***N***	K_a ($\times 10^4$ M^{-1})	K_d (µM)	***ΔG*** (kcal mol^{-1})	***ΔH*** (kcal mol^{-1})	***ΔS*** (cal $K^{-1}mol^{-1}$)
F1	-[b]	-	-	-	-0.11 ±0.04	-
F2	-	-	-	-	-0.18 ±0.07	-
F1+F2	4.6 ± 1.3	3.05 ± 0.22	32.7±2.4	-6.1	-3.19 ±0.6	9.9
Original	2.3 ± 0.3	8.70 ± 1.18	11.5 ±1.6	-6.7	-9.84 ±1.7	10.4

[a] All the titrations were performed in three times, the binding data were obtained using a one-site binding model. [b] Binding (K_a < 1000 M^{-1}) was not detectable by ITC.

2.3.5 Imprinting with individual aptamer fragments

After confirming the lack of binding for the individual free aptamer fragments, we next tested whether imprinting can rescue their binding. We hypothesize that some monomers in the gel may serve as the other half of the aptamer to form an effective binding complex. Here a few new nanogels were prepared: no DNA imprinted with adenosine (MIP), or non-imprinted (NIP); with either aptamer fragment imprinted (F1-MIP and F2-MIP), or non-imprinted (F1-NIP and F2-NIP); and with both aptamer fragments imprinted (F1F2-MIP), or non-imprinted (F1F2-NIP). Each aptamer fragment had a 5′-acrydite for co-polymerization into the gel matrix (Figure 2.1B). The used nanogels have a similar size of 200 ± 36 nm by DLS (Figure 2.2E) and were standardized containing same concentration of aptamers for binding tests through UV-vis spectroscopy. Since the tightest binding are from DNA aptamers, the aptamer concentrations were used as the binding sites of the nanogels to calculate the molar ratios in ITC.

In contrast to the free individual aptamer fragments that cannot bind adenosine (Figure 2.4A and B, Table 2.1), the imprinted gels with either fragment (F1-MIP and F2-MIP) released significant heat indicating rescued binding activity (Figure 2.5B and C, Table 2.2). Compared to the imprinted gel without aptamer (Figure 2.5A), the F1-MIP gel has increased binding affinity by 6.5-fold, and the F2-MIP gel by 13.8-fold (Table 2.2, K_a). Therefore, using DNA oligomers that alone cannot bind adenosine, the imprinted polymer has drastically improved affinity. Note that the DNA oligomers added during polymerization was only 70 μM, which was 1400-fold lower in concentration than the synthetic monomers. The fact that the DNA can still effect binding indicates the tightest binding sites are associated with DNA.

Between the two aptamer fragments, the F2 containing gels (F2-MIP) had a K_a value ~2-fold larger than that of the F1-MIP (Table 2.2). Therefore, DNA sequence still play an important role. This F1 fragment contains 5 consecutive guanines (see the sequence in the Figure 2.1B), which may promote intramolecular interactions and thus weakening adenosine binding during imprinting. DNA binding adenosine can take place via hydrogen bonding, base stacking, and hydrophobic interactions. At this moment, it is unclear whether the binding is the same as that in the original aptamer for each half aptamer, or via other interactions. On the basis of this experiment, for a given target without known aptamers, it is likely that a careful DNA sequence design is needed; not every sequence is equal. For comparison, we also made the same gels but without adenosine imprinting (Figure 2.5E-H, Table 2.2). In each case, the amount of heat was significantly less than that of their imprinted counterpart, indicating the importance of imprinting and specific binding in the imprinted gels. It needs to be noted that we plotted Figure 2.5A, E in the same way as the rest to make a consistent comparison, even though these two samples did not contain any DNA. Therefore, the molar ratio in their x axis is not an accurate representation of the number of binding cavities in the gels.

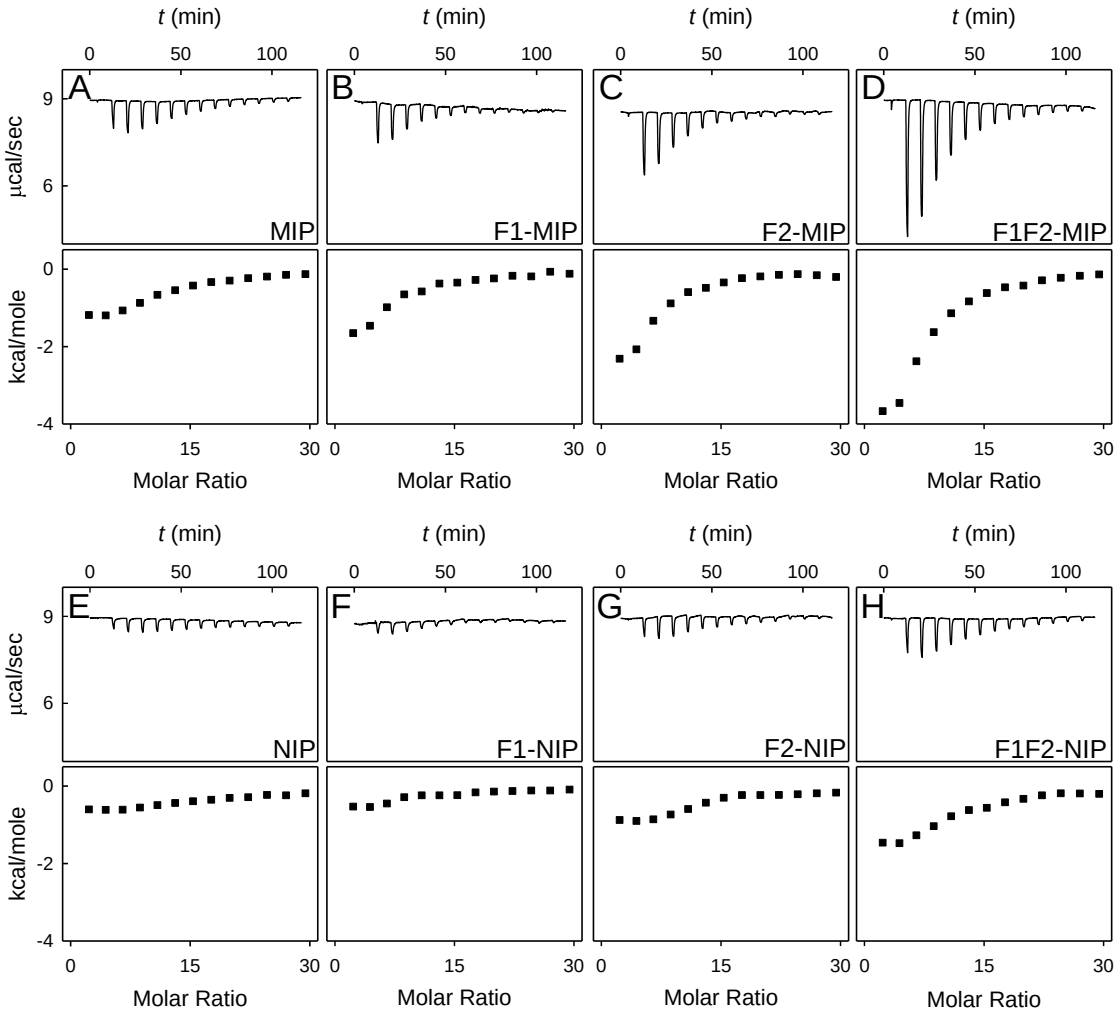

Figure 2.5 ITC titration curves obtained at 298 K for binding of adenosine by the (A) MIP, (B) F1-MIP, (C) F2-MIP, (D) F1F2-MIP, (E) NIP, (F) F1-NIP, (G) F2-NIP and (H) F1F2-NIP. The gel concentrations are around 6 mg/mL; individually adjusted to ensure that each sample contains 20 µM DNA (if imprinted with DNA). The adenosine concentration for titration was 3 mM. The DNA aptamer concentration (20 µM) was used as the binding sites of the nanogels to calculate the molar ratios. The original titration traces (top) and the integrated heat (below) of each reaction are shown.

Table 2.2. Binding data for adenosine titrating to nanogels by ITC.[a]

Nanogels	K_a ($\times 10^4$ M^{-1})	K_d (μM)	ΔG (kcal mol^{-1})	ΔH (kcal mol^{-1})	ΔS (cal $K^{-1}mol^{-1}$)
MIP	0.4 ± 0.05	250 ± 31	-4.8	-1.18 ± 0.4	12.2
F1-MIP	2.6 ± 0.2	38 ± 3.0	-6.0	-1.65 ± 0.2	14.7
F2-MIP	5.5 ± 0.4	18 ± 1.3	-6.4	-2.31 ± 0.2	13.9
F1F2-MIP	6.3 ± 0.6	16 ± 1.5	-6.5	-3.67 ± 0.6	9.64
NIP	0.06 ± 0.01	1670 ± 197	-3.7	-0.60 ± 0.1	10.4
F1-NIP	0.3 ± 0.06	330 ± 69	-4.8	-0.53 ± 0.06	14.4
F2-NIP	0.8 ± 0.1	125 ± 16	-5.3	-0.88 ± 0.05	14.8
F1F2-NIP	1.1 ± 0.1	91 ± 8	-5.5	-1.46 ± 0.4	13.6

[a] All the titrations were performed for three times. The binding data were obtained using a one-site binding model.

It is also interesting to note that the K_d measured here (16 μM adenosine for F1F2-MIP) using ITC is much tighter than that from fluorescence (0.4 mM). This is attributable to the higher DNA concentration used for preparing gels for ITC (70 μM) than for fluorescence (20 μM). Because both fragments are involved in binding, the final binding complex is tripartite (containing both fragments and adenosine). As a result, the DNA concentration difference is reflected in the apparent K_d measured (e.g., the 3.5-fold difference in DNA concentration leads to 3.5 × 3.5 =

12.25-fold difference in K_d). Considering the difference in coupling efficiency, the DNA final concentration induced effect should be ~16-fold, which is close to our observation of 25-fold. For comparison, the full aptamer (without splitting) has a K_d of ~6 μM.[58]

From this study, we could confirm that imprinting rescued the binding activity of the aptamer fragments. Although the binding of each individual fragment alone is not as strong as that of both fragments used together, it supports the feasibility of using DNA oligomers as macromonomers in MIPs.

2.3.6 Imprinting using shorter aptamer fragments

After knowing that each aptamer fragment alone can be effective in the MIPs, it is interesting to test even shorter DNA sequences. According to the structure of the aptamer, the middle 6 nucleotides in F2 (from G5 to A10) are primarily responsible for specific adenosine binding, whereas its two flanking segments contribute only to the overall aptamer folding (Figure 2.1A and B). Hence, we further shorten the F2 fragment to make F2a and F2b (See the sequences in the Figure 2.1B). To test the binding of each DNA, a few new gels incorporating these sequences were prepared, and their binding to adenosine was characterized by ITC. For the F2a imprinted gels (F2a-MIP), a considerable amount of heat was detected with a high binding constant (Figure 2.6A and Table 2.3). These values are comparable with those of the full fragment gel (F2-MIP, Figure 2.6C), indicating that the truncated nucleotides from A11 to T14 may not contribute much to adenosine binding even in the MIP gels. To push the limit, we further shortened the F2a to design F2b with only 6 nucleotides (see the sequence in the Figure 2.1B).

For the imprinted gels containing F2b (F2b-MIP), their binding affinities decreased compared with that of the full F2 fragment, but they still keep a high value of K_a (Figure 2.6B and C and Table 2.3). We reason that the 6 nucleotides from G5 to A10 are the main contributors for binding adenosine. Because neighboring bases can influence the stacking energy,[126] the moderate loss in binding may be from the loss of base stacking on this end. As controls, their corresponding NIP gels barely showed any heat release (Figure 2.6D−F and Table 2.3).

In this work, adenosine was chosen as a model target, and it happens to be a nucleoside, which may have more interactions with DNA (e.g., via base-stacking and base-pairing). Given the development of the aptamer field, we believe that this method can also be applied to other target molecules as well. For example, the cocaine aptamer has a similar binding affinity,[60] although cocaine does not resemble a nucleotide.

The full-length aptamer (27-nucleotide) was finally shortened to 6 nucleotides, and tight binding was still retained. This represents a substantial savings in the cost of DNA synthesis (scales linearly with DNA length) with higher yield and purity (scales with a power law with DNA length). Most importantly, it indicates that a low concentration of DNA can have a large influence on the binding property of MIPs.

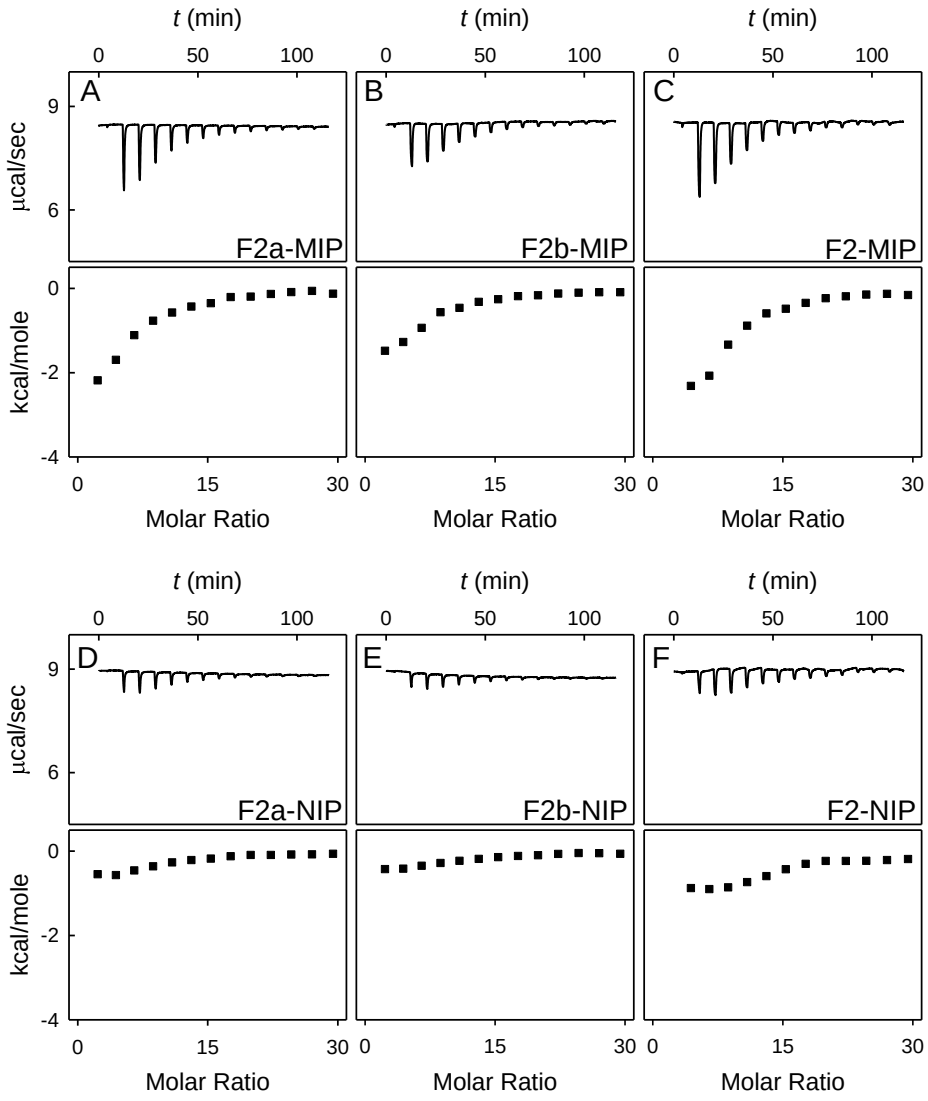

Figure 2.6 ITC titration curves obtained at 298 K for binding between adenosine with the (A) F2a-MIP, (B) F2b-MIP, (C) F2-MIP, (D) F2a-NIP, (E) F2b-NIP, and (F) F2-NIP. For all the experiments, the nanogels all contained 20 µM aptamers in the buffer A. The adenosine concentration for titration was 3 mM. The DNA aptamer concentration (20 µM) was used as the binding sites of the nanogels to calculate the molar ratios. The original titration traces (top) and the integrated heat (below) of each reaction are shown, respectively.

Table 2.3 Binding data for adenosine titrating to fragment aptamer incorporated nanogels by ITC.[a]

Nanogels	K_a ($\times 10^4$ M^{-1})	K_d (μM)	ΔG (kcal mol^{-1})	ΔH (kcal mol^{-1})	ΔS (cal $K^{-1}mol^{-1}$)
F2a-MIP	5.1±0.4	19±1.5	-6.4	-2.18 ±0.6	14.1
F2b- MIP	3.6±0.2	27±1.6	-6.2	-1.48 ±0.4	15.8
F2-MIP	5.5±0.4	18±1.3	-6.4	-2.31 ±0.2	13.9
F2a-NIP	0.4±0.06	250±38	-4.8	-0.55 ±0.06	14.3
F2b-NIP	0.6±0.05	170±14	-5.1	-0.43 ±0.08	15.7
F2-NIP	0.8±0.1	125±16	-5.3	-0.88 ±0.05	14.8

[a]All the titrations were performed were performed for three times. The binding data were obtained using a one-site binding model.

2.4 Summary

In this work, we prepared new hybrid materials using aptamer fragments as macromonomers in MIPs. The DNA aptamer for adenosine was first split into two halves used for imprinting. Compared to the synthetic monomers (AAm and NIPAAm), DNA macromonomers increased the binding affinity by up to 18-fold. DNA also allowed convenient fluorescence signaling. Compared to the free aptamer binding, MIPs doubled the binding affinity by positioning the two fragments close to each other in an optimal configuration. While each free aptamer fragment alone cannot bind adenosine, MIPs rescued their affinities. We further shortened one of the aptamer fragments, and the DNA length was pushed to as short as six nucleotides, yielding MIPs with a dissociation constant of 27 μM adenosine. This study provides a new method for

preparing functional MIP materials by combining high-affinity biopolymer fragments with imprinting.

Chapter 3 Molecular Imprinting on DNAzymes for Substrate Selectivity and Enhanced Activity

3.1 Introduction

Substrate selectivity is an important feature of enzymes. For example, glucose oxidase only converts glucose, leaving other saccharides intact.[127] Despite an excellent catalytic activity and specificity, enzymes are expensive and suffer from low yield and poor stability. In the past few decades, many enzyme mimics have been developed based on small molecules, DNA, metal complexes and nanomaterials.[128] These artificial enzymes are interesting due to their low cost and high stability. However, most of these enzyme mimics do not have the desired substrate selectivity.

Substrate selectivity in natural enzymes is often originated from a specific binding pocket. Therefore, an interesting question is whether one can engineer such pockets for substrate selectivity. At the same time, such methods might afford better enzyme stability and activity. Solving this problem will produce better enzyme mimics and deepen the fundamental understanding on molecular recognition.

DNAzymes are DNA-based catalysts. One particularly interesting DNAzyme is G-quadruplex that has peroxidase-mimicking activity with hemin as a cofactor.[65] In the presence of H_2O_2, this DNAzyme catalyzes oxidations of many substrates, such as TMB and ABTS. These substrates are commonly used since they can produce a color change upon oxidation and thus are analytically useful. While this DNAzyme is popular in many applications, its substrate selectivity was rarely explored. Recently, Willner and co-workers linked aptamers to the DNAzyme and achieved selective oxidation of the targets of the aptamers (e.g. dopamine).[68] However, aptamers

are relatively expensive and the linkage between the aptamer sequence and the DNAzyme needs to be optimized.

Molecular imprinting is an ideal method to produce enzyme-like substrate binding cavities, but related work is quite limited. Wulff and co-workers reported a esterase mimic by imprinting phosphate ester as template with amidines and a significantly enhanced activity was demonstrated.[129-130] However, the challenging problem of engineering substrate selectivity was not studied.

In this work, we aim to use this peroxidase DNAzyme as a model of enzyme mimics to introduce substrate selectivity via molecular imprinting. At the same time, the effect of MIP matrix on the stability and activity of the DNAzyme was also determined. The DNAzyme was acrydite-modified on the 5' end for copolymerization in the MIPs.

3.2 Materials and methods

3.2.1 Chemicals

The DNA samples were purchased from Integrated DNA Technologies (Coralville, USA). The sequence of G4 DNA is 5'-TTTGGGTAGGGCGGGTTGGGTATA-3'. The control DNA sequence is 5'-TTTACGCATCTGTGAAGAGAACCTGGA-3'. These DNA samples were acrydite-modified at the 5' end for polymerization. TMB and hemin were purchased from Sigma-Aldrich (St Louis, USA) and dissolved DMSO to generate freshly prepared stock solutions. ABTS, hydrogen peroxide (30 wt%) and all the monomers were also purchased from Sigma-Aldrich and diluted in fresh aqueous solution. Milli-Q water was used for all of the experiments.

3.2.2 Formation of the DNAzyme complex

4 μM DNA was dissolved in buffer B (50 mM HEPES, pH 7.6, 100 mM NaCl, and 10 mM $MgCl_2$) and heated at 90 °C for 2 min. The solution was cooled to room temperature and 8 μM hemin was added to form the DNAzyme for 1 h.

3.2.3 Preparation of imprinted nanogels

All the imprinted nanogels were prepared using the aqueous precipitation polymerization method.[47, 49] 1 mM substrate was mixed with the formed DNAzyme (4 μM) for 30 min under N_2. AAm (2.9 mg, 42 μmol), NIPAAm (4.6 mg, 42 μmol), MBAAm (crosslinker, 2.4 mg, 16 μmol), DMPA (0.5 μL) and 30 μL of SDS (60 mg/mL) were dissolved in the same buffer B to prepare a monomer solution. After purging the monomer solutions with N_2 for 20 min, polymerization was initiated by adding APS (1.0 mg) and TEMED (0.3 μL). The monomer and the DNAzyme solutions were mixed after 20 min of initiation. The final reaction volume was standardized to 1 mL. The reaction was continued for 8 h at room temperature under nitrogen and the solution was gently shaken several times after initiation. The resulting imprinted gels were collected by centrifugation at 15 000 rpm for 5 min. Then 1 mM H_2O_2 was added to react with the imprinted substrates so they were more easily removed by subsequent washing using Milli-Q water. UV-vis spectroscopy was used to confirm that the template substrates were fully washed away. The imprinted gels were freeze-dried for 24 h and weighed to determine the yield. Non-imprinted nanogels (NIPs) were also prepared and washed in the same way except that no substrate template was added during polymerization.

3.2.4 Transmission electron microscopy (TEM) and DLS

The TEM sample was prepared by dropping a gel dispersion (200 μg/mL) on a copper grid and allowed to dry overnight before imaging on a Philips CM10 microscope. The size and ζ-

potential of the gels (50 μg/mL) were measured by DLS on a Nano ZS90 Zetasizer (Malvern) at 25 °C in buffer B.

3.2.5 ITC

ITC was performed using a VP-ITC Microcalorimeter (MicroCal). Prior to each measurement, each solution and suspension was degassed to avoid air bubbles. The sample of nanogels (5 mg/mL) in HEPES buffer (50 mM, pH 7.6, 100 mM NaCl, and 10 mM $MgCl_2$, 1% v/v DMSO) was loaded in a 1.45 mL ITC cell at 25 °C. ABTS or TMB (280 μL, 1 mM) in the same buffer was titrated into the cell through a syringe (20 μL each time, except for the first injection of 2 μL). The enthalpy (ΔH) and binding constant (K_a) were obtained through fitting the titration curves to a one-site binding model. The K_d values were calculated from $1/K_a$ and $\Delta G = -RT \ln (K_a)$, where $_R$ is the gas constant. ΔS was calculated from $\Delta G = \Delta H - T\Delta S$.

3.2.6 UV–vis spectrometry and kinetics

For a typical oxidation reaction, a substrate (0.5 mM) and the free DNAzyme or nanogels (DNA 1 μM) were dissolved in buffer B. The absorption intensity of the oxidization products was measured after 5 min of reaction by adding 1 mM H_2O_2 at 25 °C. The absorption peaks of the oxidation products at 652 nm for TMB and 420 nm for ABTS were followed for kinetic measurements.

3.2.7 Catalytic saturation curves

Various concentrations of substrates (0.01, 0.05, 0.1, 0.3, 0.5, and 1 mM) were mixed with same concentration of DNAzyme or nanogels (DNA 1 μM in buffer, followed by adding H_2O_2 1 mM). The UV absorptions kinetics were monitored and then converted to concentrations through

the Beer's law: $A = \varepsilon cl$ (ε = 39 000 and 36 800 M^{-1} cm^{-1} for the products of TMB and ABTS respectively). The background oxidation by hemin alone (2 μM) was subtracted for all the kinetics. The oxidation rates (V) with different substrate concentrations were determined by fitting a straight line to the initial linear region of the kinetic curves. V_{max} and K_m were obtained by fitting the data with the Michaelis–Menten equation: $V = V_{max}[S]/(K_m + [S])$ and the k_{cat} was calculated by $V_{max} = k_{cat}[E]$, where [S] and [E] are the concentration of substrates and DNAzyme (standardized as 1 μM), respectively.

3.3 Results and discussion

3.3.1 Polymerization enhanced the activity of DNAzymes

The sequence of the G-quadruplex forming DNA (G4 DNA) and a scheme showing the formation process of the DNAzyme with hemin were shown in the Figure 3.1A. We first tested the catalytic activity of the free DNAzyme using TMB as substrate in the presence of H_2O_2. The DNAzyme converted TMB to a blue colored product, while the DNA alone or hemin alone has almost no activity (Figure 3.1B), indicating the necessity of the full DNAzyme complex. We then copolymerized the DNAzyme (with acrydite-modified) to gel nanoparticles using precipitation polymerization method. AAm and NIPAAm were used as monomers and MBAAm was used as crosslinker.

To have a complete understanding, a few gel formulations were prepared containing the full DNAzyme (i.e., with the G4 DNA and hemin, named DNAzyme-gel), the entrapped hemin alone (hemin-gel), and the G4 DNA alone (G4-gel). Finally, we also prepared a gel with a control DNA (i.e., DNA with random sequence mixed with hemin, named Ctrl-gel). The amount of DNA

in each gel was quantified by UV–vis spectroscopy and adjusted containing the same final DNA concentration of 1μM. The used gels have an average size of 216 ± 41 nm and nearly charge neutral under experimental conditions (pH 7.6) characterized by DLS. The gels have good substrate accessibility.[131-132] The average pore size of the gels is around 10 nm,[43, 133] and this size is much larger than the size of the substrate molecules (e.g., ABTS or TMB).

We then tested the activities of the gels in comparison with the free DNAzyme using TMB and ABTS. When TMB was catalyzed by the DNAzyme-gel for 5 min, the absorption peak of the oxidation product at 652 nm reached 0.23 (Figure 3.1C), while the free DNAzyme yielded a value of only 0.12. Therefore, the activity with the gel was about twice of the free DNAzyme. As controls, the hemin-gel and the G4-gel showed very small absorbance (< 0.03). The control DNA with hemin (Ctrl-gel) also failed to show activity, indicating that the full DNAzyme complex is needed for activity. We next measured their reaction kinetics (Figure 3.1D), and similar conclusions were obtained. For example, the rate of oxidization by the DNAzyme-gel is 1.7 times of that by the free DNAzyme, while the other gels were barely active.

To confirm our observation, we also tried another substrate ABTS. An enhanced activity by the DNAzyme-gel was still observed. For example, the adsorption intensity of the oxidation products by the DNAzyme-gel was 2.1 times higher than that by the free DNAzymes, and the other control gels basically had no activity (Figure 3.1E). Therefore, copolymerizing the DNAzyme into the gel matrix has enhanced its catalytic activity. We reason that the gel matrix might have stabilized the DNAzyme complex, thus enhancing its activity. This set of experiments also suggests that the gel matrix did not block substrate accessibility.

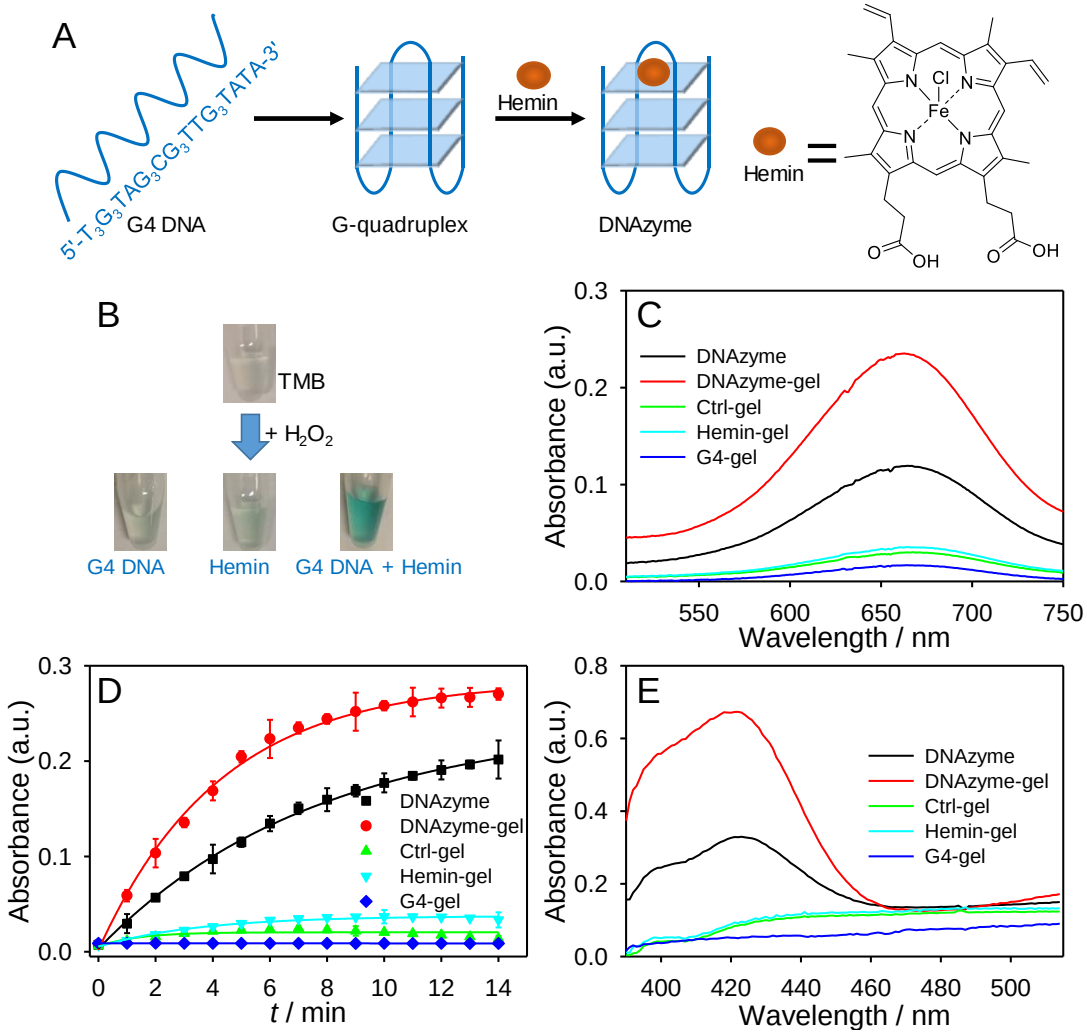

Figure 3.1 (A) A scheme of G4 DNA forming the peroxidase DNAzyme complex with hemin as a cofactor. (B) Photographs of the TMB oxidation products using the G4 DNA or hemin alone and their mixture in the presence of H_2O_2. (C) UV–vis spectra after 5 min reaction and (D) kinetics of oxidation of 0.5 mM TMB monitored at 652 nm by the free DNAzyme and the various DNA containing gels (all with 1 μM DNA and 1 mM H_2O_2) in buffer B at 25 °C. The hemin-gel only contained 2 μM hemin without DNA. (E) UV–vis spectra after 5 min reaction by using 0.5 mM ABTS as substrate monitored at 420 nm.

3.3.2 Improved activity by the gel matrix at higher temperature

To test the hypothesis of improved DNAzyme stability by the gel matrix, we next measured the activity of the gels at a higher temperature using ABTS. For the DNAzyme-gel, the activity at 40 °C ($\approx$0.36 min^{-1}) is around three times of that at 25 °C ($\approx$0.11 min^{-1}, Figure 3.2A). On the other hand, the free DNAzyme without the gel showed a similar rate at both temperatures (Figure 3.2B). We attribute our observation to that the intrinsic activity of this DNAzyme is higher at higher temperature. Oxidization by hemin itself showed a slight increase at 40 °C and this is consistent with our hypothesis (Figure 3.2C). However, the free DNAzyme complex was destabilized at the higher temperature, which has cancelled the rate enhancement. In the gel, the DNAzyme stability is higher, thus yielding a net rate enhancement. With only 41 mol% NIPAAm, the lower critical solution temperature of the gel is much higher than 40 °C.[134] In fact, we did not observe cloudiness of the gel at high temperatures, while a pure NIPAAm gel as collapsed at ~32 °C (Figure 3.2D). Thus, our observed rate enhancement might not relate to an extensive collapse of the gel at high temperature.

Polymers have been covalently linked to many protein enzymes to enhance their stability.[135-137] For example, the stability of horseradish peroxidase with polymerization was increased by more than fourfold compared to the free peroxidase at high temperature without compromising catalytic activity.[138] Our work uses the MIP gels on DNAzymes to increase enzyme stability.

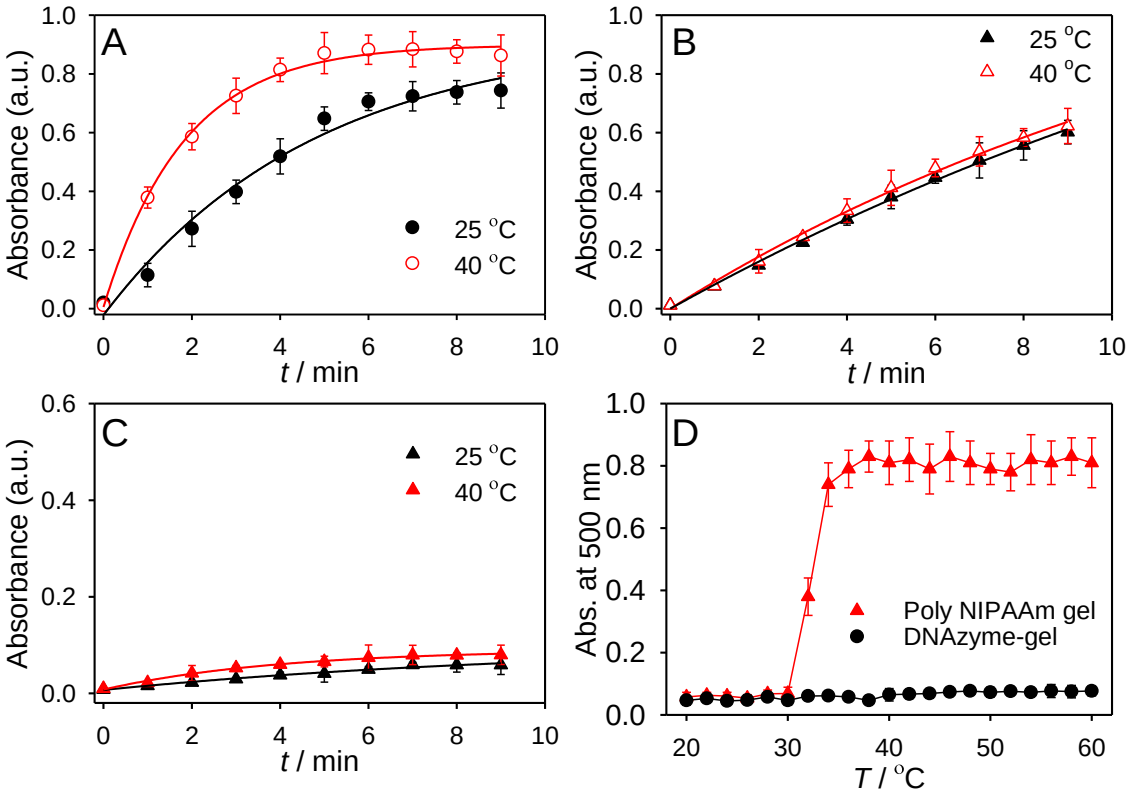

Figure 3.2 Effect of temperature on the oxidation kinetics of 0.5 mM ABTS catalysed by (A) the DNAzyme-gel, (B) the free DNAzyme and (C) free hemin (2 μM) with 1 mM of H_2O_2. The absorbance of the ABTS oxidation products was measured at 420 nm in the buffer B. The DNAzyme-gel and the free DNAzyme both contained 1 μM of the G4 DNA and 2 μM of hemin. (D) Measurement of the absorbance of two gels as a function of temperature to observe the LCST behavior. The absorption intensity of the poly-NIPAAm gel (nearly 100% NIPAAm) and the DNAzyme-gel (with 41mol% of AAM) at different temperatures was followed at 500 nm.

3.3.3 Molecular imprinting on DNAzymes

After demonstrating the feasibility of DNAzyme attachment and the stabilization effect of the gel matrix, we further aimed to engineer substrate selectivity. The DNAzyme we used is a general peroxidase that can oxidize many substrates in the presence of H_2O_2. This is easy to

understand since this DNAzyme does not have a substrate binding cavity. Our idea is to use the molecular imprinting process to create specific binding cavities using the substrate as a template (Figure 3.3A). To test the feasibility, we mixed TMB with the full DNAzyme and then performed the polymerization reaction. During this step, no H_2O_2 was added to avoid TMB oxidation. After removing the TMB template by extensive washing, the MIP gels were dispersed to have a DNA concentration of 1 μM (confirmed with UV-vis spectrometry). We named the TMB imprinted gels as T-MIP. The size and charge of this gel are similar to those made above without TMB. A TEM image of this gel is presented in Figure 3.3B. While each gel appeared irregular likely due to drying, they showed a size of around 200 nm consistent with the DLS results.

We next measured the catalytic activity. Interestingly, using TMB as a substrate, the TMB imprinted DNAzyme gel (T-MIP) showed the highest oxidation rate, more than twice of the DNAzyme-gel and four times of the free DNAzyme complex (Figure 3.3C). Therefore, molecular imprinting with the substrate can further improve the DNAzyme activity, likely due to improved absorption affinity by imprinting. To further understand the enzyme property, the rate of TMB oxidation was measured with different concentrations of TMB (Figure 3.3D). The initial oxidation rates were used where the concentration of substrate is much larger than the concentrations of enzyme and product.[139] Their catalytic parameters are summarized in the Table 3.1. The k_{cat} of T-MIP (9.2 min^{-1}) is more than three times of the DNAzyme-gel and five times of the free DNAzyme. The T-MIP also has the highest affinity to the TMB substrate as indicated from its smallest K_m of 68 μM, which is about half of that of the DNAzyme-gel. Overall, the T-MIP has an eightfold improved catalytic efficiency defined by k_{cat}/K_m than the free DNAzyme (Table 3.1, the last column). For TMB, both k_{cat} and K_m improved by imprinting.

To test the generality, we also prepared ABTS imprinted DNAzyme gels (A-MIP) with a similar observation of the catalytic efficiency enhancement (Figure 3.3E and F and Table 3.1). In this case, the increase in k_{cat} was much larger than the change in K_m, but overall the catalytic efficiency still improved to a similar extent as that for TMB. The results indicate that molecular imprinting significantly improved the catalytic rate and substrate specificity of the DNAzyme. With improved binding affinity by imprinting, the adsorbed substrate concentration around the DNAzyme might be increased by the MIP gel layers.

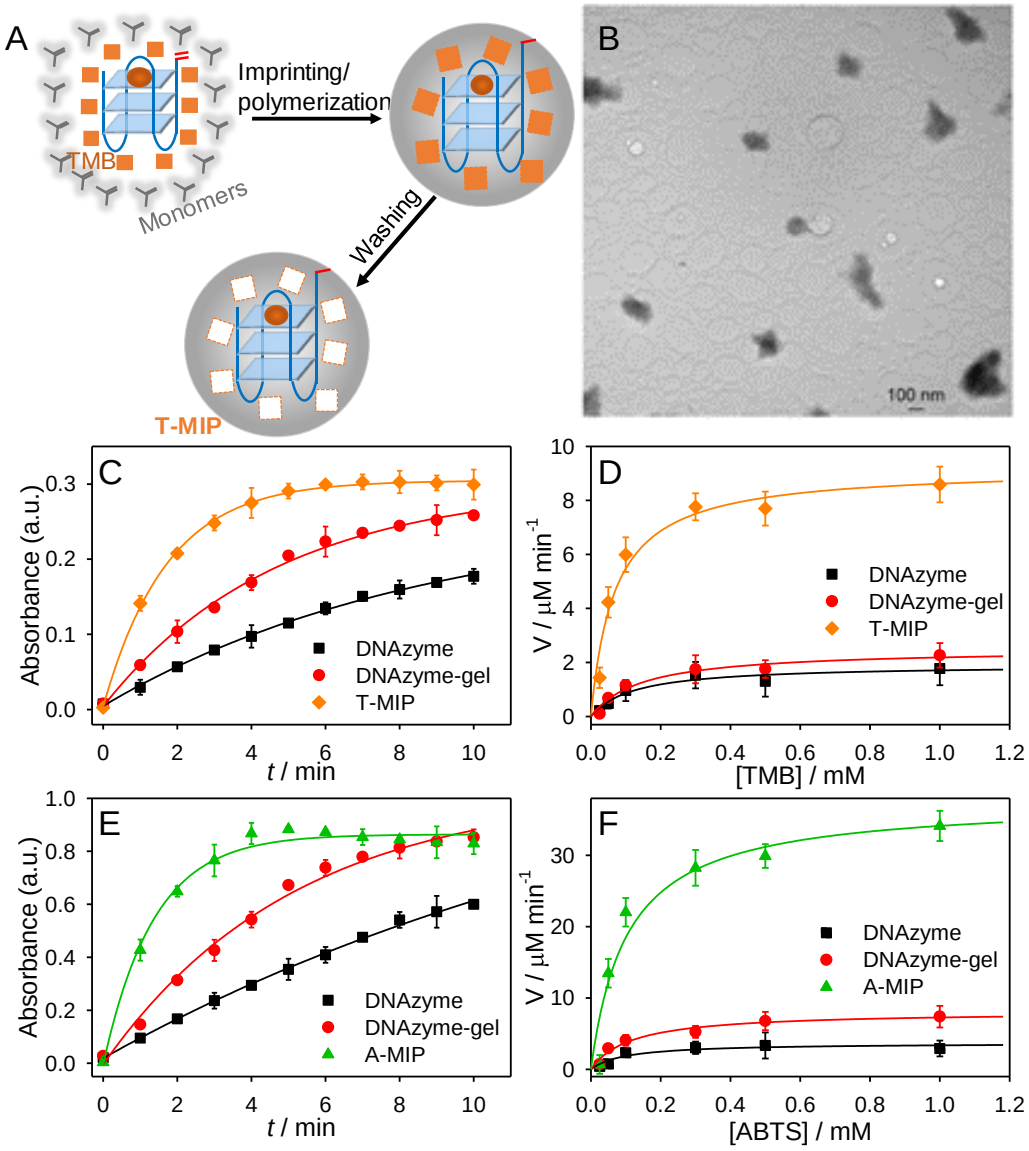

Figure 3.3 (A) A scheme of preparation of the TMB imprinted DNAzyme gels (T-MIP). (B) A TEM image of an imprinted gel (T-MIP). Kinetics of oxidation of 0.5 mM (C) TMB and (E) ABTS by the free DNAzyme and by the different gels. Catalytic rates at various concentrations of (D) TMB and (F) ABTS by the free DNAzyme and different gels. The free DNAzyme and all the gels ($\approx$5 mg/mL) have same concentration of DNA (1 μM) with 2 μM of hemin. All the reactions were with 1 mM H_2O_2 in buffer B at 25 °C.

Table 3.1 Catalytic parameters of the free DNAzyme and all the nanogels with respect to the oxidation of TMB and ABTS.[a]

Sub.	**Enzyme**	V_{max} **(μM min^{-1})**	k_{cat} **(min^{-1})**	K_m **(μM)**	k_{cat}/K_m **(10^{-2} min^{-1} μM^{-1})**
TMB	DNAzyme	1.9 ±0.2	1.9	123 ±11	1.5 ±0.02
	DNAzyme-gel	2.8 ±0.3	2.8	141 ±13	2.0 ±0.03
	T-MIP	9.2 ±0.6	9.2	68 ±8	13.5 ±0.7
	A-MIP	3.4 ±0.6	3.4	185 ±15	1.8 ±0.2
ABTS	DNAzyme	3.7 ±0.5	3.7	105 ±10	3.5 ±0.2
	DNAzyme-gel	8.1 ±0.4	8.1	116 ±18	7.0 ±0.8
	T-MIP	8.5 ±0.5	8.5	126 ±20	6.7 ±0.7
	A-MIP	38.3 ±2.4	38.3	86 ±10	44.5 ±2.5

[a] V_{max} is the maximal reaction velocity, k_{cat} is the catalytic constant, $k_{cat} = V_{max}/[E]$, and the [E] is the concentration of DNA (1 μM); K_m is the Michaelis constant.

3.3.4 Binding affinity tests

The above catalytic rates measurements support MIP binding to the corresponding substrates. To confirm the improved binding affinity, we next performed ITC. For TMB and ABTS, we respectively prepared their imprinted gels (T-MIP and A-MIP) as well as the nonimprinted (NIP) gels. When ABTS was titrated into the A-MIP, an obvious binding was detected with a K_d of 22.0 μM (Figure 3.4A and Table 3.2 for thermodynamic values). In comparison, ABTS showed a poor binding with a K_d of 78.2 μM to the T-MIP (Figure 3.4B), which is similar to titrating ABTS into the nonimprinted gel (NIP, Figure 3.4C). Figure 3.4D shows the titration of ABTS into the buffer with a minimal background. This set of experiments confirmed the specific binding of ABTS by its imprinted gel. Similarly, the specific binding TMB was also confirmed (Figure 3.4E–H, Table 3.2). The symmetrical and sharp titration peaks for each injection also support that the binding kinetics are quite fast.

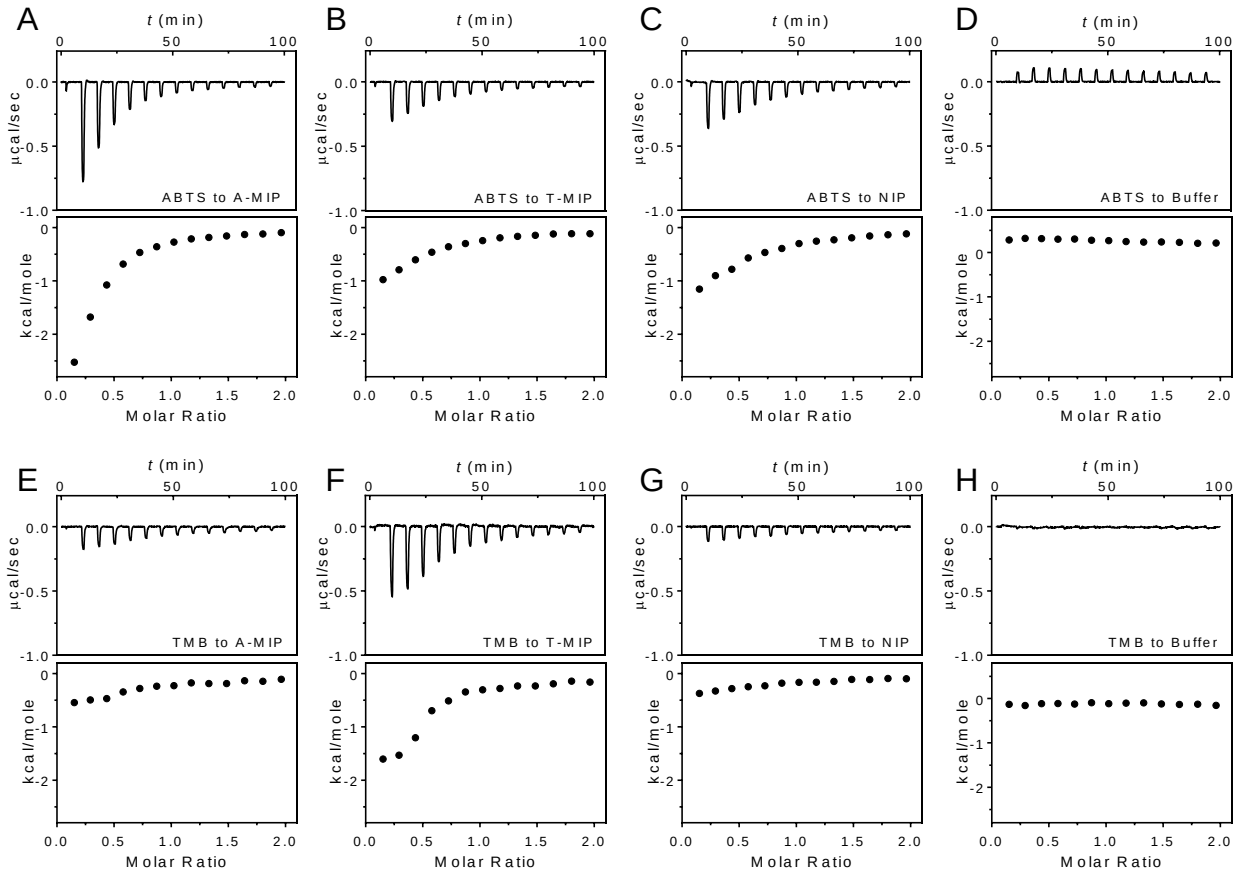

Figure 3.4 ITC titration curves obtained at 298 K (25 ℃) for binding between the substrates ABTS (A-D) or TMB (E–H) with A-MIP, T-MIP, NIP gels, and buffer. HEPES buffer (50 mM, pH 7.6, 100 mM NaCl, and 10 mM $MgCl_2$, 1% v/v DMSO) was used in all the experiments. Note that DNA was not added here. TMB and ABTS were 1 mM and all the nanogels were 5.0 mg/mL dispersed in the same buffer. The binding sites of all the nanogels were standardized to be the same to calculate the molar ratio. The original titration traces (top) and the integrated heat (below) of each reaction are shown.

Table 3.2. ITC Binding data for the substrates titrating to nanogels.[a]

Sub.	Nanogel	K_a ($\times 10^4$ M^{-1})	K_d (μM)	ΔG (kcal mol^{-1})	ΔH (kcal mol^{-1})	ΔS (cal $K^{-1}mol^{-1}$)
ABTS	A-MIP	4.6 ± 0.6	22.0 ± 2.9	-6.4	-3.2 ± 0.4	10.6
	T-MIP	1.3 ± 0.2	78.2 ± 12.2	-5.6	-1.2 ± 0.4	14.8
	NIP	1.4 ± 0.2	72.4 ± 10.5	-5.7	-1.4 ± 0.2	14.3
TMB	A-MIP	0.6 ± 0.1	169.8 ± 28.7	-5.2	-0.6 ± 0.08	15.3
	T-MIP	3.8 ± 0.2	26.4 ± 1.4	-6.2	-1.6 ± 0.1	15.6
	NIP	-[b]	-	-	-0.3 ± 0.06	-

[a] All the titrations were generally performed in duplicates, the binding data were obtained using a 1:1 binding model. [b] Binding (K_a < 1000 M^{-1}) was not detectable by ITC.

3.3.5 Enhanced specificity through imprinting

Now that we have two MIP gels containing the same DNAzyme, but respectively imprinted with TMB or ABTS, we then compared their substrate selectivity.[140] To compare the enhancement only by imprinting, the k_{cat}/K_m values of the two MIP gels were normalized to the values of the free DNAzyme for each substrate (Figure 3.5). For the T-MIP gel (imprinted with TMB), oxidizing TMB has more than eightfold enhanced catalytic efficiency while it only increased approximately onefold for oxidizing ABTS (Figure 3.5A). At the same time, the A-MIP gel imprinted with ABTS, showed > 11-fold enhanced oxidizing ABTS but < 20% for TMB (Figure 3.5B). We reason that

imprinting granted selective binding cavities that improved DNAzyme catalytic performance through specific substrate binding (see the insets for schemes in Figure 3.5).

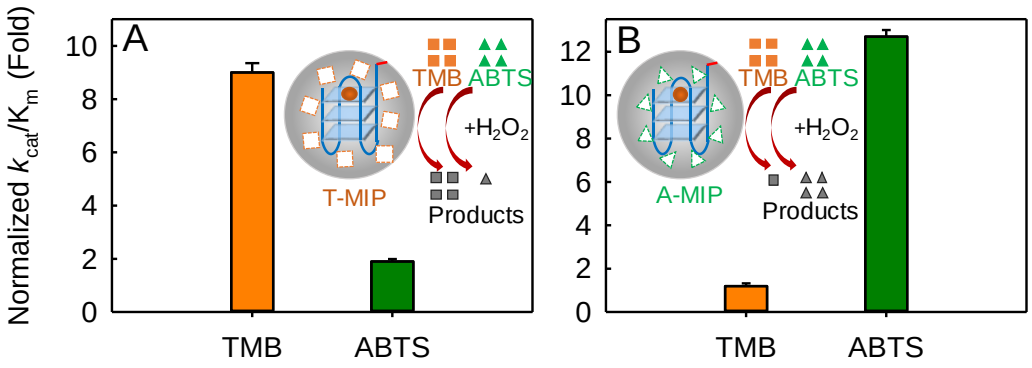

Figure 3.5 Enhancement of catalytic efficiency k_{cat}/K_m by (A) T-MIP and (B) A-MIP gels oxidizing TMB and ABTS. The fold of enhancement was calculated by normalizing the k_{cat}/K_m values of the two MIP gels to that of the free DNAzyme for each substrate. The insets are schematic presentations of the two MIP gels showing substrates selectivity due to imprinting.

3.3.6 Recycle tests

By preparing MIP gels, we have effectively created immobilized catalysts, which may allow recycling. We can readily recover the gels after each catalytic reaction by simple centrifugation. To demonstrate this, oxidization of the substrates by the two imprinted gels (A-MIP and T-MIP) were tested, respectively (Figure 3.6). After ten cycles, more than 70% of their catalytic activity were remained. The drop in activity is likely due to the loss of gels during centrifugation or damage of DNA during the reactions (e.g., each cycle losses ≈2%).[65, 141]

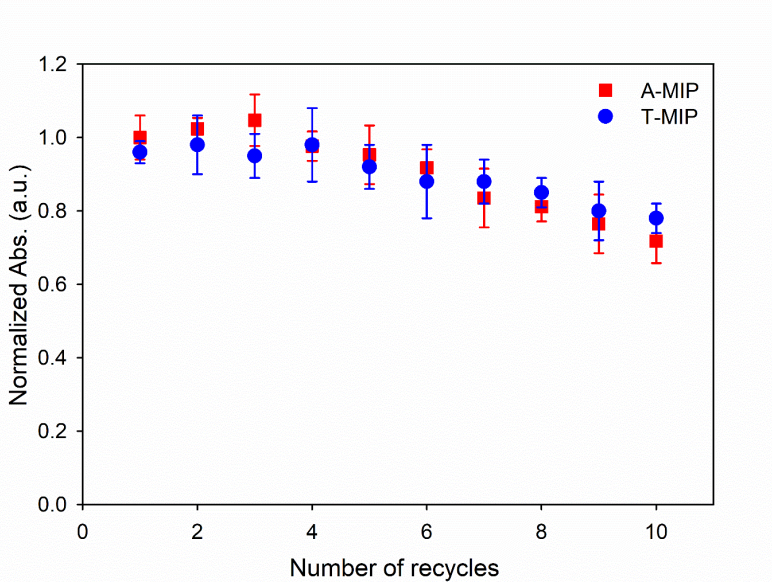

Figure 3.6 Recycle test of the imprinted DNAzyme gels. Reusability of A-MIP and T-MIP gels (~5 mg/mL, DNA 1 μM) oxidizing ABTS and TMB (0.5 mM) respectively with 1 mM H_2O_2 in the buffer B at 25 °C. The UV absorption of oxidization products by A-MIP and T-MIP gels were measured at 420 nm and 652 respectively. The normalized absorbance was calculated by divided each reading by the initial absorbance. The gels were recollected by centrifugation (15,000 rpm, 10 min) and washed with Milli-Q water (~5 mL) and then re-dispersed in the same buffer for the next reaction.

3.4 Summary

In this work, molecularly imprinted nanogels were prepared on a peroxidase mimicking DNAzyme. The gel matrix was demonstrated that enhanced the activity of the DNAzyme by two-fold. The nanogels was also resistant to high temperature. With imprinting, excellent selectivity was achieved by using two different substrate TMB and ABTS. In the best optimization, the selectivity of the DNAzyme was improved by around 11 times. This study provides a general and

powerful way to prepare functional enzyme mimics by combining molecular imprinting and artificially prepared enzymes.

Chapter 4 Intracellular Delivery of a Molecularly Imprinted Peroxidase Mimicking DNAzyme for Selective Oxidation

4.1 Introduction

For therapeutic applications, it is important to deliver drugs to cells to intervene disease related processes. Most drugs are small molecules that can diffuse across the cell membrane. Nucleic acid based drugs have been delivered by cationic lipids/polymers and viral vectors.[142-143] However, delivery of proteins, such as enzymes, has been quite challenging for many reasons. First, proteins are large in size and each protein may have a different charge and surface properties, making it difficult to achieve a generalized delivery method.[144] Second, proteins are susceptible to denaturation and degradation and they are often costly to prepare.[145] Finally, foreign proteins may be immunogenic.[146]

Such challenges might be resolved by using enzyme mimics instead of proteins. Enzyme mimics catalyze enzyme-like reactions under near physiological conditions but with lower cost and higher stability. They have been widely tested for biosensor development, environmental remediation, and medicine.[69-70] However, catalysis by enzyme mimics also has its own challenges. First, their activity is often lower than natural enzymes. At the same time, most enzyme mimics catalyze a broad range of substrates, whereas selective catalysis is critically important for intracellular applications. Many previous published reports demonstrating specificity have mainly focused on bioorthogonal reactions,[147-148] which require non-natural substrates and are more useful for imaging/diagnosis instead of therapeutics. The complicated intracellular environment also interferes with catalysis, by fouling and degradation of enzyme mimics.[149]

Nanogels have been widely studied for cellular uptake and delivery due to its stability and biocompatibility.[150] The gel shell can protect enzymes from degradation and facilitate the cellular uptake.[151] Based on our above study in the Chapter 3, we here tried to prepare a molecularly imprinted nanogel by incorporating the DNAzyme as a model of enzyme mimic to achieve selective catalysis in cells and address the abovementioned challenges.

4.2 Materials and methods

4.2.1 Chemicals

The DNA samples were purchased from Integrated DNA Technologies (IDT, Coralville, USA). The G4 DNA sequence is 5'-TTTGGGTAGGGCGGGTTGGGTATA-3' and the control DNA is 5'-GCCAGCCGAAAGGCCCTTGGC-3'. These DNA were acrydite-modified at the 5' end for polymerization. 10-acetyl-3,7-dihydroxyphenoxazine (Amplex Red, AR), TMB, hemin, fluorescein isothiocyanate isomer I (FITC) and thiazole orange were form Sigma-Aldrich (St Louis, USA) and dissolved in DMSO to generate freshly prepared stock solutions. ABTS, dopamine hydrochloride, hydrogen peroxide (30 wt%), and all the monomers were also from Sigma-Aldrich and were dissolved in fresh aqueous solution. HEPES, sodium chloride, potassium chloride, sodium carbonate, SDS and DNase I were from VWR (Mississauga, Ontario, Canada). 4',6-diamidino-2-phenylindole (DAPI), Dulbecco's phosphate-buffered saline (DPBS), fetal bovine serum (FBS), Dulbecco's modified eagle medium with nutrient mixture F-12 (DMEM/F-12), penicillin and streptomycin were from Thermo Fisher Scientific. Milli-Q water was used for all of the experiments.

4.2.2 Formation of DNAzyme complex

G4 DNA (10 μM) was dissolved in the buffer C (20 mM HEPES, pH 7.4, 100 mM NaCl, 10 mM KCl) and heated at 85°C for 2 min. The solution was then cooled to room temperature and 10 μM hemin was added to form the DNAzyme complex for one hour. The solution was diluted to 100 nM using the same buffer for oxidation tests.

4.2.3 Coupling of FITC

Freshly prepared FITC (50 mM, 25 μL) in DMSO was added to 475 μL of 2 mM allylamine in carbonate buffer (50 mM, pH 9.0) and gently stirred in dark for 4 h. The solution was then kept in a 4 °C fridge overnight and used as the stock solution for nanogel labeling.

4.2.4 Preparation of imprinted nanogels

All the imprinted nanogels were prepared using the same method as in the Chapter 3 except 20 μM AR was used as the template mixed with DNAzyme (1 μM) for imprinting. To facilitate cellular uptake, 15 mol% of DMPA were also added to the monomer solution for positively charged gels. For FITC-labeled nanogels, 1 μL of the FITC-labeled allylamine (2 mM) was also added for fluorescence. The nanogels were washed and characterized in the same as in the Chapter 3.

4.2.5 Oxidation assays

For a typical reaction, 10 μM of AR was incubated with the free DNAzyme or nanogels (DNA 100 nM) at 25°C for 30 min then added with 2 mM of H_2O_2 to initialize the oxidation in the buffer C. The fluorescence intensity and kinetics were recorded using a Varian Eclipse fluorescence spectrometer (Agilent Technologies, Santa Clara, CA) with excitation at 550 nm and emission at 585 nm at 25 °C. For the chromogenic substrates TMB, ABTS and dopamine, the

oxidization activities were determined using photography and UV–vis Spectrometry with a maximum adsorption at 652 nm, 420 nm and 480 nm, respectively.

4.2.6 DNase I Assays

DNase I was dissolved at a concentration of 10 mg/mL in Tris-HCl buffer (10 mM, pH 7.6, 50% glycerol and 2 mM $CaCl_2$). The free DNAzyme and nanogels (DNA 100 nM) were respectively dispersed in the DNase reaction buffer (10 mM Tris-HCl, pH 7.6, 2.5 mM $MaCl_2$ and 0.5 mM $CaCl_2$). To 500 μL of this solution, 0.5 μL of the 10 mg/mL DNase 1 was added and the solution was then incubated at 37°C for different time. After incubation, the nanogel samples were washed twice with buffer C then tested for the oxidation assays.

4.2.7 Cell culture

HeLa cell line was obtained from the American Type Culture Collection (ATCC, MD, USA). The cells were cultured in DMEM/F12 medium, supplemented with 10% FBS and100 U/mL penicillin, 100 μg/mL streptomycin at 37 °C using a humidified 5% CO_2 incubator.

4.2.8 Cellular uptake and confocal microscopy

HeLa cells were seeded onto 14 mm coverslips in 24-well plates with 50,000 cells per well and allowed to grow to ~60% confluency. For cellular uptake tests, the cells were first incubated with 10 μM AR and free DNAzyme or MIP gels (final DNA concentration of 100 nM) for 1 h at 37 °C. The cells were then washed twice with PBS buffer to remove non-internalized AR, DNAzyme and nanogels, and refilled with 500 μL fresh medium. The intracellular oxidation was initialized by adding a final of 2 mM H_2O_2 and the cells were further incubated for another hour at 37 °C. Then the cells were washed twice with 500 μL PBS buffer and fixed with fresh 4%

paraformaldehyde for 10 min at room temperature. The cell nucleus was counterstained using DAPI following the manufacturer's instructions. The coverslips were mounted on glass microscope slides with a drop of antifade mounting media (Sigma-Aldrich Co., USA) to reduce fluorescence photobleaching. The prepared microscope slides were visualized under a laser scanning confocal fluorescence microscope (LSM510Meta, Carl Zeiss Inc., Thornwood, NY). The color intensity of confocal images was quantified by using Image J (NIH Image).

4.3 Results and discussion

4.3.1 Catalytic activity of the free DNAzymes

In this work, we performed intracellular oxidations based on fluorescence signal. Therefore, Amplex red (AR) was chosen as the targeted substrate since its oxidation product, resorufin, is strongly fluorescent (excitation/emission maxima = 550/585 nm, see the structure in the Figure 1.7).[152] In addition, AR has been widely used in many intracellular applications with high-throughput compatibility.[153-154]

We first measured the activities of the free DNAzyme for AR oxidation in comparison with its two components: hemin alone and the G4 DNA alone. After 10 min reaction, the DNAzyme complex (G4/Hemin) had the highest oxidation activity. More than 4-fold higher activity than that of the free hemin was observed by their fluorescence spectra and photographs (Figure 4.1A and inset). A control sample (Ctrl) with a random sequence (non G4 forming DNA, see its sequence in the Method part) showed an activity similar to that of free hemin, while the free G4 DNA alone (no hemin) had almost no activity. The same trend was also observed in a kinetic assay (Figure

4.1B). Therefore, the high activity of the DNAzyme was confirmed, and a substantial fluorescence signal was produced in just 10 min.

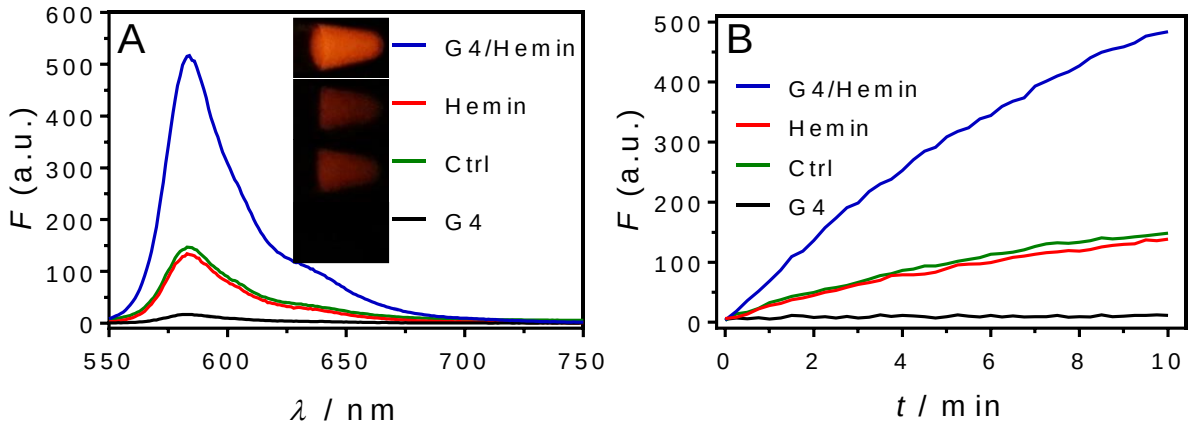

Figure 4.1 (A) Fluorescence spectra after 10 min reaction and (B) kinetics of oxidation of 10 μM AR by the DNAzyme complex, hemin alone, G4 DNA alone, and a mixture of hemin with a control DNA (Ctrl) in the presence of 2 mM H_2O_2. The inset in (A) is the fluorescence photographs of oxidized AR under UV light. 100 nM of the G4 DNA (or Ctrl DNA) and hemin were used in all the reactions in the buffer C at 25 °C.

4.3.2 Enhanced activity through imprinting

The goal of this work is to perform oxidation inside cells. Since a free DNA oligonucleotide cannot be internalized by cells, we need to deliver the DNAzyme with nanogels. In addition, we aim to achieve selective oxidation and the intended target should be preferentially oxidized. To achieve the both goals, we incorporated the DNAzyme into nanogels through imprinting and polymerization. The same method was used as in the Chapter 3 for the imprinted nanogel preparation besides AR was used the imprinting target. Furthermore, we also incorporated a fraction (15 mol%) of positively charged functional monomer, *N*-[3-

(dimethylamino)propyl]methacrylamide (DMPA), to facilitate cellular uptake.[155] The imprinted DNAzyme nanogels were collected after removing the AR template by extensive washing (confirmed by UV-vs spectroscopy).

To have a complete understanding, various nanogel formulations were prepared, including AR-imprinted DNAzyme nanogels (named MIP), non-imprinted DNAzyme nanogels (prepared the same way but in the absence of AR, named NIP), nanogels with entrapped hemin alone (no DNA, named Hemin-gel), and nanogels with the G4 DNA alone (without hemin, named G4-gel). To ensure a fair comparison, all the samples were standardized to contain the same concentration of DNAzyme (100 nM) regardless of free DNAzyme or nanogels, which was confirmed through UV−vis spectroscopy and fluorescence using thiazole orange as a DNA staining dye. All the used gels had a similar average size of around 300 nm from DLS (Figure 4.2A). With an average size of 300 nm, the molar concentration of the nanogel particles was calculated to be ~2.35 nM (e.g., dispersing 4 mg dried gels in 1 mL of buffer yielded a final gel volume of 20 µL after centrifugation). With 100 nM DNAzyme incorporated inside, each nanogel had around 42 DNAzyme molecules. As expected, all the four prepared gels were positively charged with a ζ-potential of around +14 mV (Figure 4.2B), which was attributed to the cationic monomer DMPA (15 mol%). The gel without DMPA was close to neutral (Figure 4.2B, the last bar).

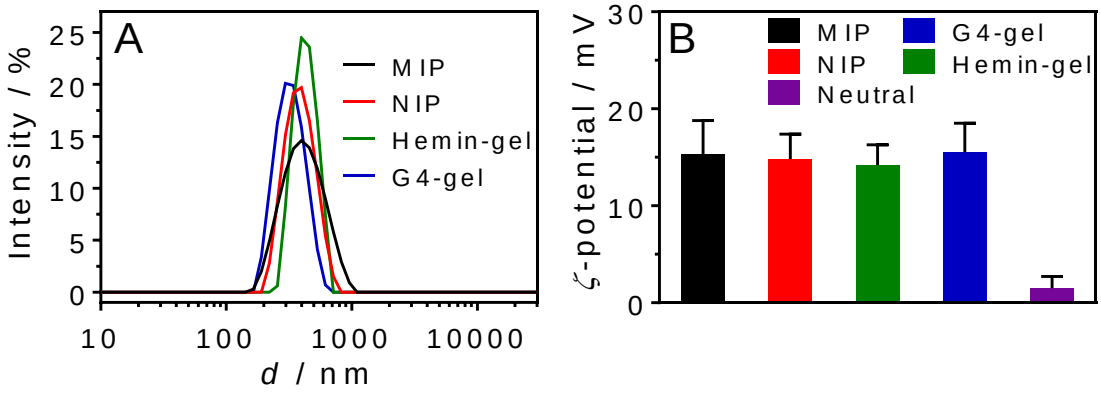

Figure 4.2 (A) The hydrodynamic size and (B) ξ-potential of various nanogels (50 μg/mL) measured by DLS in the buffer C at 25 °C. The polydispersity index (PDI) of the nanogels was below 0.1.

After characterizing the colloidal property of the nanogels, we next tested their oxidation activities with AR as a substrate. After 10 min reaction, the fluorescence spectra of the oxidized product by different gels were collected (Figure 4.3A). The MIP nanogel had the highest activity showing more than 1.6-fold higher fluorescence than that of the NIP gel and the free DNAzyme. This was also confirmed by a stronger fluorescent photograph of the MIP gel (the inset in Figure 4.3A). Therefore, molecular imprinting improved the activity of the DNAzyme. As controls, the hemin-gel and G4-gel samples showed much lower activities. Without the G4 DNA, hemin cannot be stably associated with the gels and some might be washed away during gel preparation. The fact that the free DNAzyme and the NIP nanogel had almost the same activity suggested that the secondary structure (quadruplex) of the DNAzyme in the nanogels was retained, despite the presence of cationic monomers in the gel.

To characterize their enzyme properties, we then measured their oxidation kinetics (Figure 4.3B) and calculated the catalytic rates (Figure 4.3C). The MIP nanogel showed the fastest oxidation rate of ~250 ΔF/min, which was more than 2.7-fold higher than that of the NIP gel and 3.5-fold higher than the free DNAzyme, confirming the improved activity through molecular imprinting. The activity of the NIP gel was similar to that of the free DNAzyme, suggesting that the DNAzyme had a similar conformation and activity in the gel. The higher activity of the MIP nanogel further indicated the importance of imprinting. In other words, the rate enhancement was not from simply having the polymer matrix but more likely from imprinting. The favored binding

of the substrate in the MIP might enhance enzyme-substrate interactions and thus the reaction rate. As expected, the Hemin-gel and G4-gel samples showed very slow rates.

The oxidation rate as a function of AR concentration was further measured (Figure 4.3D). After fitting the data using the Michaelis-Menten equation, the MIP gel had the highest substrate affinity with a K_m of 1.8 ± 0.6 μM, which was a few fold lower than that of the free DNAzyme (K_m = 5.5 ± 1.5 μM) and the NIP gel (K_m = 8.5 ± 1.5 μM). Therefore, imprinting indeed improved substrate binding. The high catalytic rate and lower K_m might be useful for improving specificity of the MIP gels.

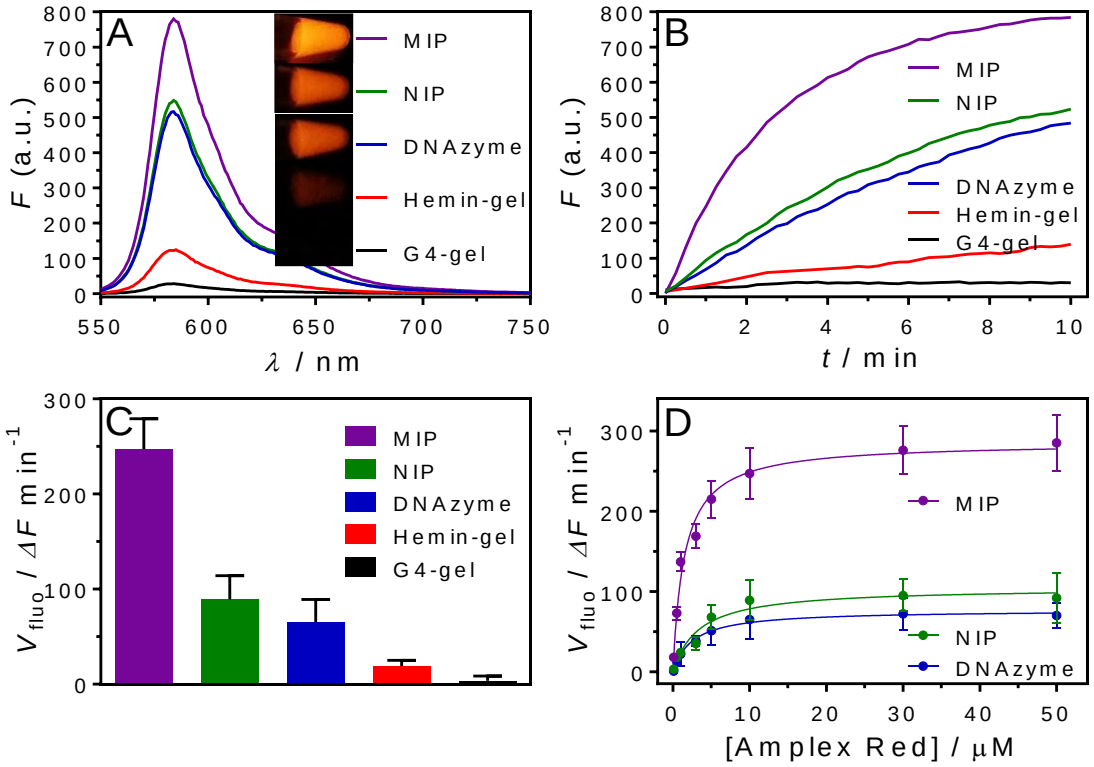

Figure 4.3 (A) Fluorescence spectra after 10 min reaction and (B) kinetics of oxidation of 10 μM AR by different nanogels and the free DNAzyme in the presence of 2 mM H_2O_2. Inset of (A): fluorescence photographs of the oxidized AR under UV light. The initial rates of the oxidation kinetics (C) with 10 μM AR and (D) as a function of AR concentration by different nanogels and

the free DNAzymes. 100 nM of the G4 DNA and hemin were used in all the reactions in the buffer C at 25 °C. All the nanogels were around 4 mg/mL containing 100 nM of the DNAzyme.

4.3.3 Enhanced selectivity through imprinting

To test the selectivity of the imprinted DNAzyme nanogels, we used three other chromogenic substrates for comparison: TMB, ABTS and dopamine. At the testing condition (the buffer C, 20 mM HEPES, pH 7.4), TMB and ABTS are negatively charged (pK_a~4.2 and 2.1, respectively), while dopamine is positive charged (pK_a ~8.9).[156] Therefore, these three substrates were representative in terms of charge interactions. Before oxidation, these substrates were all colorless, and selectivity could be determined from their color after oxidation. We mixed each substrate with the AR imprinted DNAzyme nanogels and performed the oxidation reaction (Figure 4.4A). By visual inspection, only the AR catalysis was promoted compared to the free DNAzyme, while the other three substrates were even inhibited. This trend was more obvious after quantification at their respective absorption or emission wavelengths (Figure 4.4B). Therefore, the MIP nanogels were indeed capable of selective oxidation of the imprinted AR over other substrates. Although we cannot test all possible substrates in this work, it is reasonable to believe that this imprinted DNAzyme can also selectively oxide AR inside cells, leaving other molecules less affected.

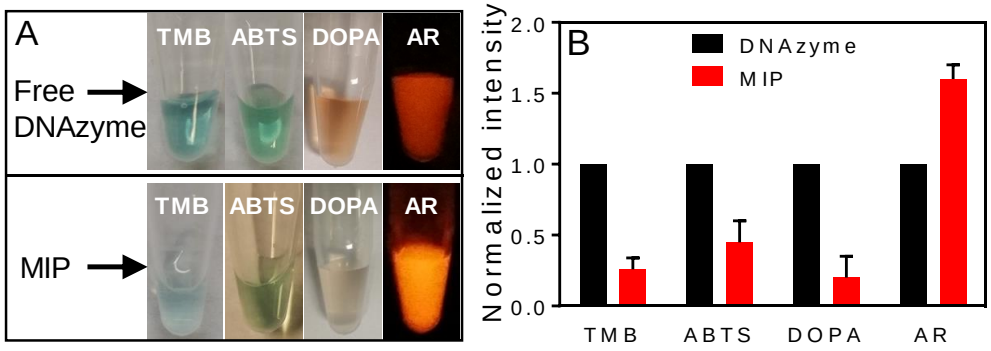

Figure 4.4 Selectivity test of four different substrates by the free DNAzyme and by the AR-imprinted nanogels (DNAzyme: 100 nM) in the presence of 2 mM H_2O_2. (B) Normalized UV-vis absorption or fluorescence intensities at the corresponding peaks from the samples in (A). The intensities of the free DNAzyme samples were normalized to be 1.

4.3.4 Enhanced stability by nanogels

After demonstrating the improved activity and specificity, we also wanted to know whether the gel matrix could protect the incorporated DNAzyme from nuclease degradation. To test this, we incubated the MIP gels with DNase I for 30 min. The gels retained good activity for AR oxidation showing only 17.6% fluorescence decrease (Figure 4.5A). In contrast, the free DNAzyme almost completely lost its activity after the DNase I treatment (Figure 4.5B). Therefore, the nanogel matrix effectively decreased enzymatic DNA degradation, which is likely due to the exclusion of the large nuclease molecules from entering into the pores of the nanogel.

For the 17.6% drop, we attributed it to the degradation of surface DNA. To further confirm this, we incubated the nanogel with DNase I for different time periods, and the fluorescence from AR oxidation by the MIP gels only dropped by ~21% even after 3 h incubation (Figure 4.5C). Therefore, we estimated that most of the DNAzymes were in the inside the gel matrix (around 80 %) that cannot be accessed by DNase I. The kinetics of the non-treated and 3 h DNase I treated samples were compared, and the rate was very similar (Figure 4.5D). Therefore, the activity of the interior and surface DNAzymes might be quite similar. Since AR is a small molecule and it can diffuse more quickly than DNase I can in the gel pores. Immobilizing DNA in hydrogels is known to facilitate long-term storage; the sample can be dried and then rehydrated before use.[157-158]

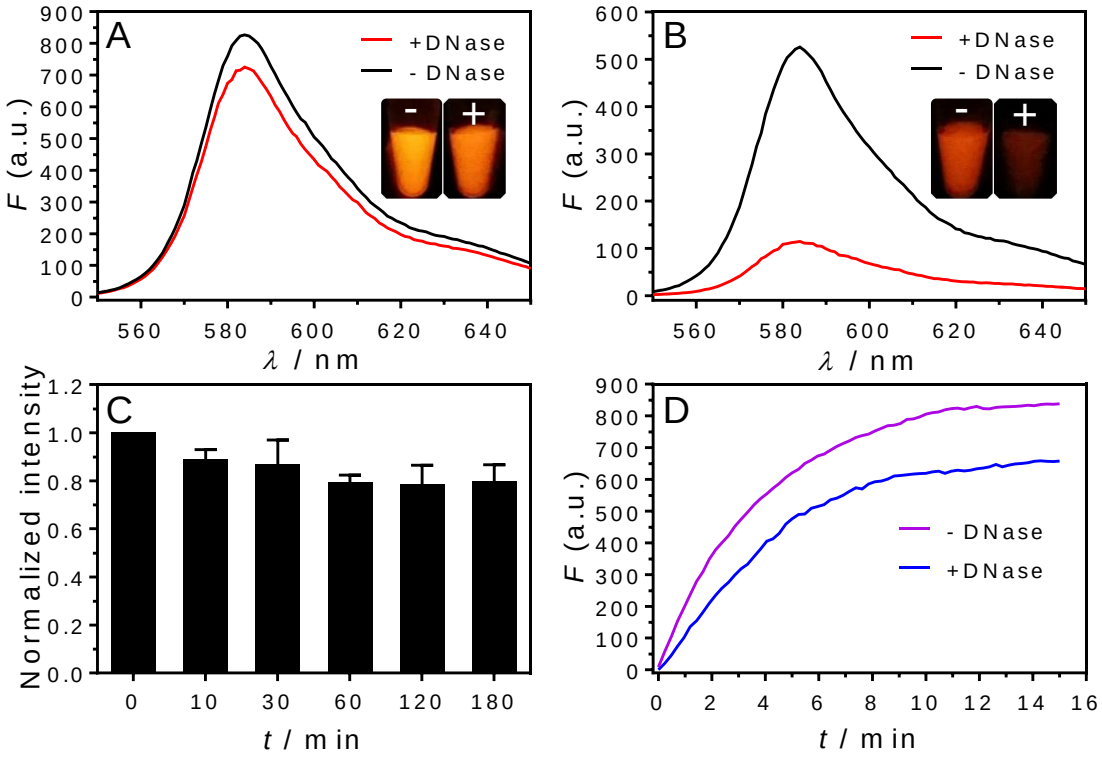

Figure 4.5 Fluorescence spectra and photographs (inset) of AR oxidation by the (A) MIP gels and (B) the free DNAzyme before and after 30 min of DNase I treatment. (C) Normalized fluorescence intensities of AR oxidation by the MIP, and the nanogels were incubated with DNase I for various time periods. (D) The kinetics of AR oxidation by the MIP nanogels without or with 3 h DNase I treatment. All the nanogels were 4 mg/mL containing 100 nM of the DNAzyme tested at 25 °C.

4.3.5 Intracellular delivery of the imprinted nanogels

With excellent activity, specificity and stability, we then measured the catalysis in living cells. To track cellular uptake of the nanogels, we covalently labelled a fluorophore to the gels. We introduced another functional monomer, allylamine, which has a primary amine group that can readily react with fluorescein isothiocyanate (FITC).[159] After linking FITC with allylamine (Figure 4.6A), the imprinted nanogels were prepared with the same procedures. After extensive washing

to remove free FITC, the resulting nanogels had a strong fluorescent signal with a maximum emission at 521 nm (Figure 4.6B) and a green fluorescence color under the UV light (inset). A fluorescent photograph of the FITC-labeled nanogels after centrifugation was also recorded to confirm that the label was on the gel matrix and no free FITC was left.

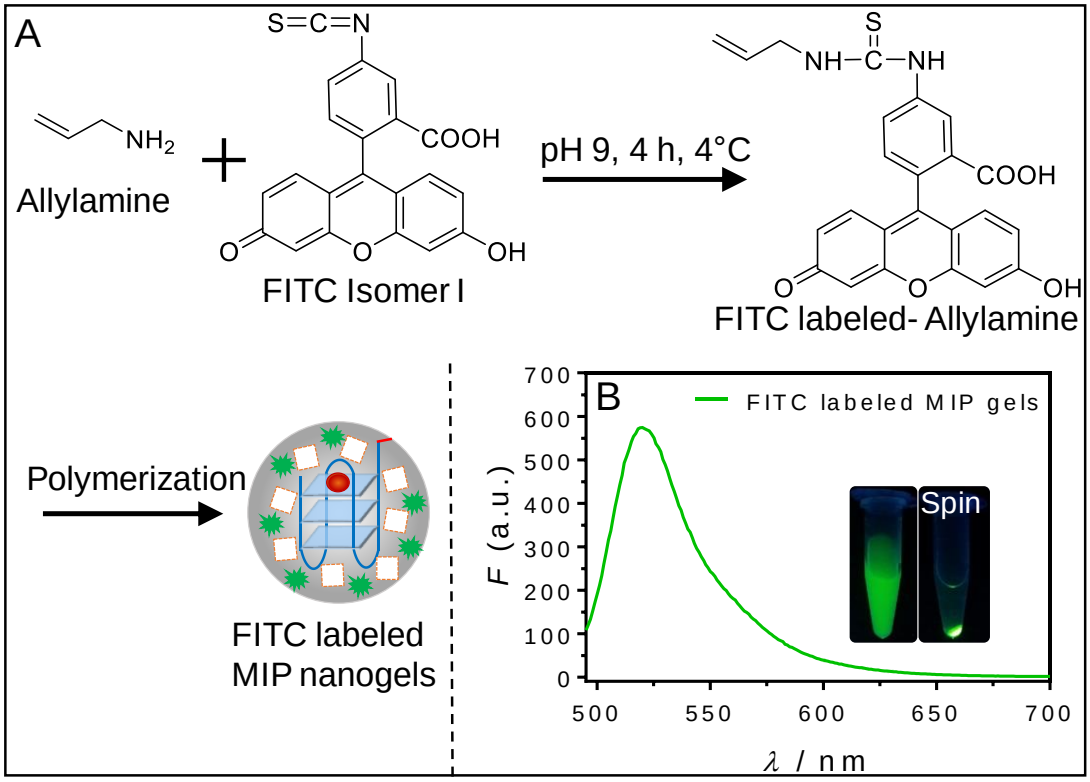

Figure 4.6 (A) A scheme showing the preparation of FITC-labeled allylamine monomer and green fluorescent MIP nanogels. (B) A fluorescence spectrum of the prepared FITC-labeled MIP nanogels (2 mg/mL, 200 nM FITC) excited at 485 nm. Inset: Dispersed FITC-labeled MIP nanogels and after centrifugation (Spin) imaged under UV light excitation.

After labeling the nanogels with FITC, we then followed their cellular uptake and the intracellular oxidation reaction. The free DNAzyme and MIP, NIP gels were all tested side-by-side. HeLa cells were chosen as a model cancer cell line. The free DNAzyme or nanogels were

incubated with the cells for uptake in the presence of the substrate AR. The culture medium was then changed to remove non-internalized AR and the enzymes. Finally, H_2O_2 was added to activate the oxidation inside the cells and the results were analyzed by confocal fluorescence microscopy. The oxidized products were red, the nanogels were green, and the cell nucleus was stained blue (Figure 4.7). No red fluorescence was measured by the free DNAzyme sample, indicating no oxidation occurred in the cells (Figure 4.7A). This might be due to poor uptake of the free DNAzyme by the cells. For the MIP gel samples, a strong green fluorescence and a strong red fluorescence were observed indicating successful internalization and oxidation (Figure 4.7B). The NIP gels were also efficiently internalized as indicated by the strong green fluorescence, but its red fluorescence was weaker (Figure 4.7C), which can be explained by its lower activity than the MIP gels. This set of experiments indicated that the imprinted DNAzymes worked inside cells in a way similar to that outside cells. Finally, we also tested the MIP samples without addition of H_2O_2 (Figure 4.7D). In this case, no red oxidized product was observed. The cell itself could produce H_2O_2 but the concentration around the nanogels was likely to be insufficient for the oxidation reaction to reach a sufficient level to be observed by our microscope.[160]

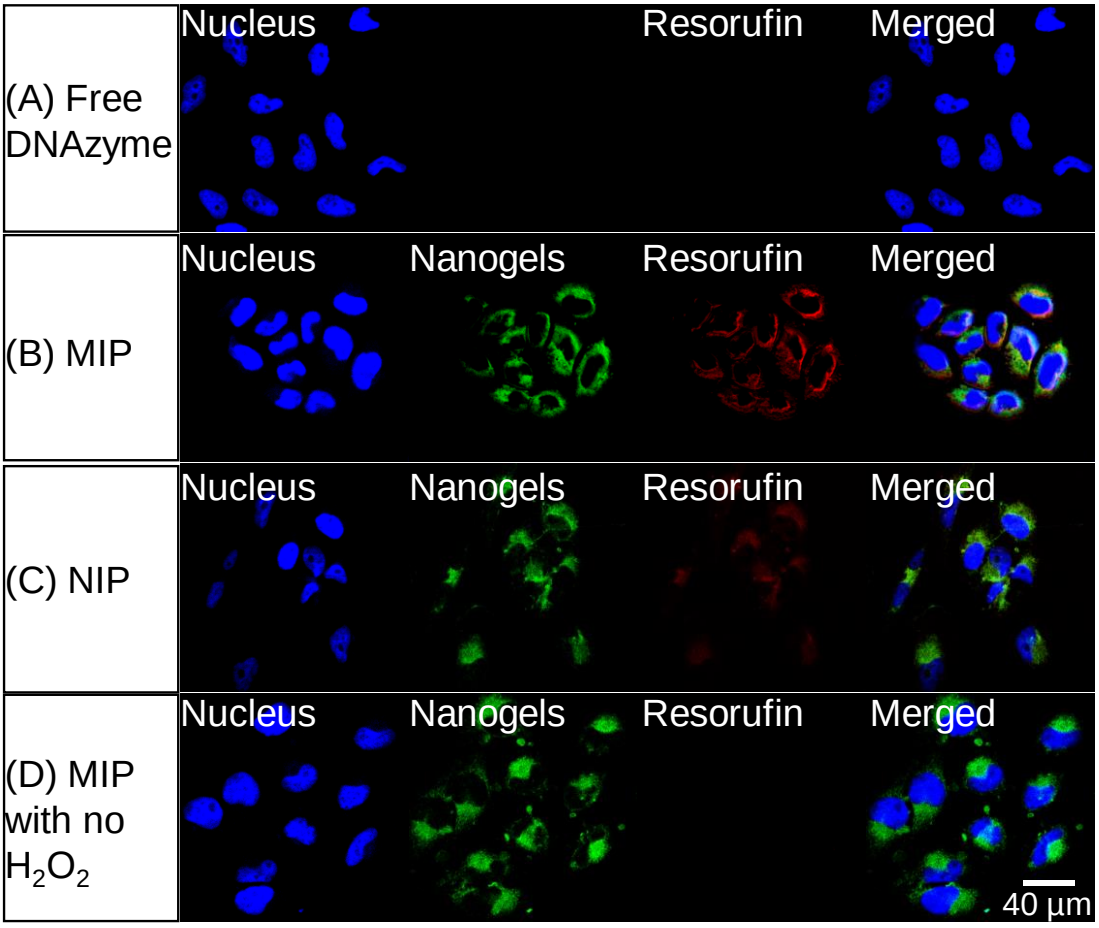

Figure 4.7 Confocal fluorescence micrographs of oxidation of AR (10 µM for incubation) in HeLa cells by (A) the free DNAzyme, (B) MIP nanogels, (C) NIP nanogels in the presence of 2 mM H_2O_2, and (D) MIP nanogels without H_2O_2 added. The initial DNA concentration was 100 nM in the cell culture medium for incubation.

To have a quantitative understanding, the fluorescence intensities of the cells were quantified (Figure 4.8A). The green intensities of the three gel samples were very close to each other indicating a similar uptake efficiency of these nanogels. This is reasonable since they all had a similar charge and imprinting did not affect internalization. For the red color indicative of the oxidation activity, the MIP gel was more than two-fold stronger than that of the NIP gel. After

normalization of the green fluorescence, the catalytic efficiency of the MIP gels was 2.6-fold higher than the NIP gels (Figure 4.8B). From the fact that the MIP sample was more effective also inside cells than the NIP sample, we concluded that molecular imprinting was still effective intracellularly.

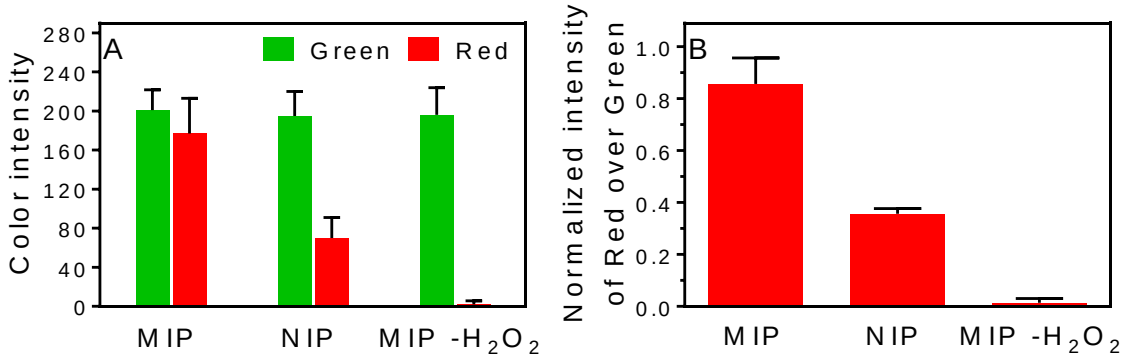

Figure 4.8 (A) Fluorescence intensity of the green and red channels of the confocal micrographs in Figure 4.7 of the MIP, NIP, and MIP with no H_2O_2 (MIP-H_2O_2) samples. (B) Normalized red fluorescence intensity from (A).

4.4 Summary

In summary, a molecularly imprinted nanogel was prepared with a peroxidase mimicking DNAzyme. After imprinting, the activity and specificity of the DNAzyme were significantly improved. At the same time, the gel matrix protected the DNAzyme from degradation by DNase I, and facilitated cellular uptake. Therefore, by using this imprinted nanogel, we provided an alternative approach for the traditional delivery of protein enzymes. Using DNAzymes can improve stability and decrease cost, while imprinting can improve the activity and specificity of the DNAzyme. By imprinting DNAzymes and other enzyme mimics (e.g., nanozymes) with other

types of catalytic activities and by using biologically relevant molecules as templates, it is possible to produce nanogels that can have a practical biomedical impact.

Chapter 5 Molecular Imprinting on Nanozymes for Substrate Specificity Improvement

5.1 Introduction

Nanozymes refer to nanomaterials that catalyze enzyme-like reactions under near physiological conditions. A diverse range of nanomaterials were discovered with oxidase, peroxidase, catalase, superoxide dismutase, and laccase mimicking activities. With much higher stability and lower cost than protein enzymes, nanozymes are attractive for various applications ranging from biosensor development, environmental remediation, to nanomedicine.[85]

While most previous work focused on catalytic activity,[161-162] substrate specificity of nanozymes has yet to be addressed. Nanozymes do not have a substrate binding pocket, a feature of most natural enzymes. Since nanozymes' reactions take place on the surface, substrates diffused to the surface can all react regardless of their shape and charge. Therefore, most nanozymes can turnover a diverse range of substrates. Substrate specificity is an important feature of enzymes, enabling its molecular recognition function. A critical step towards real enzyme mimics is to engineer substrate binding pockets. Many methods can be potentially used, such as attaching aptamers, peptides, or antibodies.[68] Using these biological ligands, however, defeats the cost and stability advantages of nanozymes.

We reason that MIPs might be ideal for creating substrate binding cavities on nanozymes since both can be prepared at a large scale and low cost. Molecular imprinting had been performed on an esterase mimic to increase catalytic activity,[129] and we had performed imprinting on DNAzymes in previous studies. In this work, we grew MIPs on three classic nanozymes with

peroxidase and oxidase like activities (e.g., iron oxides, gold nanoparticles and nanoceria). This simple method has achieved remarkable substrate specificity as well as activity enhancement.

5.2 Materials and methods

5.2.1 Chemicals

TMB was purchased form Sigma-Aldrich (St Louis, USA) and dissolved DMSO to generate a freshly prepared stock solution (100 mM). ABTS, dopamine hydrochloride, hydrogen peroxide (30 wt%) and all the acrylic monomers were also purchased from Sigma-Aldrich and dissolved freshly in water. Sodium chloride, sodium acetate, SDS, acetic acid, and HEPES were from Mandel Scientific (Guelph, ON). Milli-Q water was used for all the experiments.

5.2.2 Preparation of Fe_3O_4 NPs and other nanozymes

Fe_3O_4 NPs were prepared following literature reported methods.[163] $FeCl_2$ (0.2 M, 1.0 mL) and $FeCl_3$ solutions (0.1 M, 4.0 mL) were mixed under nitrogen gas, to which aqueous ammonia (0.2 M, 15 mL) was added drop-wise under stirring. The mixture was heated at 80 °C for 1 h under nitrogen. After cooling to room temperature, the resulting Fe_3O_4 NPs were washed by Milli-Q water until the supernatant was clear (final yield: 70.3%). Gold nanoparticles (AuNPs, 13 nm) were synthesized using the citrate reduction procedures with a concentration of ~10 nM.[164] Nanoceria (CeO_2, size ~5 nm, 20 wt% dispersed in 2.5% acetic acid from Sigma-Aldrich) was diluted in acetate buffer (20 mM, pH 4.0) for use.

5.2.3 Imprinting on nanozymes

All the imprinted nanogels were prepared using the same method as described in the Chapter 3. 60 μg/mL Fe_3O_4 NPs and 1 mM substrate (e.g., ABTS) were used for imprinting. For

the positively or negatively charged gels, DMPA (15 mol %, 10 μL) or AMPS (10 mM) was also included. The resulting imprinted gels were collected by centrifugation at 5000 rpm for 5 min. UV-vis spectroscopy was used to confirm that the template substrates were fully washed away. Non-imprinted nanogels (NIPs) were also prepared and washed in the same way except that no substrate template was added during polymerization.

5.2.4 Inductively coupled plasma mass spectrometry (ICP-MS)

To measure the Fe_3O_4 concentration in the nanogels, different gel particles (5 mg/mL) were dissolved in 5 % (w/v) nitric acid overnight. The dissolved solutions were then centrifuged at 15 000 rpm for 10 min to remove the gel shells and filtered using 0.45 μm filters. The iron content in the solutions was measured by ICP-MS (Thermo Fisher Xseries II).

5.2.5 TEM, SEM, EDX and DLS.

The particle size and morphology of the Fe_3O_4 were studied using TEM (Philips CM10). Samples (100 μg/mL) was drop-cast onto a copper grid and allowed to dry overnight at room temperature. For SEM, freeze-dried samples were dropped on a conductive carbon tape for imaging using a LEO FESEM 1530 field-emission scanning electron microscope (SEM), equipped with an EDAX Pegasus 1200 energy-dispersive X-ray analysis system (EDX). The size and ζ-potential of nanogels (50 μg/mL) were measured by DLS on a Zetasizer Nano ZS90 (Malvern) at 25 °C.

5.2.6 ITC.

ITC was performed using a VP-ITC Microcalorimeter instrument (MicroCal). Prior to measurement, each solution was degassed to remove air bubbles. The nanogels (5 mg/mL)

dispersed in acetate buffer (20 mM, pH 4, 1 % v/v DMSO) was loaded in a 1.45 mL ITC cell at 25 °C. ABTS or TMB (280 μL, 2 mM) in the same buffer was titrated into the cell (20 μL each time, except for the first injection of 2 μL). The binding parameters were analyzed with the same method as described in the Chapter 3.

5.2.7 Activity assays.

For a typical peroxidation reaction, a substrate (0.5 mM) was mixed with free Fe_3O_4 NPs (50 μg/mL) or imprinted nanogels (~5 mg/mL gel containing 50 μg/mL Fe_3O_4) in acetate buffer (20 mM, pH 4). The absorption intensity of the oxidization products (652 nm for TMB, 420 nm for ABTS, and 480 nm for dopamine) was followed after adding 10 mM H_2O_2 using an Agilent 8453A spectrometer at 25 °C. To measure the enzyme parameters, various concentrations of substrates (0.05, 0.1, 0.2, 0.3, 0.4, 0.5, 0.75, 1 mM) were mixed with free Fe_3O_4 NPs or imprinted gel particles, followed by adding H_2O_2 (10 mM). The UV absorbance was then converted to concentrations *c*, through Beer's law: $A = \varepsilon cl$ (ε = 39 000, 36 800, and 3058 M^{-1} cm^{-1} for the products of TMB, ABTS, and dopamine, respectively; *l* is the pathlength of 1 cm). The background oxidation was subtracted for all the kinetics. The catalytic parameters were obtained by using the Michaelis–Menten equation. The nanoparticle molar concentration of Fe_3O_4 was used as the nanozyme concentration. With 50 μg/mL of Fe_3O_4 nanoparticles in the gels and an average size of 30 nm, we calculated the nanoparticle molar concentration is 1.1 nM. The oxidation reactions by other nanozymes and their imprinted gels (nanoceria, 100 μg/mL; AuNPs, 10 nM) were tested in the same way.

5.3 Results and discussion

5.3.1 Fe_3O_4 NPs as a peroxidase-mimicking nanozyme.

Iron oxide nanoparticles (Fe_3O_4 NPs) are among the first reported nanozymes with peroxidase-mimicking activity.[90] We chose to study it because of its robust activity and excellent biocompatibility. We prepared Fe_3O_4 NPs using the hydrothermal method.[163] A TEM micrograph of our Fe_3O_4 NPs is shown in Figure 5.1B. The average particle size is around 30 nm and they appear aggregated because of drying on the TEM grid and we avoided strong surface capping ligands during synthesis. To confirm its peroxidase-like activity, we respectively mixed TMB and ABTS substrates with the Fe_3O_4 NPs and H_2O_2. A blue color was observed with TMB, and green color with ABTS, indicating both were oxidized (Figure 5.1A). Without the Fe_3O_4 NPs, no color change occurred for either compound, indicating the catalytic role of Fe_3O_4. If H_2O_2 was omitted, no color change occurred with Fe_3O_4 NPs alone, confirming Fe_3O_4 was a peroxidase-like nanozyme.

The Fe_3O_4 NPs can oxidize both TMB and ABTS in the presence of H_2O_2, and thus it has poor substrate specificity. We hope to create substrate binding pockets on the Fe_3O_4 NPs using MIPs to selectively oxidize only one of them. Before imprinting, we first tested the binding property of the substrate TMB and ABTS on the Fe_3O_4 NPs. We measured the ζ-potential of free Fe_3O_4 NPs to be -18.5 mV (Figure 5.1C). Adding TMB increased the charge to -11.2 mV, suggesting TMB adsorption. Adding ABTS further decreased the charge of Fe_3O_4, also suggesting adsorption. Therefore, at least a fraction of the added substrates was adsorbed by the Fe_3O_4 to enable surface imprinting.

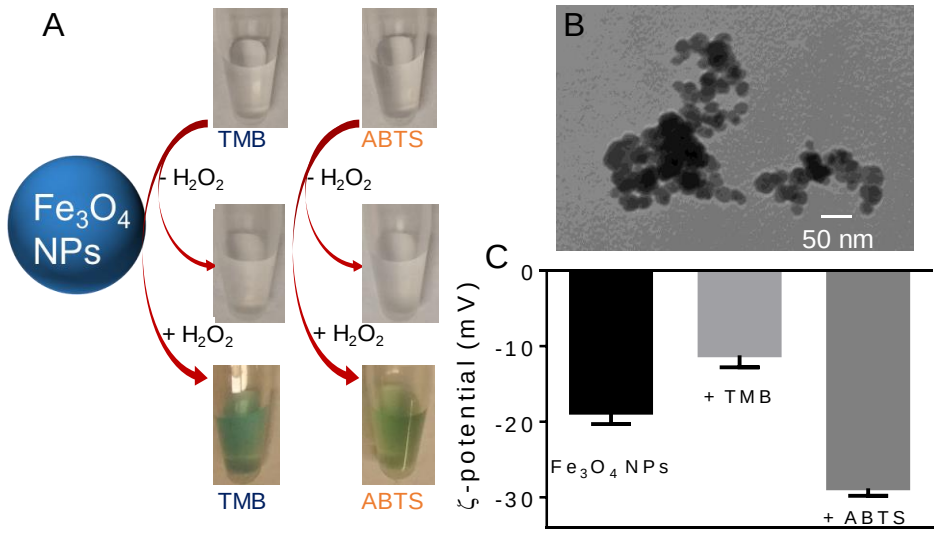

Figure 5.1 (A) Photographs showing the catalytic activity of the Fe_3O_4 NPs for oxidation of TMB and ABTS with or without H_2O_2. Fe_3O_4 NPs (50 μg/mL), 0.5 mM substrates and 10 mM H_2O_2 were used in the oxidations for 30 min in acetate buffer (20 mM, pH 4.0) at room temperature. (B) TEM micrographs of Fe_3O_4 NPs. (C) ζ-potential of the Fe_3O_4 NPs in HEPES buffer (20 mM, pH 7.6) and after adding 1 mM TMB or ABTS.

5.3.2 Imprinting on Fe_3O_4 NPs.

After confirming the adsorption, we then copolymerized the Fe_3O_4 NPs into nanogels through imprinting and polymerization using the same method as in the Chapter 3. The TMB and ABTS imprinted gels are named T-MIP and A-MIP, respectively. In addition, we also prepared the same gel but in the absence of TMB or ABTS. These control gels are named NIP only containing the Fe_3O_4 NPs. The nanogels have an average hydrodynamic size of 215 ± 28 nm characterized by DLS. To further characterize the nanogels, SEM was measured on lyophilized samples (Figure 5.2A) showing the iron oxide core entrapped in the nanogel. The EDX spectrum of the analyzed area (red square in Figure 5.2A) indicates the presence of iron along with carbon,

nitrogen and oxygen (Figure 5.2B). The nanogels had a similar iron incorporation efficiency of around 81 ± 7 % measured by ICP-MS after dissolving the Fe_3O_4 in the gels by nitric acid (Figure 5.2C).

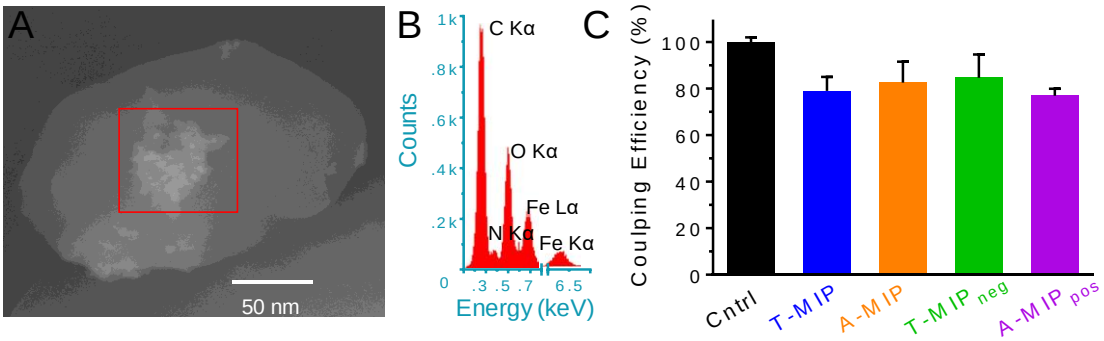

Figure 5.2 (A) An SEM micrograph of a T-MIP nanogel and (B) its EDX elemental spectrum on the analyzed area defined by the red square. (C) ICP-MS analysis of iron incorporation efficiency in the nanogels. The Fe_3O_4 NPs were dissolved by nitric acid and then diluted for ICP-MS analysis. A control sample of Fe_3O_4 NPs (60 μg/mL) without nanogels were also used for comparison. The incorporation percentages of iron in the nanogels were normalized to the initial added Fe_3O_4 in gel preparation (60 μg/mL, the first bar, Cntrl).

5.3.3 Imprinting enhanced catalytic activity of nanozymes

After preparing these imprinted nanozymes, we next measured their activity. Based on their incorporation efficiencies, all the nanogels were standardized containing the same concentration of Fe_3O_4 NPs (50 μg/mL) as the free Fe_3O_4 NPs control for our experiment. When TMB was catalyzed by free Fe_3O_4 NPs for 30 min, the absorption peak of the oxidation product at 652 nm reached 0.13 (Figure 5.3A, black trace). Next, the non-imprinted NIP sample was tested, and it has a similar activity (red trace). The results suggest that the gel layer was quite porous allowing efficient substrate diffusion to the surface.[43, 133] After we measured these control samples, the

TMB-imprinted sample (T-MIP) was measured for TMB oxidation, and it showed an increased absorbance reaching 0.23 (blue trace). Therefore, imprinted enhanced the activity by about one-fold. We next compared their reaction kinetics (Figure 5.3B), and a similar conclusion was obtained.

To test generality, we also tested the activity of the ABTS imprinted nanogels (A-MIP) (Figure 5.3 C and D). With the ABTS as the substrate, the A-MIP nanogel has an oxidation rate of 0.047 min^{-1}, 2.4-fold faster than that of the free Fe_3O_4 NPs (0.020 min^{-1}, Figure 5.3D). Overall, the imprinted nanogels slightly enhanced the catalytic activity of Fe_3O_4 NPs for its imprinted target. Modification of nanozyme surface were reported that enhanced its activity. For example, Fan and co-workers attached histidine to Fe_3O_4 NPs increasing its peroxidase-like activity by 20-fold.[161] Fluoride adsorption on nanoceria and increased its oxidase-like turnover by nearly 100-fold.[99] Shen and co-workers prepared MIP around TiO_2 as a photocatalyst also showing enhanced activity.[70]

We next measured the rates of the nanozymes at various substrate concentrations (Figure 5.3E and F). Based on the Michaelis-Menten model, their catalytic parameters are summarized in Table 5.1. The k_{cat} of T-MIP nanogel (15.0 s^{-1}) is more than twice of the free Fe_3O_4 NPs and the A-MIP gels when oxidizing TMB. The T-MIP also has the highest affinity for TMB as indicated from its smallest K_m of 218 μM. For oxidizing ABTS, the A-MIP gel has the highest activity and affinity with a k_{cat} of 70.1 s^{-1} and the smallest K_m of 135 μM. Overall, the catalytic efficiency has enhanced towards their template targets by imprinting.

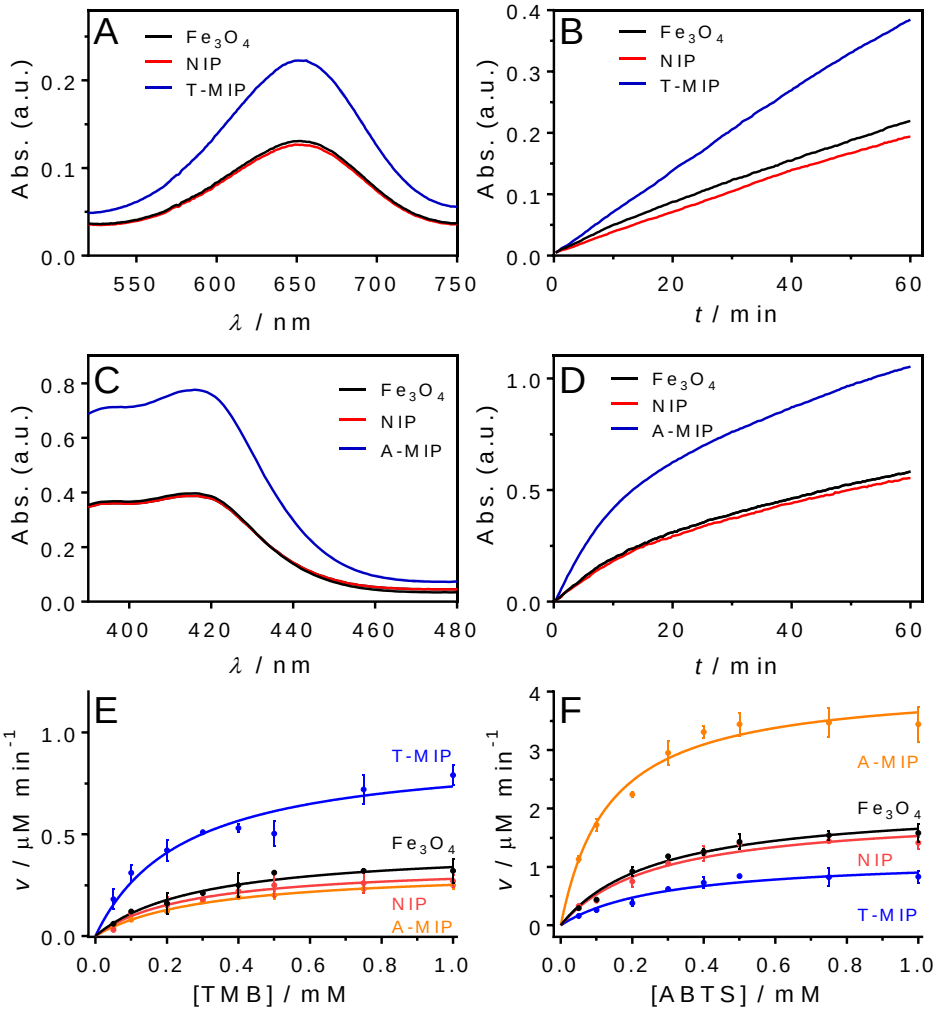

Figure 5.3 UV−vis spectra after 30 min of (A) TMB, (C) ABTS oxidations; and their kinetics of (B) TMB and (D) ABTS oxidation by free Fe_3O_4 NPs and different nanogels monitored at 652 nm and 420 nm respectively. Catalytic rates with various concentrations of (E) TMB and (F) ABTS by the free Fe_3O_4 NPs and different nanogels. The free Fe_3O_4 NPs and all the nanogels (~5 mg/mL) have the same concentration of Fe_3O_4 (50 μg/mL). All the reactions were with 10 mM H_2O_2 in acetate buffer (20 mM, pH 4) at 25 °C.

Table 5.1 Catalytic parameters of the free Fe_3O_4 NPs and the imprinted nanogels for oxidation of TMB and ABTS.[a]

Sub.	Enzyme	V_{max} (μM min^{-1})	k_{cat} (s^{-1})	K_m (μM)	k_{cat}/K_m (10^{-2} s^{-1} $μM^{-1}$)
TMB	Fe_3O_4	0.43 ± 0.04	7.1 ± 0.4	295 ± 30	2.4 ± 0.02
	NIP	0.36 ± 0.03	6.0 ± 0.3	266 ± 26	2.2 ± 0.05
	T-MIP	0.9 ± 0.04	15.0 ± 0.4	218 ± 24	6.8 ± 0.4
	T-MIPneg	3.4 ± 0.2	56.1 ± 1.7	150 ± 18	37.7 ±2.5
	A-MIP	0.3 ± 0.01	5.0 ± 0.08	316 ± 28	1.6 ± 0.1
	A-MIPpos	0.2 ± 0.04	3.3 ± 0.2	493 ± 26	0.7 ± 0.1
ABTS	Fe_3O_4	2.1 ± 0.1	35.0 ± 0.8	270 ± 34	12.9 ± 1.1
	NIP	1.9 ± 0.2	31.6 ± 1.8	267 ± 28	11.8 ± 0.03
	T-MIP	0.7 ± 0.05	11.6 ± 0.2	302 ± 26	3.8 ± 0.6
	T-MIPneg	0.4 ± 0.06	6.6 ± 0.2	360 ± 30	1.8 ± 0.02
	A-MIP	4.2 ± 0.2	70.1 ± 1.8	135 ± 22	51.8 ± 6.8
	A-MIPpos	6.5 ± 0.2	108.3 ± 1.7	93 ± 10	116.4 ± 9.5

[a] V_{max} is the maximal reaction velocity, k_{cat} is the catalytic constant, $k_{cat} = V_{max}/[E]$, and the $[E]$ is the molar concentration of Fe_3O_4 nanoparticles (1.1 nM); K_m is the Michaelis constant.

5.3.4 Imprinting enhanced specificity of nanozymes

The enhance activity may lead to better specificity, which is the main goal of the current work. Next we measured specificity by also reacting the T-MIP gel with ABTS, and A-MIP with

TMB. In general, the non-template substrate has lower activity than the template, (e.g., compare the orange and blue lines in Figure 5.3 E and F). Therefore, with this simple imprinting process, substrate specificity was achieved.

To quantify specificity, we compared their catalytic efficiency with k_{cat}/K_m.[140] T-MIP has 2.8-fold higher of k_{cat}/K_m (6.8 $\times 10^{-2}$ s^{-1} μM^{-1}) than that of bare Fe_3O_4 NPs (2.4 $\times 10^{-2}$ s^{-1} μM^{-1}, Figure 5.4A). When oxidizing ABTS, the same gel showed ~3 times lower k_{cat}/K_m than the bare Fe_3O_4 NPs (Figure 5.4B). Similarly, the A-MIP has 4-fold higher specificity than the bare Fe_3O_4 NPs for oxidizing ABTS (Figure 5.4B), but 1.5-fold lower for oxidizing TMB (Figure 5.4A). Overall, Fe_3O_4 NPs achieved a moderate substrate selectivity through imprinting.

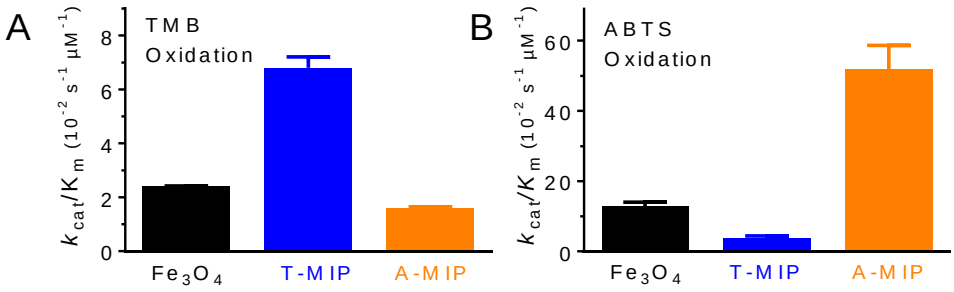

Figure 5.4 The catalytic efficiency (k_{cat}/K_m) of free Fe_3O_4 NPs and the two imprinted gels (T-MIP and A-MIP) for oxidizing (A) TMB and (B) ABTS.

5.3.5 Charged functional monomers further improve specificity and activity.

Encouraged by the above results, we aimed to further improve imprinting. The above prepared nanogels were close to neutral charged (average ξ-potential ≈ + 4.2 mV (SD ± 1.2) by DLS). Since TMB ($pK_a \approx 4.2$) carries a positive charge and ABTS ($pK_a \approx 2.1$) carries a negative charge in the reaction condition (acetate buffer, pH 4),[156] specificity might be further improved by introducing charged monomers. For this purpose, we prepared new gels by incorporating an

anionic monomer AMPS for TMB imprinting, named T-MIPneg gels, and incorporating a cationic monomer DMPA for ABTS imprinting, named as A-MIPpos gels (see the monomer structure in the Figure 5.5A). The ξ-potential of the gels were determined by DLS. The T-MIPneg gels were negatively charged with a potential of -21.4 mV (SD ±2.5) and the A-MIPpos gels were positively charged with a potential of +33.1 mV (SD ±1.4) indicating the successful incorporation of the charged monomers.

We next measured the activities of these charged gels. Their catalytic rates were determined at various concentrations of TMB and ABTS (Figure 5.5B and C), and the k_{cat} and K_m values are presented in Table 5.1. For TMB oxidation, the k_{cat} value increased 7.9-fold with the T-MIPneg gel compared to that with free Fe_3O_4 NPs, while the A-MIPpos gel even suppressed the activity by ~50% (Table 5.1). At the same time, the K_m dropped by 50% for the T-MIPneg, suggesting even tighter substrate binding. We plotted k_{cat}/K_m of these imprinted nanozymes to compare enzyme specificity (Figure 5.5D and E). The T-MIPneg has the best catalytic efficiency, 15-fold higher than that of the bare Fe_3O_4 NPs, much better than the 3-fold improvement for the T-MIP gel without the negative AMPS monomer (Figure 5.5D). At the same time, the T-MIPneg has the least efficiency for ABTS oxidation (Figure 5.5E). The same trend was also observed for the A-MIPpos gel.

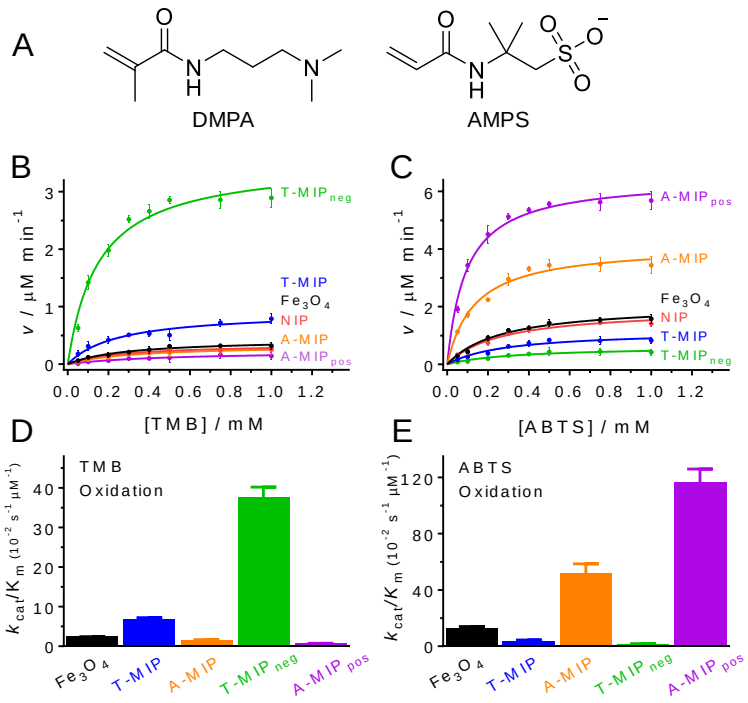

Figure 5.5 (A) The structure of the charged functional monomers. Catalytic rates in the presence of various concentrations of (B) TMB and (C) ABTS substrates by the free Fe_3O_4 NPs and different nanogels. The catalytic specificity (k_{cat}/K_m) of free Fe_3O_4 NPs and the four imprinted nanogels for oxidizing (D) TMB and (E) ABTS. The free Fe_3O_4 NPs and all the nanogels (~5 mg/mL) have the same concentration of Fe_3O_4 (50 μg/mL). All the reactions were with 10 mM H_2O_2 in acetate buffer (20 mM, pH 4) at 25 °C.

To quantify the specificity, we plotted the enhanced folds of substrate selectivity based on normalized k_{cat}/K_m values of one substrate over another (Figure 5.6). In the best case, the selectivity for TMB over ABTS using the T-MIPneg nanozyme is 98-fold (Figure 5.6A), while the selectivity for ABTS over TMB using the A-MIPpos nanozyme is 33-fold (Figure 5.6B).

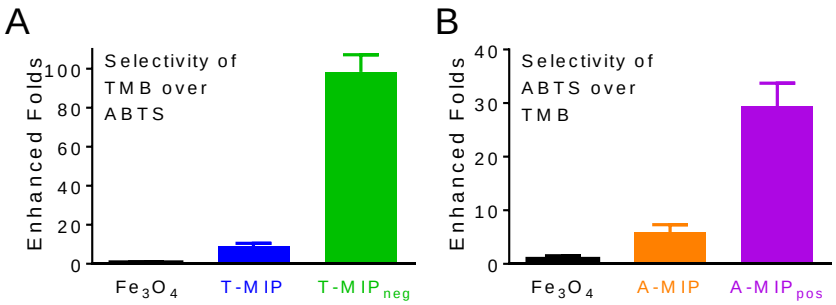

Figure 5.6 The fold of specificity enhancement of (A) bare Fe_3O_4 NPs, T-MIP, and T-MIPneg oxidizing TMB over ABTS, and (B) bare Fe_3O_4 NPs, A-MIP, and A-MIPpos oxidizing ABTS over TMB. The enhancement was calculated using normalized k_{cat}/K_m of oxidizing TMB divided that oxidizing ABTS.

5.3.6 Binding thermodynamics.

The above measurements were performed only using activity assays. The significantly enhanced specificity suggests successfully engineered substrate binding pockets. To further confirm this, and to understand the thermodynamics of binding, ITC was employed. In this experiment, TMB or ABTS was gradually titrated into the imprinted or non-imprinted nanogels, and the amount of heat released was recorded as a function of time (Figure 5.7, top panels). Most reactions released heat, which was favorable for binding. The binding site of the gel samples is ~0.4 mM as determined by UV spectroscopy after imprinting. By integrating the heat released (the lower panels), we calculated the enthalpy of the reaction. The titration curves also allow us to directly calculate the K_d of each reaction, and then the ΔG and ΔS were calculated. These thermodynamic values are listed in Table 5.2.

The T-MIP nanogels released more heat and have a higher affinity for binding TMB (Figure 5.7A, K_d = 27 μM) than binding ABTS (Figure 5.7B, K_d = 142 μM) indicating enhanced

bind specificity through imprinting. After incorporating charged monomers (T-MIPneg, Figure 5.7C and D), the binding specificity was significantly enhanced with the highest heat released and strongest affinity for TMB (Figure 5.7C, K_d = 20 μM) over binding ABTS (Figure 5.7D, no measurable binding). For ABTS imprinted gels (A-MIP and A-MIPpos), the same binding trend to ABTS was also observed (Figure 5.7E-H, Table 5.2). In general, charged monomers led to more heat release (e.g., enthalpy change). Imprinting can enhance binding affinity and selectivity to the imprinted substrates, and functional monomers further improves specificity, which explains the enhanced nanozyme specificity after imprinting.

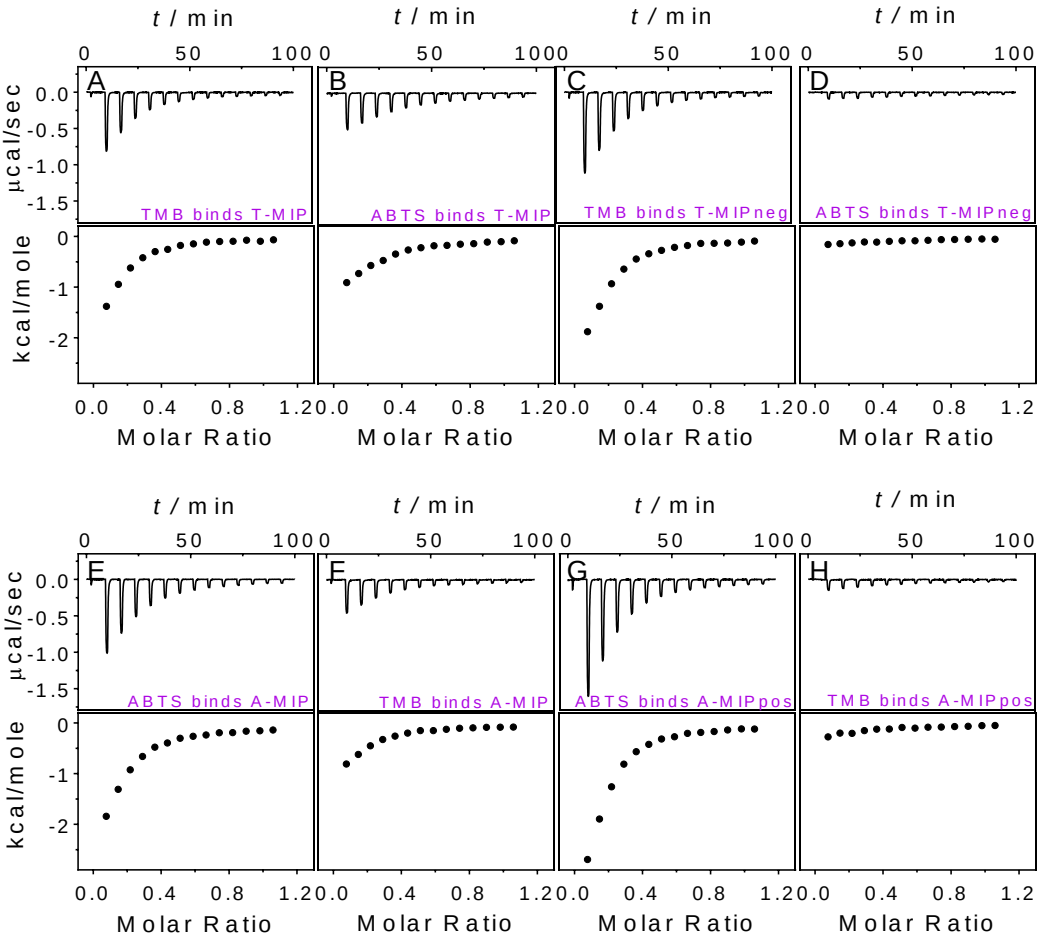

Figure 5.7 ITC traces at 298 K for binding TMB or ABTS by (A, B) T-MIP, (C, D) T-MIPneg, (E, F) A-MIP and (G, H) A-MIPpos nanogels. TMB and ABTS (2 mM) and the nanogels (5.0

mg/mL) were dispersed in the same buffer (20 mM acetate, pH 4, 1% v/v DMSO). The binding sites of the gel samples were determined as 0.4 mM and used for the calculation of molar ratio. The original titration traces (top) and the integrated heat (below) of each reaction are shown.

Table 5.2 The thermodynamic parameters of the imprinted gels calculated from ITC.[a]

Subs.	**Gel samples**	K_a ($\times 10^4$ M^{-1})	K_d (μM)	**ΔG** (kcal mol^{-1})	**ΔH** (kcal mol^{-1})	**ΔS** (cal $K^{-1}mol^{-1}$)
TMB	T-MIP	3.6 ±0.2	27.8 ±1.5	-6.1	-1.8 ±0.1	14.8
	T-MIPneg	4.8 ±0.2	20.8 ±0.8	-6.3	-2.7 ±0.2	12.4
	A-MIP	0.8 ±0.1	125.0 ±15.9	-5.3	-1.2 ±0.1	13.8
	A-MIPpos	-[b]	-	-	-0.3 ±0.02	-
ABTS	T-MIP	0.7 ±0.06	142.8 ±12.4	-5.2	-1.3 ±0.05	13.2
	T-MIPneg	-	-	-	-0.2 ±0.01	-
	A-MIP	3.9 ±0.2	25.6 ±1.3	-6.2	-2.6 ±0.1	12.2
	A-MIPpos	5.7 ±0.5	17.5 ±1.6	-6.4	-3.2 ±0.3	11.0

[a] The binding data were obtained using a one-site binding model. [b] Binding (K_a < 1000 M^{-1}) was not detectable by ITC.

5.3.7 Imprinting on other nanozymes.

So far, all our work was focused on Fe_3O_4 NPs. To test the generality of this approach, we next tried two more nanozymes: nanoceria (CeO_2) mimicking oxidase activity,[87] and AuNPs

mimicking peroxidase.[165] Different from Fe_3O_4 NPs, nanoceria can oxidize TMB and ABTS in the absence of H_2O_2 (e.g., oxidase). Therefore, these substrates are oxidized upon mixing with nanoceria, making it difficult for imprinting. Fortunately, the optimal pH for nanoceria is at pH 4.[87] Indeed, we confirmed that nanoceria is essentially non-active at pH 7.6 (20 mM HEPES, nitrogen atmosphere) but highly active at pH 4 (Figure 5.8A). This allowed us to imprint on nanoceria at pH 7.6.

These imprinted gels have similar size of 210 ± 18 nm (by DLS) as that of Fe_3O_4 containing nanogels, indicating that the growth of the gel is quite independent of the core composition. Then the activity of oxidizing TMB by free nanoceria and by different nanogels was measured (Figure 5.8B). After imprinting, the activity of nanoceria increased ~1.7-fold by T-MIP and more than 3-fold by T-MIPneg with the negatively charged (Figure 5.8B). While the T-MIP and T-MIPneg gels showed enhanced activity for TMB oxidation, they have limited activity for ABTS oxidation (Figure 5.8C) indicating the substrate selectivity was also achieved for nanoceria after imprinting.

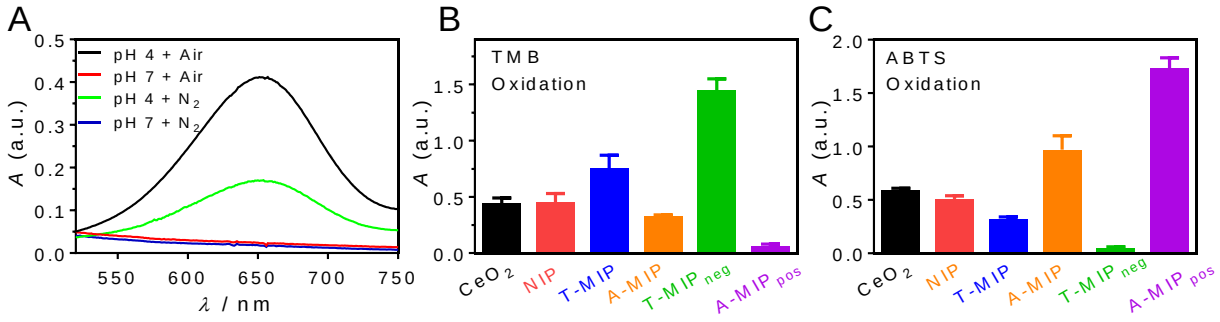

Figure 5.8 (A) The effect of pH and oxygen on the activity of nanoceria (CeO_2, 100 μg/mL) for oxidizing TMB (0.5 mM) at pH 7.6 (20 mM HEPES buffer) and pH 4.0 (20 mM acetate buffer), with or without nitrogen purge. The UV-vis spectra were measured after 30 min reaction monitored at 652 nm at 25 °C. CeO_2 NPs had no oxidation activity in the gel preparation condition (20 mM

HEPES buffer, pH 7.6, N_2 atmosphere). Oxidation of (B) TMB and (C) ABTS by free nanoceria (100 μg/mL) and different gels in the acetate buffer (20 mM, pH 4) at 25 °C.

Fe_3O_4 and nanoceria are both metal oxides, and we next tested a different type of material, AuNPs, which are also peroxidase mimics requiring H_2O_2.[165] We respectively imprinted it together with two substrates: TMB and dopamine. ABTS was not used since AuNPs cannot oxidize ABTS in the presence of H_2O_2. The dopamine imprinted nanogels were named using the same method starting with 'D-'. The enhanced activity and specificity was also observed (Figure 5.9). For example, the T-MIPneg showed the highest enhancement of 2.9-fold compared to the free AuNPs. Since dopamine has a positive charge in the test condition (pH 4.0), its best activity was observed with the D-MIPneg (Figure 5.9B).

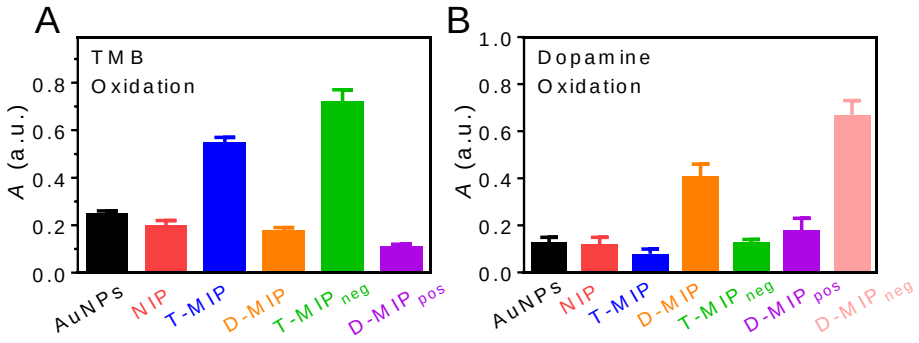

Figure 5.9 Oxidation of (A) TMB and (B) dopamine by free AuNPs (10 nM) and different gels in the acetate buffer (20 mM, pH 4) at 25 °C.

We have so far tested three nanozymes covering two types of materials (metal and metal oxide), two types of activities (oxidase and peroxidase), and three types of substrates (TMB, ABTS and dopamine). The results indicate that molecular imprinting is a general method for enhancing activity and specificity. Molecular imprinting was previously performed on TiO_2 to remove toxic

pollutants.[166-168] Some protein enzymes such as the horseradish peroxidase (HRP) are quite nonspecific and it accepts a broad range of substrates.[169] For example, HRP has a K_m of 434 μM for TMB,[90, 170] and 138 μM for ABTS, and the catalytic efficiencies for these two substrates are similar.[171] Using a similarly nonspecific peroxidase mimicking Fe_3O_4, we demonstrated excellent specificity even better than some natural enzymes. For example, the K_m of T-MIPneg for TMB is 2.9-fold lower than that of HRP, and the K_m of A-MIPpos for ABTS is also 1.5-fold lower (Table 5.1). The improvement in specificity (defined by k_{cat}/K_m) is much more significant.

In other cases, however, our ~100-fold selectivity still falls behind natural enzymes. Enzymes use a suite of mechanisms to achieve exquisite specificity, such as specific binding pockets, proofreading, and dynamic conformational changes. We only imprinted the substrate shape with simple electrostatic modulation in this case, and there is a lot more to learn from nature in future work.

5.4 Summary

In this work, molecular imprinting was successfully engineered on three different nanozymes for substrate specificity improvement. By incorporating functional monomers with charges, the activity and specificity were further improved. Under optimal conditions, specificity can reach ~100 fold. Selective substrate binding was confirmed also by ITC binding tests. With good specificity, additional advanced applications of nanozymes can be realized, including biosensors, selective destruction of disease-causing molecules and environmental contaminants, and delivery of therapeutic agents.

Chapter 6 Understanding the Catalytic Mechanism of Molecularly Imprinted Enzyme Mimics

6.1 Introduction

In the above study, we used molecular imprinting to create polymer-based substrate binding sites to address the specificity problem of the nanozymes. In addition to improved selectivity, the MIP layer also increased catalytic activity. This increased activity was quite general and was observed with DNAzymes (Chapter 3) and various nanozymes such as peroxidase-mimicking iron oxide and gold nanoparticles, oxidase-mimicking CeO_2 (Chapter 5). This increased activity suggests some fundamental processes that warrant further investigations.

To understand the catalytic mechanism of the imprinted enzyme mimics, we took a surface science approach and studied the catalysis process into three individual steps: substrate adsorption, reaction and product release. Each of these steps could be enhanced or inhibited by the MIP layer.

6.2 Materials and methods

6.2.1 Chemicals

ABTS, hydrogen peroxide (30 wt%), resorufin, and all the acrylic monomers were purchased from Sigma-Aldrich (St Louis, USA) and dissolved freshly in water. TMB, Amplex Red (AR) and hemin were also form Sigma-Aldrich and dissolved in DMSO to generate a freshly prepared stock solution. The G4 DNA (5′-acrydite-TTTGGGTAGGGCGGGTTGGGTATA) was purchased from Integrated DNA Technologies (IDT, Coralville, USA). Sodium chloride, sodium acetate, potassium chloride, SDS, acetic acid, HEPES were purchased from Mandel Scientific (Guelph, ON). Milli-Q water was used for all the experiments.

6.2.2 Preparation of imprinted nanogels

The imprinted nangels were prepared and characterized using the same method as described in above Chapters. For the DNAzyme imprinted nanogels, 20 μM AR or resorufin was mixed with the above prepared DNAzyme (1 μM) in HEPES buffer (20 mM, pH 7.4, 100 mM NaCl) for 30 min to form the initial imprinting complex in a 25 °C water bath. All the prepared gel samples were standardized to contain the same concentration of DNAzyme (100 nM) through UV−vis spectroscopy after polymerization.

6.2.3 Activity assays

For a typical peroxidation reaction, a substrate (0.5 mM) was mixed with free Fe_3O_4 NPs (50 μg/mL) or imprinted nanozyme (~5 mg/mL containing 50 μg/mL Fe_3O_4) in the buffer (20 mM acetate, pH 4). The absorption intensity of the oxidization products (652 nm for TMB, 420 nm for ABTS) was measured after adding 10 mM H_2O_2 using an Agilent 8453A spectrometer at 25 °C. To measure the enzyme parameters, various concentrations of substrate (0.05, 0.1, 0.2, 0.3, 0.4, 0.6, 0.8, 1 mM) were mixed with free Fe_3O_4 NPs (50 μg/mL) or imprinted gels in the buffer, followed by adding H_2O_2 (10 mM). The UV absorbance was then converted to concentrations *c*, through Beer's law: $A = \varepsilon cl$ (ε = 39 000 and 36 800 M^{-1} cm^{-1} for the products of TMB and ABTS respectively. *l* is the path length of 1 cm). The background oxidation in the absence of H_2O_2 was subtracted for all the kinetics. The oxidation rates (*V*) were obtained by fitting a straight line to the initial linear region of the kinetic curves. V_{max} and K_m were obtained by fitting the data with the Michaelis–Menten equation: $V = V_{max}[S]/(K_m + [S])$ and k_{cat} was calculated by $V_{max} = k_{cat}[E]$, where [*S*] and [*E*] are the concentrations of substrates and nanozyme, respectively. The molar concentration of Fe_3O_4 NPs was used as the nanozyme concentration. With 50 μg/mL of Fe_3O_4

NPs in the gels and an average size of 30 nm, we calculated the nanoparticle molar concentration to be 1.1 nM.

6.2.4 Measurement of activation energy

The activation energy (E_a) values for the Fe_3O_4 NPs and different nanogels were calculated according to the Arrhenius equation: $\ln(v)=A-E_a / RT$, in which v is the catalytic rate; A is a constant; R is the gas constant; and T is temperature.

6.2.5 AR oxidation assays

For a typical reaction, 10 mM AR was incubated with the free DNAzyme or DNAzyme-imprinted nanogels (DNA 100 nM) at 25 °C for 30 min then added with 2 mM H_2O_2 to initialize the oxidation. The fluorescence intensity and kinetics were recorded using a Varian Eclipse fluorescence spectrometer (Agilent Technologies, Santa Clara, CA) with excitation at 550 nm and emission at 585 nm.

6.2.6 ITC

Isothermal titration calorimetry (ITC) was performed using a VP-ITC Microcalorimeter instrument (MicroCal). Prior to titration, each solution was degassed to remove air bubbles. The nanogels (1 mg/mL) dispersed in HEPES buffer (20 mM, pH 7.2, NaCl 100 mM, DMSO 2%) was loaded in a 1.45 mL ITC cell at 25 °C. AR or resorufin (280 μL, 0.5 mM) dissolved in the same buffer was titrated into the cell (20 μL each time, except for the first injection of 2 μL). The enthalpy (ΔH) and binding constant (K_a) were obtained through fitting the titration curves to a one-site binding model. The K_d values were calculated from $1/K_a$ and $\Delta G = -RT \ln(K_a)$, where R is the gas constant. ΔS is calculated from $\Delta G = \Delta H - T\Delta S$.

6.3 Results and discussion

6.3.1 General catalysis mechanism

In general, a heterogeneous catalyst works as shown in the Figure 6.1. First, the substrate needs to diffuse to the catalyst surface to be adsorbed. Second, the catalytic reaction takes place to yield the product. Finally, the product desorbs to regenerate the active site. If the final step does not happen, the surface is quickly blocked by the product and the activity of the catalyst is lost. In this work, we probed the imprinted enzyme mimics for each of these steps to understand the catalytic mechanism.

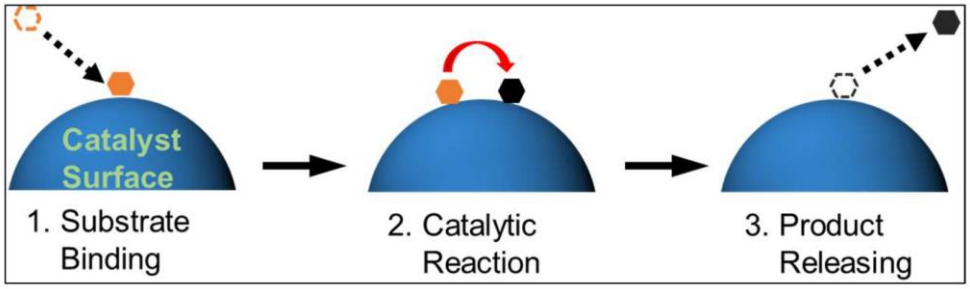

Figure 6.1 A scheme showing the reaction steps on a catalyst surface. Each step is individually studied to understand the effect of molecular imprinting.

6.3.2 Probing substrate binding

6.3.2.1 Increased local substrate concentration by imprinting

One of the most common applications of MIP is to selectively adsorb its template molecule.[172] Therefore, the substrate concentration near the enzyme mimics may be higher with the MIP, which may enhance the catalytic rate based on the mass action law (e.g., reaction rates scales with reactant concentration).[173] To quantitatively measure the effect of adsorption, we used several nanogels imprinted on Fe_3O_4 NPs, including A-MIP, A-MIPpos and NIP. The gels were

respectively mixed with ABTS for adsorption tests. The nanogels were prepared and characterized using the same method as described in the Chapter 5. The bare Fe_3O_4 NPs were also tested for comparison. After adsorptions, the adsorbed ABTS was determined by measuring the absorbance of the supernatant solutions after centrifugation (Figure 6.2A). To determine selectivity of adsorption, TMB was also tested as a control (Figure 6.2B). The adsorption percentages were quantified in the Figure 6.2C.

The bare Fe_3O_4 nanozyme adsorbed very little of ABTS or TMB, and this is understandable due to its limited surface area. The A-MIPpos gel adsorbed 41.4% of the added ABTS (Figure 6.2C). Since the total gel volume was ~10 μL (determined after centrifugation) dispersed in 200 μL of the substrate solution, the gel volume fraction was only 5%. Therefore, the ABTS concentration in the A-MIPpos gels increased by 8.4-fold (42%/5%). The non-charged A-MIP and NIP gels had a lower volume fraction of 2.5% (5 μL/200 μL). They adsorbed 18.1% and 6.2% of the total ABTS, (Figure 6.2C), and thus their local substrate concentrations increased by 7.2- and 2.5-fold respectively. Therefore, the local substrate concentrations in the MIP gels were enriched (Figure 6.2E), which might directly contribute to the enhanced catalytic activity.

In contrast, the two ABTS-imprinted MIP gels adsorbed very little TMB (Figure 6.2B and E). We compared the concentration of ABTS over TMB in these materials (Figure 6.2D). The A-MIPpos gel adsorbed 8.5-fold of ABTS than TMB, and the A-MIP gel adsorbed 3.6-fold. The NIP gel and bare Fe_3O_4 had no selective adsorptions. Therefore, selective substrate adsorption by imprinting might be the first reason of specific catalysis (Figure 3E).

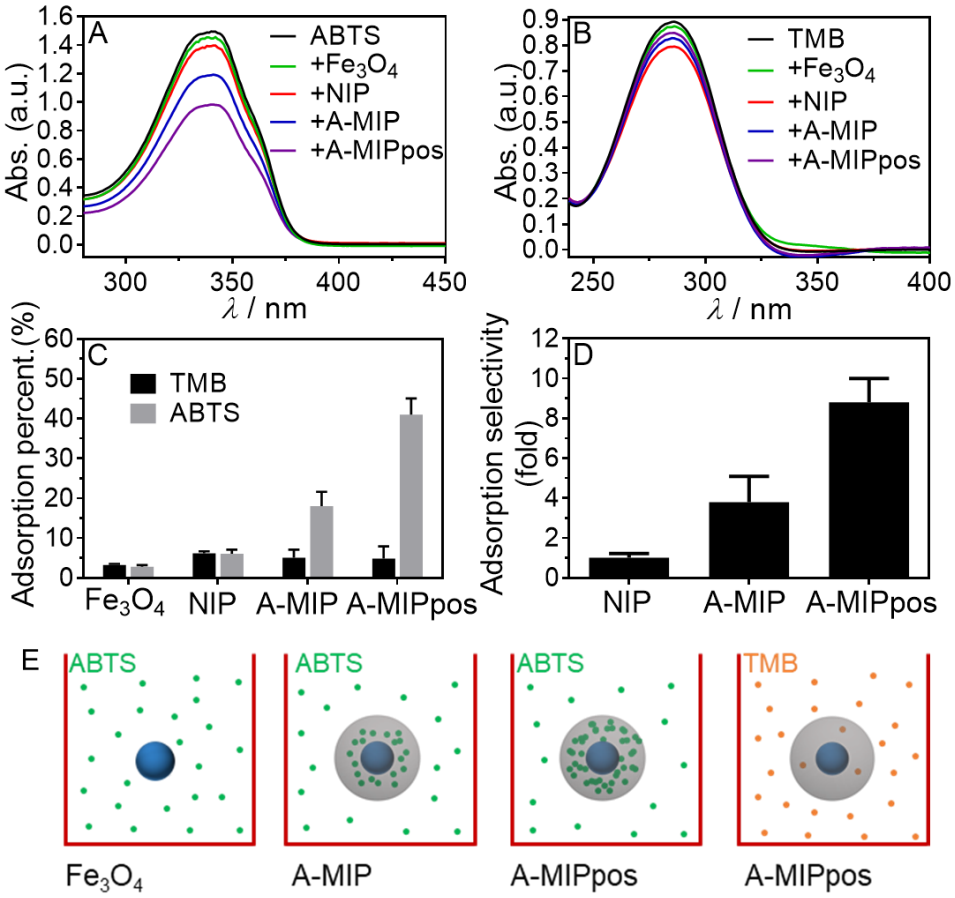

Figure 6.2 The UV-vis spectra of (A) ABTS and (B) TMB before and after adsorption by the bare Fe_3O_4 nanozyme and different imprinted or non-imprinted nanogels. (C) Adsorption percentages calculated from the spectra in (A, B). (D) Selectivity improvement of adsorption of ABTS over TMB by various gels. An initial concentration of 40 μM of ABTS and TMB in the acetate buffer (20mM, pH 4) was used for the tests. Fe_3O_4 (50 μg) or the nanogels (1 mg each) were incubated for 20 min and the supernatants were measured using UV-vis spectrometry. (E) A scheme showing substrate adsorption by the free Fe_3O_4 nanozyme and various MIP gels.

6.3.2.2 Substrate pre-incubation for probing molecular transportation.

With a thick gel layer, substrate diffusion to the nanozyme surface might take more time. The substrates were all pre-incubated for the above reactions (i.e., H_2O_2 added after adding

substrates). To understand substrate transportation kinetics, we then measured reactions without pre-incubation (i.e., added H_2O_2 and substrate at same time). The A-MIP, NIP gels and the bare Fe_3O_4 were all tested (Figure 6.3A-C, red curves). For the bare Fe_3O_4 and the A-MIP gel, within the first 5 min, the absorbance reached 0.12 (initial rate ~0.24 min^{-1}). For the NIP gel, the absorbance was only 0.05 (rate ~0.01 min^{-1}). At 20 min, the bare Fe_3O_4 absorbance was ~0.3, while the MIP was ~0.4. Therefore, for the MIP sample, the gel layer had a very fast substrate transportation kinetics. The same gel layer, if not imprinted, molecular transportation was much slower. Compared with the pre-incubated reactions (also plotted in the Figure 6.3A-C black curves), the samples without pre-incubation had slower initial rates (red curves). For example, the A-MIP gel without pre-incubation (0.24 min^{-1}) was slower initially than the pre-incubated one (0.61 min^{-1}), but they caught up to reach a similar rate after 8 min of reaction (Figure 6.3A). It is reasonable since substrate diffusing needs time in the beginning and the MIP gel layer with fast transportation was less affected once the steady-state kinetics were established.

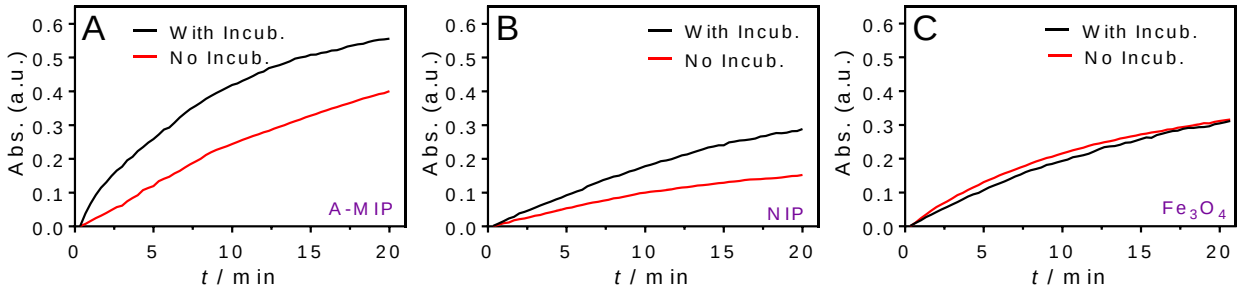

Figure 6.3 The kinetics of ABTS oxidation by (A) A-MIP, (B) NIP gels and (C) free Fe_3O_4 with or without 10 min of pre-incubation with ABTS. The free Fe_3O_4 and all the gels (~5 mg/mL) had the same concentration of Fe_3O_4 (50 μg/mL). All the reactions used 0.5 mM ABTS and 10 mM H_2O_2 in acetate buffer (20mM, pH 4) at 25 °C.

6.3.3 Probing the catalytic reaction.

The above studies probed the substrate adsorption step. MIP enriched the substrate near the nanozyme surface and thus can accelerate the reaction. We then probed the catalytic reaction by measuring the activation energy (E_a). The kinetics of ABTS oxidation by the MIP gels were measured at different temperatures (Figure 6.4A and D). For comparison, the free Fe_3O_4 nanozyme and NIP gels were also measured (Figure 6.4B and C). The E_a was calculated from the slope of the Arrhenius plot (Figure 6.4E). Our gels contained only 40 mol% of NIPAAm, and the lower critical solution temperature of the gels was higher than 40 °C,[134] and thus the gels remained dispersed in water during this experiment (10 – 40 °C). The E_a of the A-MIPpos gel was 13.8 kJ/mol, 2.1-fold lower than the free Fe_3O_4 nanozyme. For the A-MIP gel, its E_a was 19.7 kJ/mol, 1.5-fold lower than the Fe_3O_4. Therefore, the MIP gel layer lowered the E_a of the nanozyme. The NIP gel as control had an even higher E_a than the free nanozyme suggesting the importance of imprinting. Other strategies have also been made on nanozyme to improve its catalysis, e.g., surface modification and immobilization.[174-177] Our imprinted system clearly lowered E_a. Compared with protein enzyme (e.g., horseradish peroxidase, E_a ~ 40 kJ/mol),[178] our system had a lower E_a. At this moment, it is difficult to determining what the rate limiting step is in the reaction. The MIP layer on the Fe_3O_4 nanoparticle can selectively absorb specific template substrate used for imprinting. It is likely that the rate-limiting step would be the delivery of substrates to the reactive interface of the Fe_3O_4.

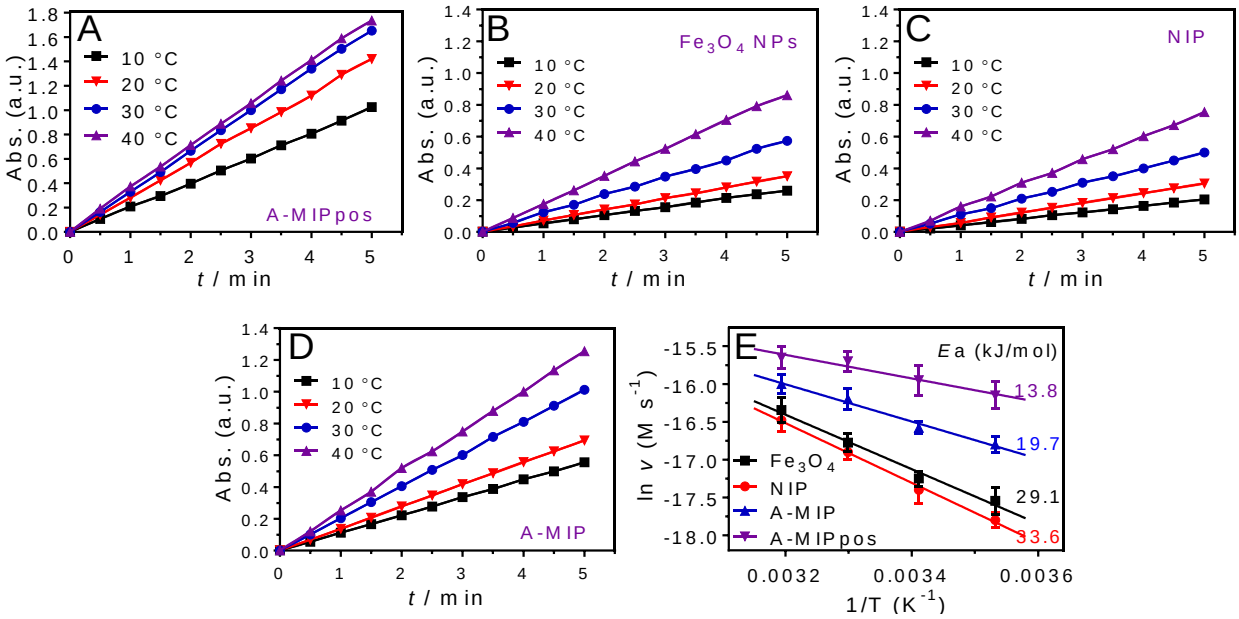

Figure 6.4 The kinetics of ABTS oxidation by (A) the A-MIPpos gel, (B) bare Fe_3O_4 NPs, (C) NIP and (D) A-MIP nanogels measured at different temperatures. (E) The Arrhenius plot of the bare Fe_3O_4 nanozymes and different gels to measure their E_a. The free Fe_3O_4 and all the gels had the same concentration of Fe_3O_4 (50 μg/mL). All the reactions were with 10 mM H_2O_2 in acetate buffer (20 mM, pH 4).

6.3.4 Probing product release.

We have so far probed substrate adsorption and measured the E_a. Aside from these, product release is also an important step. For example, tight product adsorption may inhibit the reaction. Therefore, we further studied product release of the imprinted nanozyme.

To do this, instead of imprinting the substrate, we imprinted the product and such gels might inhibit product release. For this experiment, we did not use ABTS or TMB since they cannot be completely oxidised and we could not get the pure oxidation products (Figure 6.5A). Therefore, we used Amplex red (AR) and its product, resorufin, can be obtained as a pure chemical. Since

Fe_3O_4 could not efficiently catalyse the peroxidation of AR, we used the acrydite-modified DNAzyme here. The activity of the DNAzyme catalysing AR oxidation has been studied in the Chapter 4.

To have a complete understanding, three type of gels were prepared: the substrate AR imprinted (AR-MIP), the product resorufin imprinted (RES-MIP), and non-imprinted (NIP) (Figure 6.5B). Their catalytic activities were then respectively measured for oxidizing AR. The free DNAzyme (without gel) was also measured for comparison (Figure 6.5C). The NIP gel has a similar rate as the free DNAzyme. The AR-MIP has the fastest rate of 225 ΔF min^{-1}, 2.3-fold enhanced than the free DNAzyme or the NIP gel (97 ΔF min^{-1}), which was expected from the substrate imprinting gels. Interestingly, the RES-MIP showed a lower rate (by 1.8-fold) than the free DNAzyme.

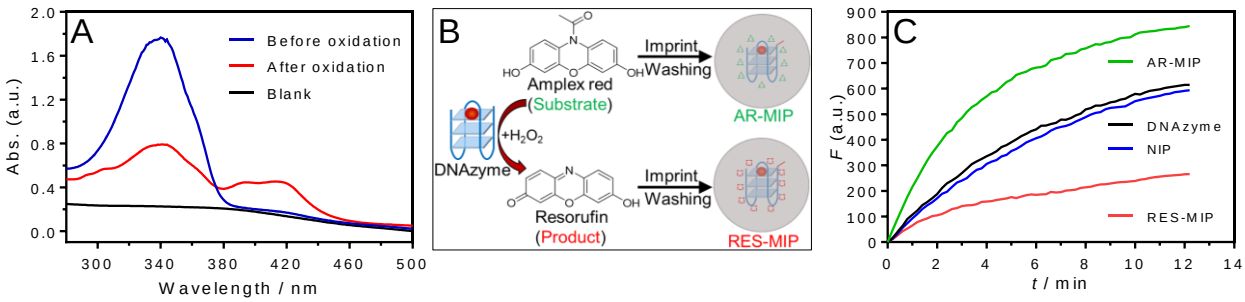

Figure 6.5 (A) The UV-vis spectra of 0.5 mM ABTS before and after oxidized by A-MIPpos gel (4 mg/mL) for 24 h in the buffer A at 25 °C. 10 mM H_2O_2 was added. The substrate ABTS and its oxidized product have the maximum adsorption at 340 nm and 420 nm respectively. After 24 h reaction, 40% of ABTS was still not oxidized. (B) A scheme of preparing the AR substrate imprinted (AR-MIP) and resorufin product imprinted gels (RES-MIP) on the DNAzyme. (C) The kinetics of AR oxidation by free DNAzyme and different gels. 100 nM of the DNAzyme and

hemin were used in the buffer (20 mM HEPES, pH 7.2, NaCl 100 mM) at 25 °C. 10 μM AR were used and all the gels were around 4 mg/mL containing 100 nM of the DNAzyme.

From the NIP and RES-MIP comparison, the product release step might contribute to the slower kinetics of RES-MIP. The unreleased products might occupy the active sites around the DNAzyme therefore inhibited the reaction. On the other hand, our substrate imprinted gels should have no problem of product release, and it may even promote product release (e.g., less tight product binding). To confirm this, we performed ITC to directly measure binding.

We respectively titrated AR and resorufin (RES) into the three type of gels: AR-MIP, RES-MIP and NIP, and the amount of heat released was recorded as a function of time (top panels, Figure 6.6). The background heat for the titrations into the buffer was also measured (Figure 6.6D and H). By integrating the heat (the lower panels), we directly obtained the enthalpy and dissociation constant, K_d, which allowed further calculation of ΔG and ΔS (Table 6.1). The AR-MIP gel had a stronger affinity for AR (Figure 6.6A, K_d =40.0 μM) than the RES-MIP and NIP gels (Figure 6.6B and C), indicating the importance of target imprinting. For the product resorufin, the RES-MIP gel had the strongest binding (Figure 6.6F, K_d =2.9 μM). The gel layer with strong product binding effectively prevented product release and inhibited the catalytic activity. On another hand, the AR-MIP gel and NIP gel essentially had no binding to resorufin (Figure 6.6E and G), suggesting that the non-imprinted gel layers did not specifically retain the product, and this could also be helpful for achieving catalytic turnover of the AR-imprinted gels. Overall, concentrating the substrate by the MIP enhanced the catalytic rate, while its prevention of product binding could be important for catalytic turnovers.

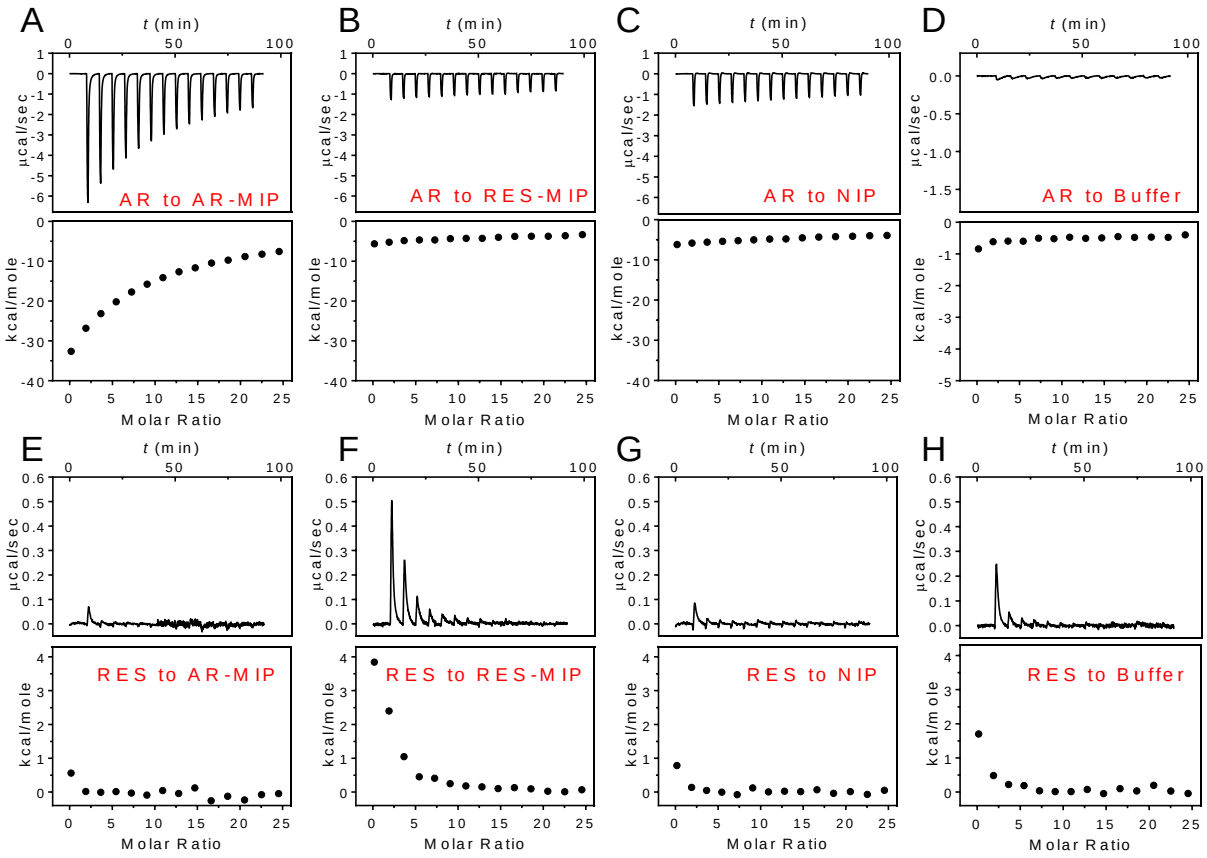

Figure 6.6 ITC traces at 298 K (25 °C) for binding (A-D) AR or (E-H) resorufin (RES) by different gels and the buffer. AR and resorufin (0.5 mM stock solution) and the gels (1 mg/mL) were dispersed in HEPES buffer (20 mM, pH 7.2, 100 mM NaCl, 2% DMSO). The binding site of the gels was estimated to be 4 µM as determined by UV spectroscopy after imprinting. The original titration traces (top) and the integrated heat (below) of each reaction are shown.

Table 6.1. The thermodynamic parameters of the imprinted nanogels calculated from ITC measured at 298.15 K.[a]

Substrate	Gel samples	K_a ($\times 10^5$ M^{-1})	K_d (μM)	ΔG (kcal mol^{-1})	ΔH (kcal mol^{-1})	ΔS (cal $K^{-1}mol^{-1}$)
AR	AR-MIP	0.25 ± 0.06	40.0	-5.9	-35.4 ±3.9	-98.6
	RES-MIP	-[b]	-	-	-5.6 ±0.5	-
	NIP	0.02 ± 0.01	500.0	-4.4	-7.0 ±0.8	8.7
Resorufin	AR-MIP	-	-	-	0.6 ±0.05	-
	RES-MIP	3.4 ±0.8	2.9	-7.5	4.7 ±0.4	40.9
	NIP	-	-	-	0.8 ±0.3	-

[a] The binding data were obtained using a one-site binding model. [b] Binding (K_a < 1000 M^{-1}) was not detectable by ITC.

It is also interesting to notice that AR-imprinted gel released heat upon AR binding, while the resorufin-imprinted gel absorbed heat upon resorufin binding. Therefore, resorufin binding is entropy driven and it is likely due to the more hydrophobic structure of resorufin. In this part, we studied AR mainly because of its oxidation products are commercially available.

Based on the above results, the enhanced activity can be explained by the enriched substrate adsorption and lowered E_a of the reaction. In addition, the MIP gels did not retain the products,

facilitating turnover of the active sites. Noted that the rate enhancement in these steps may overlap. The enhanced activity also has a significant contribution to the selectivity. Thus the imprinted nanozyme acted as a better enzyme mimic. At the same time, the transportation of the substrate was not affected by the MIP layer.

6.4 Summary

In summary, the catalytic mechanism of the imprinted enzyme mimics was studied into three separated steps: substrate adsorption, reaction, and product release. Imprinting enriched the substrate concentration near the nanozyme surface and contributed to the activity enhancement. The MIP gel layer has a fast molecular transportation kinetic compared to the NIP sample confirmed by the pre-incubation tests. The substrate-imprinted gels also lowered the reaction energy barrier with the lowest activation energy (E_a). The MIP gels did not retain the products confirmed with ITC tests. This study has rationalized improved activity and specificity of imprinted enzyme mimics and may guide further rational design of such materials.

Chapter 7 Conclusions and Future Work

7.1. Conclusions and original contributions

In this thesis work, molecular imprinting was combined with functional DNAs and nanozymes to improve the binding affinity and achieving selective catalysis. In addition, the catalytic activity was also significantly increased in the same process. Incorporation of DNA aptamers improved the binding affinity and signaling of MIPs. At the same time, MIP rescued the aptamer fragments that had no affinity. Some DNAzymes have peroxidase mimicking activity but lack substrate selectivity. Imprinting on the DNAzymes improved the substrate selectivity by around 10-fold. The method was also successfully applied to nanozymes mimicking oxidase and peroxidase activities. At the best optimization, the substrate selectivity was enhanced around 100-fold. Besides the improved specificity, imprinting also increased the activity of the enzyme mimics. Our subsequent mechanistic study demonstrated that specific adsorption of the imprinted substrate by the MIP gel to reach a high low substrate concentration is the major reason of the enhanced activity.

In Chapter 2, for the first time, we prepared new hybrid materials using aptamer fragments as macromonomers in MIPs. All the previous work used full-length aptamers to prepare MIPs. Using aptamer fragments can reduce the cost of DNA synthesis while still improving the MIP binding and signaling properties. We showed that even DNA sequences that cannot bind the target molecule can still be quite effective upon imprinting. Different DNA sequences perform differently in MIPs, and rational DNA sequence design is likely to be important for target molecules without known aptamers. We summarize our findings in the following aspects: (1) DNA help MIPs. Compared to the two synthetic monomers (AAm and NIPAAm), DNA

macromonomers increased the binding affinity by up to 18-fold. For optimal performance, the DNA sequence needs to be carefully designed and screened. (2) Imprinting helps aptamers. When both fragments are used, a fully functional aptamer can form. Compared to the free aptamer binding, the imprinted material has double the binding affinity by positioning the two fragments close to each other in an optimal configuration. This is consistent with previous reports using full-length aptamers. (3) It might be possible to *de novo* design DNA sequences to bind a given target molecule optimally without known aptamers. In this aspect, computer modeling might be a powerful tool to predict DNA oligomer sequences. (4) DNA may also allow convenient signaling. Over the past two decades, the analytical chemistry of aptamer has significantly advanced. By introducing such knowledge to MIPs, new and better biosensors might be produced. Overall, combining DNA oligomers and MIPs is a promising method for obtaining new functional materials.

In Chapter 3, molecular imprinting was used to solve the problem of poor specificity of enzyme mimics. Although many enzyme mimics have been developed in the past few decades, the problem of low specificity had rarely been addressed. We demonstrate a simple, cost-effective, and general yet highly effective method to create substrate binding pockets for a peroxidase mimicking DNAzyme by molecular imprinting. With imprinting, more than ten-fold of substrate selectivity was achieved by comparing two substrates TMB and ABTS. In addition, the catalytic activity of the DNAzyme was also enhanced by the polymer matrix compared to the free DNAzyme. In this case, the imprinted gel also stabilized the DNAzymes and was resistant at high temperature. Therefore, we proposed a general and powerful way to achieve functional enzyme mimics by combining molecular imprinting and enzyme mimics.

In Chapter 4, the imprinted nanogels were demonstrated to be an efficient method for intracellular catalysis. The activity and specificity of the DNAzyme were significantly improved. The imprinted nanogels showed excellent selectivity by using three different substrates. At the same time, the gel matrix protected the DNAzyme from degradation by DNase I and facilitated cellular uptake. Therefore, by using this imprinted nanogel, we provided an alternative approach for the traditional delivery of protein enzymes. DNAzymes have excellent stability and a low cost, while imprinting can improve the activity and specificity of the DNAzyme. By imprinting DNAzymes and other enzyme mimics (e.g., nanozymes) with other types of catalytic activities and by using biologically relevant molecules as templates, it is possible to produce nanogels that may have a practical biomedical impact.

In Chapter 5, molecular imprinting was further used on nanozymes. By using similarly cost-effective and robust MIPs, we solved an intrinsic problem of the nanozyme: lack of specificity. With molecular imprinting, we successfully engineered substrate binding pockets on three different nanozymes. By incorporating functional monomers with charges, the activity and specificity were further improved. Selective substrate binding was confirmed also by ITC and its thermodynamic parameters were obtained for fundamental insights. With good specificity, additional advanced applications of nanozymes can be realized, including biosensors, selective destruction of disease-causing molecules and environmental contaminants, and delivery of therapeutic agents.

In Chapter 6, the catalytic mechanism of imprinted enzyme mimics was illuminated. By taking a surface science approach, the catalytic process was studied into three separated steps: adsorption of the substrate, reaction, and product release. Through imprinting, the local substrate concentration was enriched by around 8-fold. The increased substrate concentration might be the

most important reason of the activity enhancement. Diffusion of the substrate across the imprinted gel layer is studied by a pre-incubation experiment, highlighting the difference between imprinted and non-imprinted gel layers. MIP layer had a faster molecular transportation kinetics. The activation energy was also measured, and the substrate imprinted sample had the lowest activation energy of 13.8 kJ mol^{-1}. Product release was also found to be improved by imprinting as studied by ITC. This study has rationalized the reason for improved activity and specificity of imprinted enzyme mimics and may guide further rational design of such hybrid materials.

7.2. Future work

The results presented in the thesis proved that molecular imprinting is an efficient approach to create specific binding sites on artificial enzymes. In addition, the catalytic activity is also enhanced due to enriched low substrate concentration. Functional DNAs and nanozymes are potent functional materials and their combination with MIP is an interesting way of forming hybrid materials with improved affinity and may lead to new signaling mechanisms. Several future research directions could be carried on.

First, DNA aptamer fragments used in the MIP could be optimized for further improvements. The formation of an initial binding complex is critical for imprinting effectivity. DNA aptamers binding with the targets could be tighter at lower temperatures and with stronger ionic strength. Therefore, the stronger binding complex enables higher affinity of prepared MIPs. A challenge might be difficult polymerization at the low temperature. Researchers may need to find different initialization methods, e.g., photo-initialization,[50] to perform polymerization and imprinting.

Second, more work could be carried out on the development of signaling mechanisms using DNA in MIPs. Signaling of binding events has been a major challenge for MIPs. Most binding measurements have relied on QCM or other mass/refractive index-based methods. DNA is known for its versatility in signal transduction and this is a promising direction. Various nanomaterials such as UCNPs and QDs coupled with DNA to achieve this goal have been reported,[179] and more advanced signal transduction designs could be performed by using fluorescently labeled DNA.

Third, formulation of the imprinted gel layers needs to be further optimized. For example, the gel layer thickness could be adjusted and the effect on molecular transportation needs to be evaluated. The gel pore sizes could be determined and adjusted by changing the crosslinker percentage. Beside acrylamide-based polymers, other type of matrix such as polydopamine could be utilized to perform imprinting on enzyme mimics.

References

(1) Ye, L.; Mosbach, K. Molecularly imprinted microspheres as antibody binding mimics. *React. Funct. Polym.* **2001,** *48*, 149-157.

(2) Wulff, G.; Liu, J. Design of biomimetic catalysts by molecular imprinting in synthetic polymers: the role of transition state stabilization. *Acc. Chem. Res.* **2011,** *45*, 239-247.

(3) Haupt, K. Peer reviewed: molecularly imprinted polymers: the next generation. *Anal. Chem.* **2003,** *75*, 376-383.

(4) Alexander, C.; Andersson, H. S.; Andersson, L. I.; Ansell, R. J., et al. Molecular imprinting science and technology: a survey of the literature for the years up to and including 2003. *J. Mol. Recognit.* **2006,** *19*, 106-180.

(5) Wulff, G.; Poll, H. G. Enzyme-analogue built polymers, 23. Influence of the structure of the binding sites on the selectivity for racemic resolution. *Makromol. Chem.* **1987,** *188*, 741-748.

(6) Ikegami, T.; Mukawa, T.; Nariai, H.; Takeuchi, T. Bisphenol A-recognition polymers prepared by covalent molecular imprinting. *Anal. Chim. Acta* **2004,** *504*, 131-135.

(7) Cieplak, M.; Szwabinska, K.; Sosnowska, M.; Chandra, B. K., et al. Selective electrochemical sensing of human serum albumin by semi-covalent molecular imprinting. *Biosens. Bioelectron.* **2015,** *74*, 960-966.

(8) Awino, J. K.; Gunasekara, R. W.; Zhao, Y. Selective recognition of d-aldohexoses in water by boronic acid-functionalized, molecularly imprinted cross-linked micelles. *J. Am. Chem. Soc.* **2016,** *138*, 9759-9762.

(9) Mayes, A.; Whitcombe, M. Synthetic strategies for the generation of molecularly imprinted organic polymers. *Adv. Drug Del. Rev.* **2005,** *57*, 1742-1778.

(10) Gaeta, M.; Oliveri, I. P.; Fragalà, M. E.; Failla, S., et al. Chirality of self-assembled achiral porphyrins induced by chiral Zn (II) Schiff-base complexes and maintained after spontaneous dissociation of the templates: a new case of chiral memory. *Chem. Commun.* **2016,** *52*, 8518-8521.

(11) Ye, L.; Mosbach, K. Molecular imprinting: synthetic materials as substitutes for biological antibodies and receptors. *Chem. Mater.* **2008,** *20*, 859-868.

(12) Komiyama, M.; Mori, T.; Ariga, K. Molecular Imprinting: Materials Nanoarchitectonics with Molecular Information. *Bull. Chem. Soc. Jpn.* **2018,** *91*, 1075-1111.

(13) Arshady, R.; Mosbach, K. Synthesis of substrate - selective polymers by host - guest polymerization. *Makromol. Chem.* **1981,** *182*, 687-692.

(14) Vlatakis, G.; Andersson, L. I.; Müller, R.; Mosbach, K. Drug assay using antibody mimics made by molecular imprinting. *Nature* **1993,** *361*, 645.

(15) Chen, L.; Xu, S.; Li, J. Recent advances in molecular imprinting technology: current status, challenges and highlighted applications. *Chem. Soc. Rev.* **2011,** *40*, 2922-2942.

(16) Karim, K.; Breton, F.; Rouillon, R.; Piletska, E. V., et al. How to find effective functional monomers for effective molecularly imprinted polymers? *Adv. Drug Del. Rev.* **2005,** *57*, 1795-1808.

(17) Yuan, Y.; Yang, Y.; Ma, X.; Meng, Q., et al. Molecularly Imprinted Porous Aromatic Frameworks and Their Composite Components for Selective Extraction of Uranium Ions. *Adv. Mater.* **2018,** *30*, 1706507.

(18) Dai, S.; Burleigh, M.; Ju, Y.; Gao, H., et al. Hierarchically imprinted sorbents for the separation of metal ions. *J. Am. Chem. Soc.* **2000,** *122*, 992-993.

(19) Hoshino, Y.; Koide, H.; Urakami, T.; Kanazawa, H., et al. Recognition, neutralization, and clearance of target peptides in the bloodstream of living mice by molecularly imprinted polymer nanoparticles: a plastic antibody. *J. Am. Chem. Soc.* **2010,** *132*, 6644-6645.

(20) Boitard, C.; Bée, A.; Ménager, C.; Griffete, N. Magnetic protein imprinted polymers: a review. *J. Mater. Chem. B* **2018,** *6*, 1563-1580.

(21) Ogiso, M.; Minoura, N.; Shinbo, T.; Shimizu, T. Detection of a specific DNA sequence by electrophoresis through a molecularly imprinted polymer. *Biomaterials* **2006,** *27*, 4177-4182.

(22) Ren, K.; Zare, R. N. Chemical recognition in cell-imprinted polymers. *ACS Nano* **2012,** *6*, 4314-4318.

(23) Dickert, F.; Hayden, O. Bioimprinting of polymers and sol− gel phases. Selective detection of yeasts with imprinted polymers. *Anal. Chem.* **2002,** *74*, 1302-1306.

(24) Whitcombe, M. J.; Kirsch, N.; Nicholls, I. A. Molecular imprinting science and technology: a survey of the literature for the years 2004–2011. *J. Mol. Recognit.* **2014,** *27*, 297-401.

(25) Cacho, C.; Turiel, E.; Martin-Esteban, A.; Ayala, D., et al. Semi-covalent imprinted polymer using propazine methacrylate as template molecule for the clean-up of triazines in soil and vegetable samples. *J. Chromatogr.* **2006,** *1114*, 255-262.

(26) Whitcombe, M. J.; Rodriguez, M. E.; Villar, P.; Vulfson, E. N. A new method for the introduction of recognition site functionality into polymers prepared by molecular imprinting: synthesis and characterization of polymeric receptors for cholesterol. *J. Am. Chem. Soc.* **1995,** *117*, 7105-7111.

(27) Türker, A. R. Separation, preconcentration and speciation of metal ions by solid phase extraction. *Sep. Purif. Rev.* **2012,** *41*, 169-206.

(28) Díaz-García, M. E.; Laínño, R. B. Molecular imprinting in sol-gel materials: Recent developments and applications. *Microchim. Acta* **2005,** *149*, 19-36.

(29) Zhang, H. Water-compatible molecularly imprinted polymers: promising synthetic substitutes for biological receptors. *Polymer* **2014,** *55*, 699-714.

(30) Cormack, P. A.; Elorza, A. Z. Molecularly imprinted polymers: synthesis and characterisation. *J. Chromatogr. B* **2004,** *804*, 173-182.

(31) Odian, G. *Principles of polymerization*, John Wiley & Sons: 2004.

(32) Billmeyer, F. *Textbook of polymer science*, Wiley: 1984; Vol. 19842, p 361-484.

(33) Wulff, G. Molecular imprinting in cross - linked materials with the aid of molecular templates—a way towards artificial antibodies. *Angew. Chem. Int. Ed.* **1995,** *34*, 1812-1832.

(34) Vaughan, A. D.; Sizemore, S. P.; Byrne, M. E. Enhancing molecularly imprinted polymer binding properties via controlled/living radical polymerization and reaction analysis. *Polymer* **2007,** *48*, 74-81.

(35) Baggiani, C.; Anfossi, L.; Baravalle, P.; Giovannoli, C., et al. Selectivity features of molecularly imprinted polymers recognising the carbamate group. *Anal. Chim. Acta* **2005,** *531*, 199-207.

(36) Yan, H.; Row, K. Characteristic and synthetic approach of molecularly imprinted polymer. *Int. J. Mol. Sci.* **2006,** *7*, 155-178.

(37) Jing, T.; Gao, X.-D.; Wang, P.; Wang, Y., et al. Determination of trace tetracycline antibiotics in foodstuffs by liquid chromatography–tandem mass spectrometry coupled with selective molecular-imprinted solid-phase extraction. *Anal. Bioanal. Chem.* **2009,** *393*, 2009–2018.

(38) Tan, C. J.; Chua, H. G.; Ker, K. H.; Tong, Y. W. Preparation of bovine serum albumin surface-imprinted submicrometer particles with magnetic susceptibility through core− shell miniemulsion polymerization. *Anal. Chem.* **2008,** *80*, 683-692.

(39) Pérez, N.; Whitcombe, M. J.; Vulfson, E. N. Molecularly imprinted nanoparticles prepared by core - shell emulsion polymerization. *J. Appl. Polym. Sci.* **2000,** *77*, 1851-1859.

(40) Cecchini, A.; Raffa, V.; Canfarotta, F.; Signore, G., et al. In vivo recognition of human vascular endothelial growth factor by molecularly imprinted polymers. *Nano Lett.* **2017,** *17*, 2307-2312.

(41) Yoshimatsu, K.; Reimhult, K.; Krozer, A.; Mosbach, K., et al. Uniform molecularly imprinted microspheres and nanoparticles prepared by precipitation polymerization: The control of particle size suitable for different analytical applications. *Anal. Chim. Acta* **2007,** *584*, 112-121.

(42) Chen, Z.; Ye, L. Controlling size and uniformity of molecularly imprinted nanoparticles using auxiliary template. *J. Mol. Recognit.* **2012,** *25*, 370-376.

(43) Ye, L.; Cormack, P. A.; Mosbach, K. Molecularly imprinted monodisperse microspheres for competitive radioassay. *Anal. Commun.* **1999,** *36*, 35-38.

(44) Poma, A.; Turner, A. P.; Piletsky, S. A. Advances in the manufacture of MIP nanoparticles. *Trends Biotechnol.* **2010,** *28*, 629-637.

(45) Kunath, S.; Panagiotopoulou, M.; Maximilien, J.; Marchyk, N., et al. Cell and tissue imaging with molecularly imprinted polymers as plastic antibody mimics. *Adv. Healthc. Mater.* **2015,** *4*, 1322-1326.

(46) Wang, C.; Javadi, A.; Ghaffari, M.; Gong, S. A pH-sensitive molecularly imprinted nanospheres/hydrogel composite as a coating for implantable biosensors. *Biomaterials* **2010,** *31*, 4944-4951.

(47) Pan, G.; Guo, Q.; Cao, C.; Yang, H., et al. Thermo-responsive molecularly imprinted nanogels for specific recognition and controlled release of proteins. *Soft Matter* **2013,** *9*, 3840-3850.

(48) Ye, L. Molecularly imprinted polymers with multi-functionality. *Anal. Bioanal. Chem.* **2016,** *408*, 1727-1733.

(49) Hoshino, Y.; Kodama, T.; Okahata, Y.; Shea, K. J. Peptide imprinted polymer nanoparticles: a plastic antibody. *J. Am. Chem. Soc.* **2008,** *130*, 15242-15243.

(50) Cutivet, A.; Schembri, C.; Kovensky, J.; Haupt, K. Molecularly imprinted microgels as enzyme inhibitors. *J. Am. Chem. Soc.* **2009,** *131*, 14699-14702.

(51) Daoud Attieh, M.; Zhao, Y.; Elkak, A.; Falcimaigne-Cordin, A., et al. Enzyme-Initiated Free-Radical Polymerization of Molecularly Imprinted Polymer Nanogels on a Solid Phase with an Immobilized Radical Source. *Angew. Chem.* **2017,** *129*, 3387-3391.

(52) Miyata, T.; Jige, M.; Nakaminami, T.; Uragami, T. Tumor marker-responsive behavior of gels prepared by biomolecular imprinting. *Proc. Natl. Acad. Sci.* **2006,** *103*, 1190-1193.

(53) Bowen, J. L. Detection of lipopolysaccharide pyrogens by molecularly imprinted polymers. PhD Thesis Cardiff University, 2011.

(54) Dechtrirat, D.; Gajovic-Eichelmann, N.; Bier, F. F.; Scheller, F. W. Hybrid material for protein sensing based on electrosynthesized MIP on a mannose terminated self‐assembled monolayer. *Adv. Funct. Mater.* **2014,** *24*, 2233-2239.

(55) Wilson, D. S.; Szostak, J. W. In vitro selection of functional nucleic acids. *Annu. Rev. Biochem.* **1999,** *68*, 611-647.

(56) Tuerk, C.; Gold, L. Systematic evolution of ligands by exponential enrichment: RNA ligands to bacteriophage T4 DNA polymerase. *Science* **1990,** *249*, 505-510.

(57) Famulok, M.; Hartig, J. S.; Mayer, G. Functional aptamers and aptazymes in biotechnology, diagnostics, and therapy. *Chem. Rev.* **2007,** *107*, 3715-3743.

(58) Huizenga, D. E.; Szostak, J. W. A DNA aptamer that binds adenosine and ATP. *Biochemistry* **1995,** *34*, 656-665.

(59) Liu, J.; Lu, Y. Fast colorimetric sensing of adenosine and cocaine based on a general sensor design involving aptamers and nanoparticles. *Angew. Chem. Int. Ed.* **2006,** *45*, 90-94.

(60) Stojanovic, M. N.; De Prada, P.; Landry, D. W. Aptamer-based folding fluorescent sensor for cocaine. *J. Am. Chem. Soc.* **2001,** *123*, 4928-4931.

(61) Xue, X.; Wang, F.; Liu, X. One-step, room temperature, colorimetric detection of mercury (Hg2+) using DNA/nanoparticle conjugates. *J. Am. Chem. Soc.* **2008,** *130*, 3244-3245.

(62) Joyce, G. F. Directed evolution of nucleic acid enzymes. *Annu. Rev. Biochem.* **2004,** *73*, 791-836.

(63) Liu, M.; Zhang, Q.; Chang, D.; Gu, J., et al. A DNAzyme feedback amplification strategy for biosensing. *Angew. Chem.* **2017,** *129*, 6238-6242.

(64) Silverman, S. K. Catalytic DNA: scope, applications, and biochemistry of deoxyribozymes. *Trends Biochem. Sci.* **2016,** *41*, 595-609.

(65) Travascio, P.; Witting, P. K.; Mauk, A. G.; Sen, D. The peroxidase activity of a hemin−DNA oligonucleotide complex: free radical damage to specific guanine bases of the DNA. *J. Am. Chem. Soc.* **2001,** *123*, 1337-1348.

(66) Li, W.; Li, Y.; Liu, Z.; Lin, B., et al. Insight into G-quadruplex-hemin DNAzyme/RNAzyme: adjacent adenine as the intramolecular species for remarkable enhancement of enzymatic activity. *Nucleic Acids Res.* **2016,** *44*, 7373-7384.

(67) Li, F.; Wang, C.; Guo, W. Multifunctional Poly‐N‐Isopropylacrylamide/DNAzyme Microgels as Highly Efficient and Recyclable Catalysts for Biosensing. *Adv. Funct. Mater.* **2018,** *28*, 1705876.

(68) Golub, E.; Albada, H. B.; Liao, W.-C.; Biniuri, Y., et al. Nucleoapzymes: hemin/G-quadruplex DNAzyme–aptamer binding site conjugates with superior enzyme-like catalytic functions. *J. Am. Chem. Soc.* **2015,** *138*, 164-172.

(69) Wang, X. Y.; Hu, Y. H.; Wei, H. Nanozymes in bionanotechnology: from sensing to therapeutics and beyond. *Inorg. Chem. Front.* **2016,** *3*, 41-60.

(70) Shen, X.; Zhu, L.; Liu, G.; Tang, H., et al. Photocatalytic removal of pentachlorophenol by means of an enzyme-like molecular imprinted photocatalyst and inhibition of the generation of highly toxic intermediates. *New J. Chem.* **2009,** *33*, 2278-2285.

(71) Liu, J.; Cao, Z.; Lu, Y. Functional nucleic acid sensors. *Chem. Rev.* **2009,** *109*, 1948-1998.

(72) Poma, A.; Brahmbhatt, H.; Pendergraff, H. M.; Watts, J. K., et al. Generation of novel hybrid aptamer–molecularly imprinted polymeric nanoparticles. *Adv. Mater.* **2015,** *27*, 750-758.

(73) Liu, J. Oligonucleotide-functionalized hydrogels as stimuli responsive materials and biosensors. *Soft Matter* **2011,** *7*, 6757-6767.

(74) Roh, Y. H.; Ruiz, R. C.; Peng, S.; Lee, J. B., et al. Engineering DNA-based functional materials. *Chem. Soc. Rev.* **2011,** *40*, 5730-5744.

(75) Bai, W.; Gariano, N. A.; Spivak, D. A. Macromolecular amplification of binding response in superaptamer hydrogels. *J. Am. Chem. Soc.* **2013,** *135*, 6977-6984.

(76) Ghanbari, K.; Roushani, M. A nanohybrid probe based on double recognition of an aptamer MIP grafted onto a MWCNTs-Chit nanocomposite for sensing hepatitis C virus core antigen. *Sensors Actuat. B Chem.* **2018,** *258*, 1066-1071.

(77) Li, S.; Liu, C.; Yin, G.; Zhang, Q., et al. Aptamer-molecularly imprinted sensor base on electrogenerated chemiluminescence energy transfer for detection of lincomycin. *Biosens. Bioelectron.* **2017,** *91*, 687-691.

(78) You, M.; Yang, S.; Tang, W.; Zhang, F., et al. Molecularly imprinted polymers-based electrochemical DNA biosensor for the determination of BRCA-1 amplified by SiO2@ Ag. *Biosens. Bioelectron.* **2018,** *112*, 72-78.

(79) Li, Q.; Fei, Y.; Gao, L.; Yu, Y., et al. G-Quadruplex DNA with an Apurinic Site as a Soft Molecularly Imprinted Sensing Platform. *Anal. Chem.* **2018,** *90*, 5552-5556.

(80) Liu, X.; Ren, J.; Su, L.; Gao, X., et al. Novel hybrid probe based on double recognition of aptamer-molecularly imprinted polymer grafted on upconversion nanoparticles for enrofloxacin sensing. *Biosens. Bioelectron.* **2017,** *87*, 203-208.

(81) Geng, Y.; Guo, M.; Tan, J.; Huang, S., et al. A fluorescent molecularly imprinted polymer using aptamer as a functional monomer for sensing of kanamycin. *Sensors Actuat. B Chem.* **2018,** *268*, 47-54.

(82) Brahmbhatt, H.; Poma, A.; Pendergraff, H.; Watts, J., et al. Improvement of DNA recognition through molecular imprinting: hybrid oligomer imprinted polymeric nanoparticles (oligoMIP NPs). *Biomater. Sci.* **2016,** *4*, 281-287.

(83) Poma, A.; Brahmbhatt, H.; Watts, J. K.; Turner, N. W. Nucleoside-tailored molecularly imprinted polymeric nanoparticles (MIP NPs). *Macromolecules* **2014,** *47*, 6322-6330.

(84) Mourão, C. A.; Bokeloh, F.; Xu, J.; Prost, E., et al. Dual-Oriented Solid-Phase Molecular Imprinting: Toward Selective Artificial Receptors for Recognition of Nucleotides in Water. *Macromolecules* **2017,** *50*, 7484-7490.

(85) Wei, H.; Wang, E. Nanomaterials with enzyme-like characteristics (nanozymes): next-generation artificial enzymes. *Chem. Soc. Rev.* **2013,** *42*, 6060-6093.

(86) Tokuyama, H.; Yamago, S.; Nakamura, E.; Shiraki, T., et al. Photoinduced biochemical activity of fullerene carboxylic acid. *J. Am. Chem. Soc.* **1993,** *115*, 7918-7919.

(87) Asati, A.; Santra, S.; Kaittanis, C.; Nath, S., et al. Oxidase-Like Activity of Polymer-Coated Cerium Oxide Nanoparticles. *Angew. Chem. Int. Ed.* **2009,** *48*, 2308-2312.

(88) Comotti, M.; Della Pina, C.; Matarrese, R.; Rossi, M. The Catalytic Activity of "Naked" Gold Particles. *Angew. Chem. Int. Ed.* **2004,** *43*, 5812-5815.

(89) Luo, W.; Zhu, C.; Su, S.; Li, D., et al. Self-catalyzed, self-limiting growth of glucose oxidase-mimicking gold nanoparticles. *ACS Nano* **2010,** *4*, 7451-7458.

(90) Gao, L.; Zhuang, J.; Nie, L.; Zhang, J., et al. Intrinsic peroxidase-like activity of ferromagnetic nanoparticles. *Nat. Nanotechnol.* **2007,** *2*, 577-583.

(91) Cai, R.; Yang, D.; Peng, S. J.; Chen, X. G., et al. Single Nanoparticle to 3D Supercage: Framing for an Artificial Enzyme System. *J. Am. Chem. Soc.* **2015,** *137*, 13957-13963.

(92) Zhang, L.; Han, L.; Hu, P.; Wang, L., et al. TiO2 nanotube arrays: intrinsic peroxidase mimetics. *Chem. Commun.* **2013,** *49*, 10480-10482.

(93) Pirmohamed, T.; Dowding, J. M.; Singh, S.; Wasserman, B., et al. Nanoceria exhibit redox state-dependent catalase mimetic activity. *Chem. Commun.* **2010,** *46*, 2736-2738.

(94) Korsvik, C.; Patil, S.; Seal, S.; Self, W. T. Superoxide dismutase mimetic properties exhibited by vacancy engineered ceria nanoparticles. *Chem. Commun.* **2007**, 1056-1058.

(95) Liang, H.; Lin, F.; Zhang, Z.; Liu, B., et al. Multicopper Laccase Mimicking Nanozymes with Nucleotides as Ligands. *ACS Appl. Mater. Interfaces* **2017,** *9*, 1352-1360.

(96) Manea, F.; Houillon, F. B.; Pasquato, L.; Scrimin, P. Nanozymes: Gold-nanoparticle-based transphosphorylation catalysts. *Angew. Chem. Int. Ed.* **2004,** *43*, 6165-6169.

(97) Zheng, X.; Liu, Q.; Jing, C.; Li, Y., et al. Catalytic Gold Nanoparticles for Nanoplasmonic Detection of DNA Hybridization. *Angew. Chem. Int. Ed.* **2011,** *50*, 11994-11998.

(98) Liang, M. M.; Fan, K. L.; Pan, Y.; Jiang, H., et al. Fe3O4 Magnetic Nanoparticle Peroxidase Mimetic-Based Colorimetric Assay for the Rapid Detection of Organophosphorus Pesticide and Nerve Agent. *Anal. Chem.* **2013,** *85*, 308-312.

(99) Liu, B.; Huang, Z.; Liu, J. Boosting the oxidase mimicking activity of nanoceria by fluoride capping: rivaling protein enzymes and ultrasensitive F- detection. *Nanoscale* **2016,** *8*, 13562-13567.

(100) Wang, N.; Zhu, L. H.; Wang, D. L.; Wang, M. Q., et al. Sono-assisted preparation of highly-efficient peroxidase-like Fe3O4 magnetic nanoparticles for catalytic removal of organic pollutants with H2O2. *Ultrason. Sonochem.* **2010,** *17*, 526-533.

(101) Gao, L. Z.; Fan, K. L.; Yan, X. Y. Iron Oxide Nanozyme: A Multifunctional Enzyme Mimetic for Biomedical Applications. *Theranostics* **2017,** *7*, 3207-3227.

(102) Zhang, L.; Liu, B.; Dong, S. Bifunctional nanostructure of magnetic core luminescent shell and its application as solid-state electrochemiluminescence sensor material. *J. Phys. Chem. B* **2007,** *111*, 10448-10452.

(103) Sudimack, J.; Lee, R. J. Targeted drug delivery via the folate receptor. *Adv. Drug Del. Rev.* **2000,** *41*, 147-162.

(104) Jiang, Z.; Kun, L.; Ouyang, H.; Liang, A., et al. A simple and sensitive fluorescence quenching method for the determination of H_2O_2 using rhodamine B and Fe_3O_4 nanocatalyst. *J. Fluoresc.* **2011,** *21*, 2015-2020.

(105) Wei, H.; Wang, E. Fe3O4 magnetic nanoparticles as peroxidase mimetics and their applications in H2O2 and glucose detection. *Anal. Chem.* **2008,** *80*, 2250-2254.

(106) Duan, D.; Fan, K.; Zhang, D.; Tan, S., et al. Nanozyme-strip for rapid local diagnosis of Ebola. *Biosens. Bioelectron.* **2015,** *74*, 134-141.

(107) Zhang, D.; Zhao, Y.-X.; Gao, Y.-J.; Gao, F.-P., et al. Anti-bacterial and in vivo tumor treatment by reactive oxygen species generated by magnetic nanoparticles. *J. Mater. Chem. B* **2013,** *1*, 5100-5107.

(108) Gao, L.; Yan, X. Nanozymes: an emerging field bridging nanotechnology and biology. *Sci China Life Sci* **2016,** *59*, 400-402.

(109) Rajeshkumar, S.; Naik, P. Synthesis and biomedical applications of cerium oxide nanoparticles–a review. *Biotechnol. Rep.* **2018,** *17*, 1-5.

(110) Karakoti, A.; Singh, S.; Dowding, J. M.; Seal, S., et al. Redox-active radical scavenging nanomaterials. *Chem. Soc. Rev.* **2010,** *39*, 4422-4432.

(111) Asati, A.; Kaittanis, C.; Santra, S.; Perez, J. M. pH-tunable oxidase-like activity of cerium oxide nanoparticles achieving sensitive fluorigenic detection of cancer biomarkers at neutral pH. *Anal. Chem.* **2011,** *83*, 2547-2553.

(112) Lin, Y. H.; Ren, J. S.; Qu, X. G. Nano-Gold as Artificial Enzymes: Hidden Talents. *Adv. Mater.* **2014,** *26*, 4200-4217.

(113) Hermann, T.; Patel, D. J. Adaptive recognition by nucleic acid aptamers. *Science* **2000,** *287*, 820-825.

(114) Haupt, K.; Mosbach, K. Molecularly imprinted polymers and their use in biomimetic sensors. *Chem. Rev.* **2000,** *100*, 2495-2504.

(115) Mahony, J.; Nolan, K.; Smyth, M.; Mizaikoff, B. Molecularly imprinted polymers—potential and challenges in analytical chemistry. *Anal. Chim. Acta* **2005,** *534*, 31-39.

(116) Jolly, P.; Tamboli, V.; Harniman, R. L.; Estrela, P., et al. Aptamer–MIP hybrid receptor for highly sensitive electrochemical detection of prostate specific antigen. *Biosens. Bioelectron.* **2016,** *75*, 188-195.

(117) Sharma, A. K.; Heemstra, J. M. Small-molecule-dependent split aptamer ligation. *J. Am. Chem. Soc.* **2011,** *133*, 12426-12429.

(118) Solomon, J. J.; Fedyk, J.; Mukai, F.; Segal, A. Direct alkylation of 2′-deoxynucleosides and DNA following in vitro reaction with acrylamide. *Cancer Res.* **1985,** *45*, 3465-3470.

(119) Dizdaroglu, M.; Jaruga, P.; Birincioglu, M.; Rodriguez, H. Free radical-induced damage to DNA: mechanisms and measurement. *Free Radic. Biol. Med.* **2002,** *32*, 1102-1115.

(120) Liao, Y.-J.; Shiang, Y.-C.; Huang, C.-C.; Chang, H.-T. Molecularly imprinted aptamers of gold nanoparticles for the enzymatic inhibition and detection of thrombin. *Langmuir* **2012,** *28*, 8944-8951.

(121) Helwa, Y.; Dave, N.; Froidevaux, R.; Samadi, A., et al. Aptamer-functionalized hydrogel microparticles for fast visual detection of mercury (II) and adenosine. *ACS Appl. Mater. Interfaces* **2012,** *4*, 2228-2233.

(122) Huang, P.-J. J.; Liu, J. Flow cytometry-assisted detection of adenosine in serum with an immobilized aptamer sensor. *Anal. Chem.* **2010,** *82*, 4020-4026.

(123) Xiang, Y.; Tong, A.; Lu, Y. Abasic site-containing DNAzyme and aptamer for label-free fluorescent detection of Pb2+ and adenosine with high sensitivity, selectivity, and tunable dynamic range. *J. Am. Chem. Soc.* **2009,** *131*, 15352-15357.

(124) Zhang, Z.; Oni, O.; Liu, J. New insights into a classic aptamer: binding sites, cooperativity and more sensitive adenosine detection. *Nucleic Acids Res.* **2017,** *45*, 7593-7601.

(125) Lin, C. H.; Patei, D. J. Structural basis of DNA folding and recognition in an AMP-DNA aptamer complex: distinct architectures but common recognition motifs for DNA and RNA aptamers complexed to AMP. *Chem. Biol.* **1997,** *4*, 817-832.

(126) Yakovchuk, P.; Protozanova, E.; Frank-Kamenetskii, M. D. Base-stacking and base-pairing contributions into thermal stability of the DNA double helix. *Nucleic Acids Res.* **2006,** *34*, 564-574.

(127) Adams Jr, E. C.; Mast, R. L.; Free, A. H. Specificity of glucose oxidase. *Arch. Biochem. Biophys.* **1960,** *91*, 230-234.

(128) Kuah, E.; Toh, S.; Yee, J.; Ma, Q., et al. Enzyme mimics: advances and applications. *Chem. Eur. J.* **2016,** *22*, 8404-8430.

(129) Liu, J.-q.; Wulff, G. Molecularly Imprinted Polymers with Strong Carboxypeptidase A-Like Activity: Combination of an Amidinium Function with a Zinc-Ion Binding Site in Transition-State Imprinted Cavities. *Angew. Chem. Int. Ed.* **2004,** *43*, 1287-1290.

(130) Wulff, G.; Gross, T.; Schönfeld, R. Enzyme models based on molecularly imprinted polymers with strong esterase activity. *Angew. Chem. Int. Ed.* **1997,** *36*, 1962-1964.

(131) Zhu, Z.; Guan, Z.; Jia, S.; Lei, Z., et al. Au@ Pt Nanoparticle Encapsulated Target-Responsive Hydrogel with Volumetric Bar-Chart Chip Readout for Quantitative Point-of-Care Testing. *Angew. Chem. Int. Ed.* **2014,** *53*, 12503-12507.

(132) Li, C.; Rowland, M. J.; Shao, Y.; Cao, T., et al. Responsive double network hydrogels of interpenetrating DNA and CB [8] host–guest supramolecular systems. *Adv. Mater.* **2015,** *27*, 3298-3304.

(133) Wang, J.; Gonzalez, A. D.; Ugaz, V. M. Tailoring bulk transport in hydrogels through control of polydispersity in the nanoscale pore size distribution. *Adv. Mater.* **2008,** *20*, 4482-4489.

(134) Priest, J. H.; Murray, S. L.; Nelson, R. J.; Hoffman, A. S. Lower Critical Solution Temperatures of Aqueous Copolymers of *N*-Isopropylacrylamide and Other *N*-Substituted Acrylamides. In *Reversible Polymeric Gels and Related Systems*; Russo, P. S., Ed.; American Chemical Society: 1987; Chapter 18, pp 255-264.

(135) Wei, W.; Du, J.; Li, J.; Yan, M., et al. Construction of robust enzyme nanocapsules for effective organophosphate decontamination, detoxification, and protection. *Adv. Mater.* **2013,** *25*, 2212-2218.

(136) Schulz, J. D.; Patt, M.; Basler, S.; Kries, H., et al. Site-Specific Polymer Conjugation Stabilizes Therapeutic Enzymes in the Gastrointestinal Tract. *Adv. Mater.* **2016,** *28*, 1455-1460.

(137) Keefe, A. J.; Jiang, S. Poly (zwitterionic) protein conjugates offer increased stability without sacrificing binding affinity or bioactivity. *Nat. Chem.* **2012,** *4*, 59.

(138) Yan, M.; Ge, J.; Liu, Z.; Ouyang, P. Encapsulation of single enzyme in nanogel with enhanced biocatalytic activity and stability. *J. Am. Chem. Soc.* **2006,** *128*, 11008-11009.

(139) Schnell, S. Validity of the Michaelis–Menten equation–steady-state or reactant stationary assumption: that is the question. *The FEBS journal* **2014,** *281*, 464-472.

(140) Hedstrom, L. Enzyme Specificity and Selectivity. In *eLS*; John Wiley & Sons, Ltd: 2001.

(141) Shumayrikh, N.; Huang, Y. C.; Sen, D. Heme activation by DNA: isoguanine pentaplexes, but not quadruplexes, bind heme and enhance its oxidative activity. *Nucleic Acids Res.* **2015,** *43*, 4191-4201.

(142) Zhou, L.; Ren, J.; Qu, X. Nucleic acid-templated functional nanocomposites for biomedical applications. *Mater. Today* **2017,** *20*, 179-190.

(143) Li, Y. L.; Maciel, D.; Rodrigues, J.; Shi, X. Y., et al. Biodegradable Polymer Nanogels for Drug/Nucleic Acid Delivery. *Chem. Rev.* **2015,** *115*, 8564-8608.

(144) Zhu, S. W.; Nih, L.; Carmichael, S. T.; Lu, Y. F., et al. Enzyme-Responsive Delivery of Multiple Proteins with Spatiotemporal Control. *Adv. Mater.* **2015,** *27*, 3620-3625.

(145) Dean, S. N.; Turner, K. B.; Medintz, I. L.; Walper, S. A. Targeting and delivery of therapeutic enzymes. *Ther. Deliv.* **2017,** *8*, 577-595.

(146) Hermeling, S.; Crommelin, D. J. A.; Schellekens, H.; Jiskoot, W. Structure-immunogenicity relationships of therapeutic proteins. *Pharm. Res.* **2004,** *21*, 897-903.

(147) Tonga, G. Y.; Jeong, Y.; Duncan, B.; Mizuhara, T., et al. Supramolecular regulation of bioorthogonal catalysis in cells using nanoparticle-embedded transition metal catalysts. *Nat. Chem.* **2015,** *7*, 597-607.

(148) Wang, F.; Zhang, Y.; Du, Z.; Ren, J., et al. Designed heterogeneous palladium catalysts for reversible light-controlled bioorthogonal catalysis in living cells. *Nat. Commun.* **2018,** *9*, 1209.

(149) Zhou, Y.; Liu, B.; Yang, R.; Liu, J. Filling in the Gaps between Nanozymes and Enzymes: Challenges and Opportunities. *Bioconj. Chem.* **2017,** *28*, 2903-2909.

(150) Sharma, A.; Garg, T.; Aman, A.; Panchal, K., et al. Nanogel-an advanced drug delivery tool: Current and future. *Artif. Cell. Nanomed. Biotechnol.* **2016,** *44*, 165-177.

(151) Li, D.; van Nostrum, C. F.; Mastrobattista, E.; Vermonden, T., et al. Nanogels for intracellular delivery of biotherapeutics. *J. Control. Release* **2017,** *259*, 16-28.

(152) Fan, D.; Zhu, J.; Zhai, Q.; Wang, E., et al. Cascade DNA logic device programmed ratiometric DNA analysis and logic devices based on a fluorescent dual-signal probe of a G-quadruplex DNAzyme. *Chem. Commun.* **2016,** *52*, 3766-3769.

(153) Zielonka, J.; Zielonka, M.; VerPlank, L.; Cheng, G., et al. Mitigation of NADPH Oxidase 2 Activity as a Strategy to Inhibit Peroxynitrite Formation. *J. Biol. Chem.* **2016,** *291*, 7029-7044.

(154) Santillo, M. F.; Liu, Y. T. A fluorescence assay for measuring acetylcholinesterase activity in rat blood and a human neuroblastoma cell line (SH-SY5Y). *J. Pharmacol. Toxicol. Methods* **2015,** *76*, 15-22.

(155) Cho, E. C.; Xie, J.; Wurm, P. A.; Xia, Y. Understanding the role of surface charges in cellular adsorption versus internalization by selectively removing gold nanoparticles on the cell surface with a I2/KI etchant. *Nano Lett.* **2009,** *9*, 1080-1084.

(156) Perrin, D. D. Dissociation contants of inorganic acids and bases in aqueous solution. *Pure Appl. Chem.* **1969,** *20*, 133-236.

(157) Um, S. H.; Lee, J. B.; Park, N.; Kwon, S. Y., et al. Enzyme-catalysed assembly of DNA hydrogel. *Nat. Mater.* **2006,** *5*, 797-801.

(158) Dave, N.; Chan, M. Y.; Huang, P.-J. J.; Smith, B. D., et al. Regenerable DNA-functionalized hydrogels for ultrasensitive, instrument-free mercury (II) detection and removal in water. *J. Am. Chem. Soc.* **2010,** *132*, 12668-12673.

(159) Strobel, M.; Lyons, C. S.; Mittal, K. *Plasma surface modification of polymers: relevance to adhesion*, VSP: Utrecht, The Netherlands, 1994.

(160) Malinouski, M.; Zhou, Y.; Belousov, V. V.; Hatfield, D. L., et al. Hydrogen peroxide probes directed to different cellular compartments. *PLoS One* **2011,** *6*, e14564.

(161) Fan, K.; Wang, H.; Xi, J.; Liu, Q., et al. Optimization of Fe3O4 nanozyme activity via single amino acid modification mimicking an enzyme active site. *Chem. Commun.* **2017,** *53*, 424-427.

(162) Liu, B.; Liu, J. Accelerating peroxidase mimicking nanozymes using DNA. *Nanoscale* **2015,** *7*, 13831-13835.

(163) Philipse, A. P.; Van Bruggen, M. P.; Pathmamanoharan, C. Magnetic Silica Dispersions: Preparation and Stability of Surface-modified Silica Particles with a Magnetic Core. *Langmuir* **1994,** *10*, 92-99.

(164) Liu, J.; Lu, Y. Preparation of aptamer-linked gold nanoparticle purple aggregates for colorimetric sensing of analytes. *Nat. Protoc.* **2006,** *1*, 246-252.

(165) Jv, Y.; Li, B. X.; Cao, R. Positively-charged gold nanoparticles as peroxidiase mimic and their application in hydrogen peroxide and glucose detection. *Chem. Commun.* **2010,** *46*, 8017-8019.

(166) Li, Y. X.; Li, Y. J.; Huang, L. H.; Bin, Q., et al. Molecularly imprinted fluorescent and colorimetric sensor based on TiO_2@$Cu(OH)_2$ nanoparticle autocatalysis for protein recognition. *J. Mater. Chem. B* **2013,** *1*, 1256-1262.

(167) Shen, X. T.; Zhu, L. H.; Wang, N.; Zhang, T., et al. Selective photocatalytic degradation of nitrobenzene facilitated by molecular imprinting with a transition state analog. *Catal. Today* **2014,** *225*, 164-170.

(168) Shen, X. T.; Zhu, L. H.; Huang, C. X.; Tang, H. Q., et al. Inorganic molecular imprinted titanium dioxide photocatalyst: synthesis, characterization and its application for efficient and selective degradation of phthalate esters. *J. Mater. Chem.* **2009,** *19*, 4843-4851.

(169) Morawski, B.; Quan, S.; Arnold, F. H. Functional expression and stabilization of horseradish peroxidase by directed evolution in Saccharomyces cerevisiae. *Biotechnol. Bioeng.* **2001,** *76*, 99-107.

(170) Guo, Y.; Deng, L.; Li, J.; Guo, S., et al. Hemin-Graphene Hybrid Nanosheets with Intrinsic Peroxidase-like Activity for Label-free Colorimetric Detection of Single-Nucleotide Polymorphism. *ACS Nano* **2011,** *5*, 1282-1290.

(171) O'Brien, A. M.; Smith, A. T.; Ó'Fágáin, C. Effects of phthalic anhydride modification on horseradish peroxidase stability and activity. *Biotechnol. Bioeng.* **2003,** *81*, 233-240.

(172) Andersson, L. I.; Paprica, A.; Arvidsson, T. A Highly Selective Solid Phase Extraction Sorbent for Pre-concentration of Sameridine Made by Molecular Imprinting. *Chromatographia* **1997,** *46*, 57-62.

(173) Baek, H. K.; Van Wart, H. E. Elementary steps in the reaction of horseradish peroxidase with several peroxides: kinetics and thermodynamics of formation of compound 0 and compound I. *J. Am. Chem. Soc.* **1992,** *114*, 718-725.

(174) Huang, Y.; Lin, Y.; Ran, X.; Ren, J., et al. Self-Assembly and Compartmentalization of Nanozymes in Mesoporous Silica-Based Nanoreactors. *Chem. Eur. J.* **2016,** *22*, 5705-5711.

(175) Vernekar, A. A.; Das, T.; Mugesh, G. Vacancy-Engineered Nanoceria: Enzyme Mimetic Hotspots for the Degradation of Nerve Agents. *Angew. Chem. Int. Ed.* **2016,** *55*, 1412-1416.

(176) Devi, H. S.; Singh, H. P. Unique Dual Responsive Activity of a Platinum Nanozyme Stabilized by a Green Solvent: Deep Eutectic Solvents. *New J. Chem.* **2018,** *42*, 12369-12373.

(177) Sun, Y.; Zhao, C.; Gao, N.; Ren, J., et al. Stereoselective Nanozyme Based on Ceria Nanoparticles Engineered with Amino Acids. *Chem. Eur. J.* **2017,** *23*, 18146-18150.

(178) Mogharrab, N.; Ghourchian, H.; Amininasab, M. Structural stabilization and functional improvement of horseradish peroxidase upon modification of accessible lysines: experiments and simulation. *Biophys. J.* **2007,** *92*, 1192-1203.

(179) Tan, J.; Guo, M.; Tan, L.; Geng, Y., et al. Highly efficient fluorescent QDs sensor for specific detection of protein through double recognition of hybrid aptamer-molecular imprinted polymers. *Sensors Actuat. B Chem.* **2018,** *274*, 627-635.